EARLY-AGE HYDRATION AND VOLUME CHANGE OF CALCIUM SULFOALUMINATE CEMENT-BASED BINDERS

BY

PIYUSH CHAUNSALI

DISSERTATION

Submitted in partial fulfillment of the requirements
for the degree of Doctor of Philosophy in Civil Engineering
in the Graduate College of the
University of Illinois at Urbana-Champaign, 2015

Urbana, Illinois

Doctoral Committee:

Assistant Professor Paramita Mondal, Chair and Director of Research
Professor Leslie J. Struble
Professor David A. Lange
Associate Professor Riyadh Hindi, St. Louis University

ABSTRACT

Shrinkage cracking is a predominant deterioration mechanism in structures with high surface-to-volume ratio. One way to allay shrinkage-induced stresses is to use calcium sulfoaluminate (CSA) cement whose early-age expansion in restrained condition induces compressive stress that can be utilized to counter the tensile stresses due to shrinkage. In addition to enhancing the resistance against shrinkage cracking, CSA cement also has lower carbon footprint than that of Portland cement. This dissertation aims at improving the understanding of early-age volume change of CSA cement-based binders. For the first time, interaction between mineral admixtures (Class F fly ash, Class C fly ash, and silica fume) and OPC-CSA binder was studied. Various physico-chemical factors such as the hydration of ye'elimite (main component in CSA cement), amount of ettringite (the main phase responsible for expansion in CSA cement), supersaturation with respect to ettringite in cement pore solution, total pore volume, and material stiffness were monitored to examine early-age expansion characteristics.

This research validated the crystallization stress theory by showing the presence of higher supersaturation level of ettringite, and therefore, higher crystallization stress in CSA cement-based binders. Supersaturation with respect to ettringite was found to increase with CSA dosage and external supply of gypsum. Mineral admixtures (MA) altered the expansion characteristics in OPC-CSA-MA binders with fixed CSA cement. This study reports that fly ash (FA) behaves differently depending on its phase composition. The Class C FA-based binder (OPC-CSA-CFA) ceased expanding beyond two days unlike other OPC-CSA-MA binders. Three factors were found to govern expansion of CSA cement-based binders: 1) volume fraction of ettringite in given pore volume, 2) saturation level of ettringite, and 3) dynamic modulus.

Various models were utilized to estimate the macroscopic tensile stress in CSA cement-based binders without taking into account the viscoelastic effects. For the first time, model based

on poromechanics was used to calculate the macroscopic tensile stress that develops in CSA cement-based binders due to crystallization of ettringite. The models enabled a reasonable prediction of tensile stress due to crystallization of ettringite including the failure of an OPC-CSA binder which had high CSA cement content. Elastic strain based on crystallization stress was calculated and compared with the observed strain. A mismatch between observed and calculated elastic strain indicated the presence of early-age creep. Lastly, the application of CSA cement in concretes is discussed to link the paste and concrete behavior.

Dedicated to my parents

ACKNOWLEDGMENTS

First of all, I would like to express my deep gratitude to my advisor, Prof. Paramita Mondal, for giving me an opportunity to work with her. This dissertation would not have been possible without her constant support and constructive criticism. The freedom in doing research with her has helped me grow as an independent researcher. I am also immensely grateful to my PhD thesis committee members – Prof. Leslie Struble, Prof. David Lange, and Prof. Riyadh Hindi for their time, helpful advice, and constructive criticism. I have been fortunate to have Prof. Struble in number of courses which really improved my understanding of cement-based materials. She has been a constant source of inspiration for her critical technical writing. Sometimes people get lost in their small world and don't realize the "Big Picture" which really means transferring the ideas to practice. Prof. Lange, through his lectures, has made me realize the importance of this aspect. I have also had privilege of working with Prof. Hindi on a collaborative project which laid the foundation of this dissertation. His knowledge of structural aspects has been critical in understanding the applicability of my research.

I would like to acknowledge the support from Illinois Department of Transportation through Illinois Center of Transportation which has made this research possible. The feedback of IDOT personnel: Dr. Daniel Tobias, Doug Dirks, Matthew W. Mueller, and James M. Krstulovich, Jr., during the course of the project is really appreciated. I would also like to acknowledge the support of Ravindar K. and Kavita Kinra Fellowship which I received in the first two years of doctoral program.

I have been fortunate to share my research with Prof. George Scherer (Princeton University) who provided his insightful and critical feedback on the part of this dissertation related to the calculation of crystallization stress. I also acknowledge helpful discussions with

Dr. Mauro Sardela (Material Research Laboratory at UIUC) on X-ray diffraction analysis. I thank Tim Prunkard and machine shop staff of Newmark Structural Laboratory for helping with the fabrication of pore solution extraction device and corrugated tube test apparatus which were used extensively in this research. I have also had chance to work with outstanding undergraduate students: Daniel Borup, Ilan Cohn, Jacob Scott, Xiazhi Zhang, and Haiyang Zhao who have also contributed toward various aspects of this research.

The stay in Urbana-Champaign could not have been better without the company of my fellow students from CEE. I would like to acknowledge Sravanthi Pulligilla, Seungmin Lim, Peter Stynoski, Bin Zhang, Will Hunnicutt, Xu Chen, Di Wu, Jacob Henschen, and Alexander Brand for their help and wonderful company. I especially remember innumerous discussions with Sravanthi and Seungmin about the research and other aspects of life. I would like to thank my roommate, Tarun, for enlightening me with his enormous knowledge of world around us, and for encouraging the appreciation and pursuit for history, music, and food. I specially thank Arun L. Gain, Saurabh Singh, Harshitha Menon, Hari Gajendran, Varun Gupta, Jeevaka Somaratna, Daniel Castaneda, James Bittner, William Wilson, and John Sanders for their amazing company.

The support and unconditional love of my parents has always been a constant source of encouragement since my childhood. I dedicate this thesis to my parents who have always believed in my ability, and instilled the pursuit of knowledge.

Table of Contents

LIST OF SYMBOLS XII

CHAPTER 1: INTRODUCTION 1

1.1 MOTIVATION 1

1.1.1 Shrinkage Reducing Admixtures (SRAs) 2

1.1.2 Light -Weight Aggregates 2

1.1.3 Expansive Cements 2

1.2 RESEARCH OBJECTIVES 6

1.3 ORGANIZATION OF THESIS 7

CHAPTER 2: LITERATURE REVIEW 9

2.1 MANUFACTURING OF CALCIUM SULFOALUMINATE CEMENT 9

2.2 HYDRATION OF CALCIUM SULFOALUMINATE CEMENT 10

2.2.1 Heat of Hydration 11

2.2.2 Pore Solution Chemistry 12

2.3 EXPANSION MECHANISM 12

2.4 FACTORS AFFECTING EXPANSION OF CSA CEMENT 16

2.4.1 Supersaturation 16

2.4.2 Amount of Ettringite 16

2.4.3 Effect of Calcium Sulfate 17

2.4.4 Effect of Water-to-Cementitious Ratio 18

2.4.5 Effect of Lime 19
2.4.6 Effect of Mineral Admixtures 20
2.5 MODELING OF CRYSTALLIZATION STRESS 21
2.6 CONCLUSIONS 24
CHAPTER 3: MATERIALS, MIXTURE PROPORTIONS AND METHODS 25
3.1 MATERIALS 25
3.2 MIXTURE PROPORTIONS 27
3.3 METHODS 27
3.3.1 Unrestrained Deformation Using Corrugated Tube and Prism Test 27
3.3.2 Method to Stop Cement Hydration 30
3.3.3 X-ray Diffraction (XRD) 30
3.3.4 Thermogravimetric (TG) Analysis 33
3.3.5 Scanning Electron Microscopy 33
3.3.6 Isothermal Conduction Calorimetry 34
3.3.7 Pore Solution Analysis and Thermodynamic Modeling 34
3.3.8 Capillary Porosity 36
3.3.9 Compressive Strength 37
3.3.10 Tensile Strength 37
3.3.11 Dynamic Modulus 37

CHAPTER 4: EARLY-AGE VOLUME CHANGE OF CSA CEMENT-BASED BINDERS……..39

4.1 INTRODUCTION 39

4.2 EARLY-AGE VOLUME CHANGE, POROSITY AND DYNAMIC MODULUS…. 39

4.2.1 OPC-CSA Binder 39

4.2.2 OPC-CSA-MA Binder 43

4.3 CONCLUSIONS 48

CHAPTER 5: EARLY-AGE HYDRATION OF CSA CEMENT-BASED BINDERS 50

5.1 INTRODUCTION 50

5.2 HEAT OF HYDRATION 50

5.2.1 OPC-CSA Binder 50

5.2.2 OPC-CSA-MA Binder 53

5.3 HYDRATION PROGRESS 57

5.3.1 OPC-CSA Binder 57

5.3.2 OPC-CSA-MA Binder 62

5.4 THERMOGRAVIMETRIC ANALYSIS 68

5.5 PORE SOLUTION CHEMISTRY 70

5.5.1 OPC-CSA Binder 70

5.5.2 OPC-CSA-MA Binder 74

5.6 CONCLUSIONS 81

CHAPTER 6: FACTORS INFLUENCING EARLY-AGE EXPANSION 82

6.1 RATE OF YE'ELIMITE HYDRATION 82

6.2 AMOUNT OF ETTRINGITE IN PORE VOLUME 83

6.3 SUPERSATURATION 85

6.4 DYNAMIC MODULUS 86

6.5 CONCLUSIONS 87

CHAPTER 7: ESTIMATION OF CRYSTALLIZATION STRESS AND ITS INFLUENCE ON EXPANSION 88

7.1 ESTIMATION OF CRYSTALLIZATION STRESS 88

7.1.1 OPC-CSA Binder 88

7.1.2 OPC-CSA-MA Binder 90

7.2 COMPARISON BETWEEN MEASURED AND CALCULATED STRAIN 93

7.3 CONCLUSIONS 95

CHAPTER 8: EARLY-AGE BEHAVIOR OF CONCRETE 96

8.1 INTRODUCTION 96

8.2 BACKGROUND 96

8.2.1 Restrained Expansion of Concretes 96

8.2.2 Mechanical Properties and Long-Term Creep 97

8.3 MIXTURE PROPORTIONS 98

8.4 METHODS 99
8.4.1 Restrained Expansion 99
8.4.2 Compressive Strength 100
8.5 RESULTS 100
8.5.1 Early-Age Properties 100
8.5.2 Restrained Expansion and Shrinkage of Expansive Concretes 101
8.5.3 Mechanical Properties of Expansive Concretes 103
8.6 CONCLUSIONS 104
CHAPTER 9: CONCLUSIONS AND FUTURE DIRECTIONS 106
9.1 THESIS SUMMARY 106
9.2 PRIMARY CONCLUSIONS 107
9.3 RECOMMENDATIONS FOR FUTURE WORK 109
REFERENCES 112
APPENDIX A. RIETVELD REFINEMENT OF OPC-CSA BINDERS 124
APPENDIX B. RIETVELD REFINEMENT OF OPC-CSA-MA BINDERS 133
APPENDIX C. RIETVELD RFINEMENT OF OPC-CSA-CFA-GYP BINDER 142
APPENDIX D. ESTIMATION OF AMORPHOUS CONTENT USING INTERNAL STANDARD 145

List of Symbols

The following abbreviations have been used in this thesis:

$C = CaO$ $A = Al_2O_3$ $S = SiO_2$ $\hat{S} = SO_3$ $F = Fe_2O_3$ $H = H_2O$

OPC = ordinary Portland cement

CSA = calcium sulfoaluminate

$C_4A_3\hat{S} = 4CaO.3Al_2O_3.SO_3$

$C_3S = 3CaO.SiO_2$

$C_2S = 2CaO.SiO_2$

$C_3A = 3CaO.Al_2O_3$

$C_4AF = 4CaO.Al_2O_3.Fe_2O_3$

Ettringite = $3CaO.Al_2O_3.3CaSO_4.32H_2O$

Monosulfate = $3CaO.Al_2O_3.CaSO_4.12H_2O$

Monocarbonate = $3CaO.Al_2O_3.CaCO_3.12H_2O$

Hemicarbonate = $3CaO.Al_2O_3.0.5CaCO_3.12H_2O$

Gypsum = $C\hat{S}H_2$

Hemihydrate = $C\hat{S}H_{0.5}$

Anhydrite = $C\hat{S}$

C-S-H = amorphous calcium silicate hydrate gel

CHAPTER 1: INTRODUCTION

1.1 MOTIVATION

Concrete structures with large surface-to-volume ratio often suffer from shrinkage cracking. Cracking increases the maintenance cost, and also facilitates the ingress of aggressive chemicals such as chloride and sulfate ions resulting in degradation. Therefore, mitigation of cracking in concrete elements such as bridge decks remains a challenging problem across the United States of America. Concrete cracks when the tensile stress due to shrinkage exceeds the tensile strength of concrete. Figure 1.1 describes the evolution of tensile stress due to shrinkage and material strength with time. In concrete, stress relaxation at early-age reduces the magnitude of the tensile stress which prolongs the cracking time.

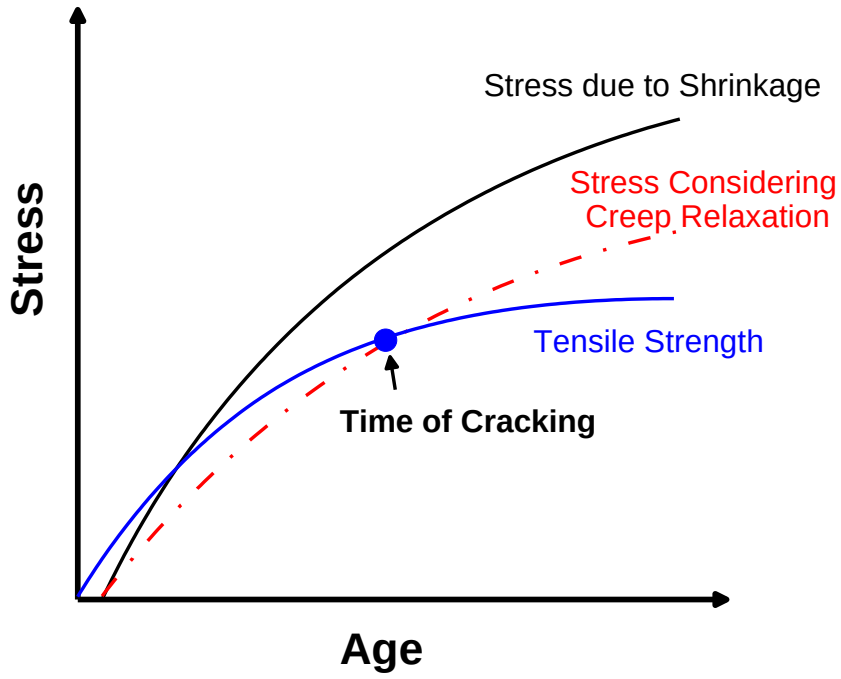


Figure 1.1 Schematic showing the onset of cracking due to the development of tensile stress

Shrinkage of concrete is derived from calcium silicate hydrate (C-S-H) which is the main hydration product of Portland cement. Hence, there have been efforts to optimize concrete mixture proportion by minimizing the paste content and improving aggregate grading. In the last four decades, there has been substantial research in devising ways to prevent early-age shrinkage cracking. Few of the existing shrinkage-mitigation techniques are mentioned below:

1.1.1 Shrinkage Reducing Admixtures (SRAs)

Shrinkage reducing admixture lowers the surface tension of water, thus reduces the capillary tensile stress developed due to drying [Sato et al., 1983; Ai and Young, 1997; Berke et al., 1997; Bentz et al. 2001]. This reduction in tensile stress has been proven to be effective in reducing the shrinkage of concrete. The SRAs have been shown to reduce both the drying and autogenous shrinkage [Berke et al., 1997; Weiss, 1999; D'Ambrosia et al., 2001]. One downside of using SRA is that they have been found to decrease the compressive strength of concrete by 10-15% [Weiss, 1999].

1.1.2 Light -Weight Aggregates

Light-weight aggregates (LWAs) have been shown to be effective in mitigating the autogenous shrinkage (self-desiccation) of concrete which is significant at low water-to-cement (w/c) ratios [Jensen and Hansen, 2001; Bentur et al., 2001; Bentz et al., 2004; Lura et al., 2006]. The higher porosity of LWAs makes them suitable as water reservoirs. The absorbed water is released later to facilitate hydration.

1.1.3 Expansive Cements

Expansive cements were developed to compensate for drying shrinkage of concrete. Figure 1.2 (a) shows the schematic of shrinkage-compensation achieved by using expansive cement. Although expansive cement also shrinks, the net shrinkage is reduced due to initial

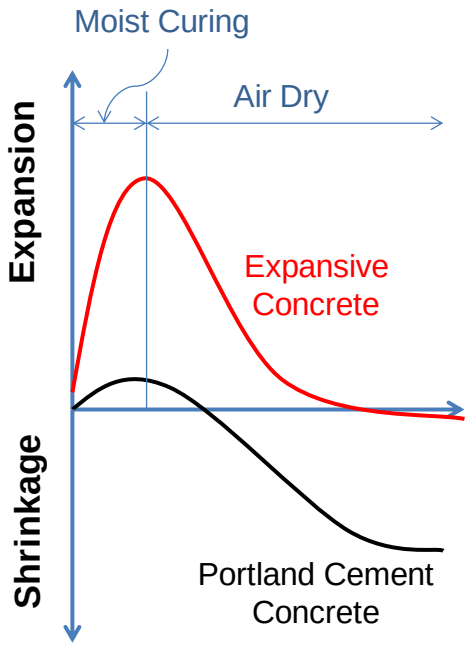
expansion. In the presence of restraint (internal or external), the expansion occurring at early age results in development of compressive stress which counteracts the tensile stress generated due to drying shrinkage (Figure 1.2 (b)). ACI 223-R10 committee specifies four different types of expansive cements: Type K, Type M, Type S, and Type G. Type K, Type M, and Type S expand due to the formation of ettringite whereas Type G forms calcium hydroxide crystals. Following are the descriptions of each of these cements according to ACI 223-R10:

Type K: blend of OPC, ye'elimite ($C_4A_3\hat{S}$) and calcium sulfate ($C\hat{S}$)

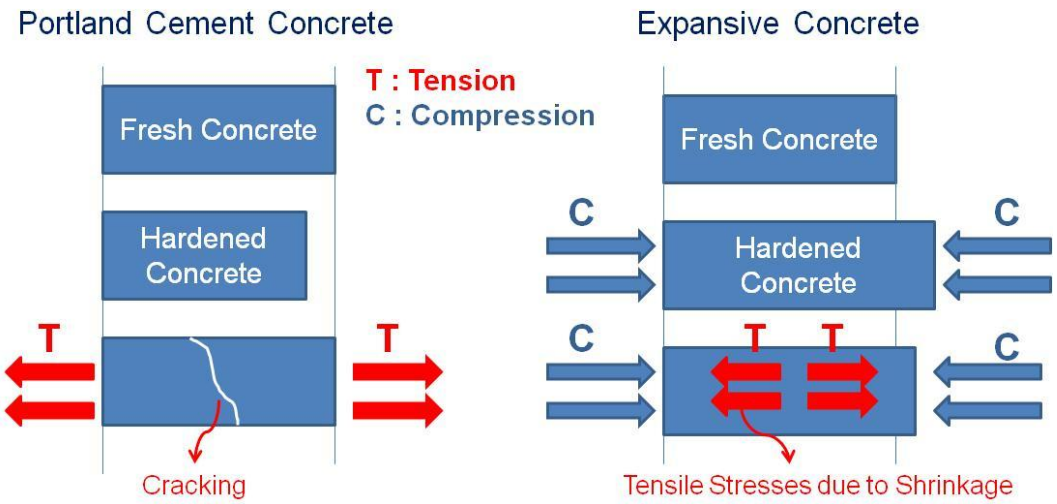
Type M: blend of OPC, mono calcium aluminate (CA) and calcium sulfate ($C\hat{S}$)

Type S: blend of OPC, tri calcium aluminate (C_3A) and calcium sulfate ($C\hat{S}$)

Type G: blend of OPC, free lime and alumina



(a)



(b)

Figure 1.2 Comparison between Portland cement concrete and expansive concrete with respect to: (a) volume change, and (b) stress development

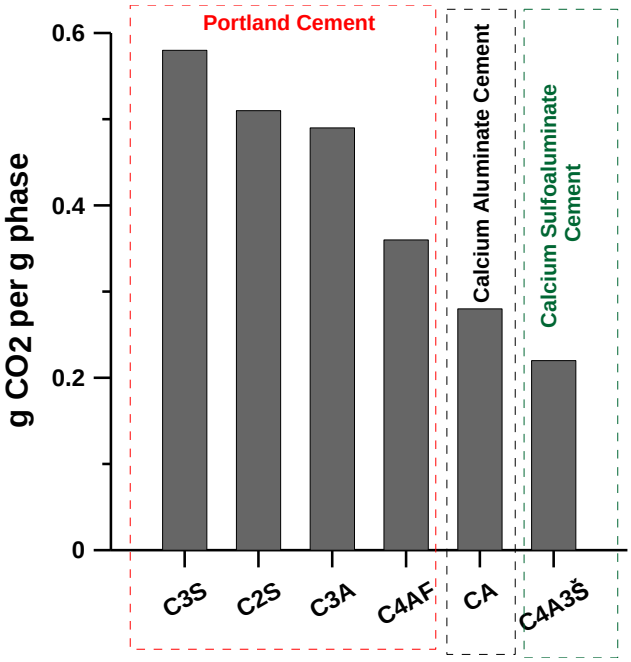


Figure 1.3 Amount of CO_2 released (during calcination process only) for various cementitious phases [Gartner, 2004]

Among the above-mentioned expansive cements, Type K cement is of particular interest as its main component, ye'elimite or calcium sulfoaluminate ($C_4A_3\hat{S}$), has lower carbon footprint than the phases present in Portland cement. Ye'elimite and C_2S are also the main phases of calcium sulfoaluminate cement which has been promoted for being an environmentally friendly binder [Mehta, 1980; Valenti et al., 1987; Glasser and Zhang, 2001; Odler, 2003; Gartner, 2004; Damtoft et al., 2008; Juenger et al., 2011]. Figure 1.3 shows the CO_2 released during the formation of various constituents of Portland cement, calcium aluminate cement (CAC), and calcium sulfoaluminate (CSA) cement through calcination process. Since the constituents of Portland cement have higher demand for limestone, they produce higher CO_2 than calcium monoaluminate and calcium sulfoaluminate phases. Additionally, the CSA clinker can be manufactured at lower kiln temperature (~1250°C) and has higher porosity than Portland cement clinker [Mehta, 1980; Ali et al., 1994; Sherman et al., 1995; Zhang, 2000], both of which

contribute toward reducing the overall energy demand. Thus, it is evident that the CSA-based cement can be utilized as shrinkage-compensating and environmentally friendly binder.

1.2 RESEARCH OBJECTIVES

Long-term performance of CSA cement-based concrete is mainly governed by the time, duration, and extent of early-age expansion. Therefore, it becomes important to get better understanding of various factors influencing expansion characteristics of CSA cement. The current research aims at understanding early-age volume change taking place during the hydration of CSA cement-based binders. The amount of ettringite, saturation level of ettringite in the pore solution, pore structure features (porosity and pore size distribution), availability of water, temperature, and material stiffness were identified as the factors governing expansion characteristics of CSA cement. Two different binder systems: OPC-CSA and OPC-CSA-MA, where MA stands for mineral admixtures, were examined in the current study to understand how various above-mentioned factors are linked to expansion. The interaction between mineral admixtures (Class C FA, Class F FA, and silica fume) and OPC-CSA blend was investigated for the first time. This thesis can broadly be divided into two sections: 1) early-age volume change, hydration and modeling for crystallization stress in CSA cement pastes, and 2) early-age behavior of restrained CSA cement-based concrete. Physical factors such as material stiffness and pore structure features were monitored by determining dynamic modulus and capillary porosity, respectively. Chemical factors such as the hydration of ye'elimite and the amount of ettringite were monitored through X-ray diffraction. Pore solution was extracted to determine the elemental composition (Na, K, Ca, S, Al, and Si) of the pore solution. Subsequently, a geochemical modeling program (GEMS-PSI) was utilized to estimate the saturation level of ettringite in the pore solution. Once the saturation level of ettringite was determined, the

maximum crystallization stress arising from supersaturation was calculated. Subsequently, various models were utilized to estimate the macroscopic tensile stresses developed in CSA cement-based binders. One of the models used in this study was based on poromechanics which was applied in CSA cement-based system for the first time. Finally, the calculated tensile stresses were compared with the measured tensile strengths. At the end, expansion behavior of restrained concrete incorporating CSA cement was also studied to link the behavior of paste and concrete.

1.3 ORGANIZATION OF THESIS

This thesis attempts to examine various physico-chemical factors influencing early-age volume change of CSA cement-based binders. The thesis is broadly organized into two parts: paste study (Chapters 2-7) and concrete study (Chapter 8). A detailed literature review on early-age hydration and expansion mechanism of CSA cement is presented in Chapter 2. Various physico-chemical factors influencing the expansion behavior and modeling of crystallization stress are discussed. Materials, mixture proportions, and methods are discussed in Chapter 3. Since the motivation behind the current study was to understand and explain the early-age volume change of CSA cement-based binders, the observations on early-age volume change of CSA cement-based binders are presented in Chapter 4. More specifically, the effect of CSA cement, mineral admixtures, and gypsum addition on expansion behavior of OPC-CSA and OPC-CSA-MA binders was studied. Chapter 4 also discusses the physical changes (change in porosity and dynamic modulus) occurring during the expansion process. The hydration kinetics and phase evolution of CSA cement-based binders are presented in Chapter 5. Pore solution analyses and the estimation of saturation levels of ettringite are also discussed in Chapter 5. Chapter 6 summarizes the various factors which were found critical in understanding early-age

expansion of CSA cement-based binders. Chapter 7 shows that application of various models in estimating the tensile stress due to crystallization of ettringite. The calculated tensile stresses were compared with tensile strength of paste samples. Chapter 8 reports the studies on concrete samples in order to establish a link between early-age volume change of paste and concrete. The concrete study consisted of early-age properties, early-age volume change, long-term drying shrinkage, and mechanical properties. Finally, Chapter 9 presents the conclusions, and proposes the future work.

CHAPTER 2: LITERATURE REVIEW

2.1 MANUFACTURING OF CALCIUM SULFOALUMINATE CEMENT

The very first expansive cement developed by Alexander Klein for achieving shrinkage-compensation was based on calcium sulfoaluminate (CSA) clinker [Klein and Troxell, 1958; Klein et al., 1961]. The raw materials used for making CSA cement are bauxite, limestone, clay, and calcium sulfate. The major chemical reactions occurring in the $CaO\text{-}SiO_2\text{-}Al_2O_3\text{-}SO_3$ system during the formation of CSA clinker from raw materials such as limestone, clay, calcium sulfate and bauxite have been summarized as below [Zhang, 2000]:

$$CaCO_3 \xrightarrow{\sim 900^oC} CaO + CO_2$$

$$2CaO + Al_2O_3 + SiO_2 \xrightarrow{900\text{-}950^oC} C_2AS$$

$$3CaO + Al_2O_3 + CaSO_4 \xrightarrow{950\text{-}1000^oC} C_4A_3\hat{S}$$

$$3CaO + 3C_2AS + CaSO_4 \xrightarrow{1050\text{-}1150^oC} C_4A_3\hat{S} + 3C_2S$$

$$2CaO + SiO_2 \xrightarrow{1050\text{-}1150^oC} C_2S$$

$$2C_2S + CaSO_4 \xrightarrow{1150\text{-}1250^oC} 2C_2S.C\hat{S}$$

$$2C_2S.C\hat{S} \xrightarrow{1300^oC} 2C_2S + C\hat{S}$$

Calcium sulfoaluminate cements have been used commercially in China for the last four decades [Zhang, 2000]. Chinese researchers have developed the following formula to derive the optimal sulfate for different types of CSA cements which can be prepared by adjusting the gypsum content:

$$C_T = 0.13\ M\ (A/\hat{S})$$

where C_T is the weight ratio: gypsum/clinker, M is the molar ratio: gypsum/$C_4A_3\hat{S}$, A is the weight percentage of $C_4A_3\hat{S}$ in clinker, and $\hat{S}$ is the weight percentage of SO_3 in gypsum. The value of M can be chosen according to specific types of cement. For example, M value is in between 0-1.5 for rapid hardening cement whereas M values falls in range of 1.5-2.5 and 2.5-6.0 for expansive and self-stressing cements.

2.2 HYDRATION OF CALCIUM SULFOALUMINATE CEMENT

Calcium sulfoaluminate cement is produced by grinding $C_4A_3\hat{S}$ and C_2S with various amounts of gypsum ($C\hat{S}H_2$) and/or anhydrite ($C\hat{S}$). The following reactions have been suggested to take place in CSA cement [Mehta and Klein, 1966; Collepardi et al., 1972; Mehta, 1973 a; Zhang, 2000]:

$$C_4A_3\hat{S} + 18H \longrightarrow C_3A.C\hat{S}.12H + 2AH_3 \quad (1)$$

$$C_4A_3\hat{S} + 2C\hat{S}H_2 + 34H \longrightarrow C_3A.3C\hat{S}.32H + 2AH_3 \quad (2)$$

$$C_4A_3\hat{S} + 6CH + 8C\hat{S}H_2 + 74H \longrightarrow 3C_3A.3C\hat{S}.32H \quad (3)$$

$$C_2S + H \longrightarrow C\text{-}S\text{-}H \quad (4)$$

where C = CaO, A = Al_2O_3, $\hat{S}$ = SO_3, S = SiO_2, H = H_2O

The C-S-H formed from CSA cement has been reported to have lower Ca/Si ratio than that in Portland cement [Zhang, 2000]. From the above reactions, it is evident that the hydration products of CSA cement are $C_3A.3C\hat{S}.32H$ (ettringite), C-S-H, and amorphous AH_3. It has been shown that the reaction (1) does not lead to expansion whereas reaction (2) and (3) lead to expansion due to the formation of ettringite [Mehta, 1967]. Therefore, the presence of calcium sulfate is essential for expansion as it leads to the formation of ettringite. In presence of lime and gypsum, increased amount of ettringite is formed which is highlighted in reaction (3). Therefore, the hydration of $C_4A_3\hat{S}$ results in larger amount of ettringite following reaction (3) in a C_3S-

based system, compared to a C_2S-based system where reaction (2) is favored [Collepardi and Turriziani, 1972]. However, Kasselouri et al. (1995) observed the non-expansive nature of CSA cement when the greatest amount of ettringite formed in the inner vacant spaces at early-age.

2.2.1 Heat of Hydration

Figure 2.1 shows heat evolution during hydration of ye'elimite with and without presence of gypsum. Without gypsum, the pure ye'elimite phase shows two maxima in the heat flow curve. The first one occurs immediately after adding water, and can be attributed to heat of wetting. The second peak occurs after a dormant period at around 14 hours. The dormant period is reduced as the gypsum content is increased [Winnefeld and Barlag, 2010]. It is noted that there is a presence of second maximum (or peak) after initial dormant period in the mixture with ye'elimite/gypsum molar ratio of 1:1. The second maximum occurred due to the depletion of gypsum and formation of monosulfate; upon further addition of gypsum, the peak disappeared [Winnefeld and Barlag, 2010]. From the calorimetric plot, it is very clear that calcium sulfate plays an important role in controlling the reaction of ye'elimite. It should also be noted that CSA cement contains mainly two forms of calcium sulfate: gypsum or anhydrite or both. Hence, the difference in the dissolution kinetics of gypsum and anhydrite also affects the hydration of ye'elimite [Sahu et al., 1991]. The faster dissolution kinetics of gypsum accelerates the hydration of ye'elimite [Winnefeld and Barlag, 2010].

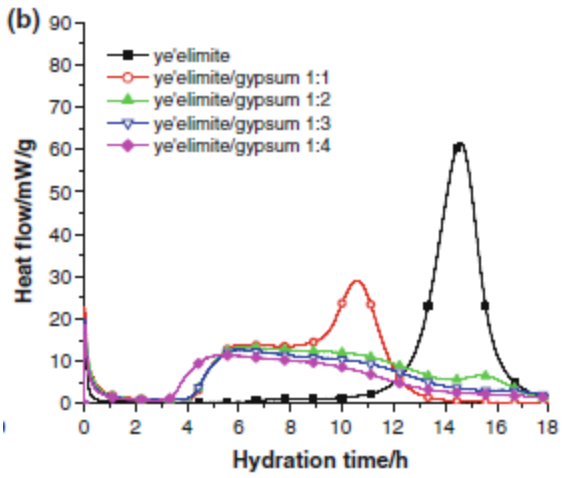


Figure 2.1 Heat evolution during hydration of pure ye'elimite with and without gypsum addition [Winnefeld and Barlag, 2010]

2.2.2 Pore Solution Chemistry

The pH of pore solution of CSA cement has been found to be lower than that of Portland cement, and within a range ~11.2 to ~12.8 [Andac and Glasser, 1999; Winnefeld and Lothenbach, 2010]. Winnefeld and Lothenbach (2010) studied the effect of two forms of calcium sulfate (i.e., anhydrite and gypsum) on the pore solution composition of CSA cement. The pore solution was found to be saturated with gypsum until later ages due the faster dissolution kinetics of gypsum. On the contrary, the pore solution was undersaturated with respect to anhydrite from very early age due to its slower dissolution kinetics of anhydrite.

2.3 EXPANSION MECHANISM

There have been primarily two theories proposed to describe the underlying mechanism of expansion due to ettringite precipitation in CSA cements.

- **Crystallization Stress Theory** [Ping and Beaudoin, 1992; Scherer, 2004; Steiger, 2005; Flatt and Scherer, 2008; Bizzozero, 2014]: According to this theory, the expansion takes place when ettringite is formed in small pores in a supersaturated pore solution. The role

of supersaturation in exerting stress has been depicted long time ago. In 1916, Taber showed that a crystal can grow if it is placed in a supersaturated solution and the crystallization pressure developed due to the growth of the crystal is enough to lift a certain weight (Figure 2.2). However, when two crystals, one loaded and one unloaded, are in contact with a supersaturated solution, the unloaded crystal grows to consume the supersaturation (Figure 2.2). In a saturated solution in absence of evaporation, the loaded crystal would dissolve while the unloaded crystal grows, indicating the role of pressure on solubility of the crystal. These experiments were performed under equilibrium conditions without considering kinetics and transport of ions.

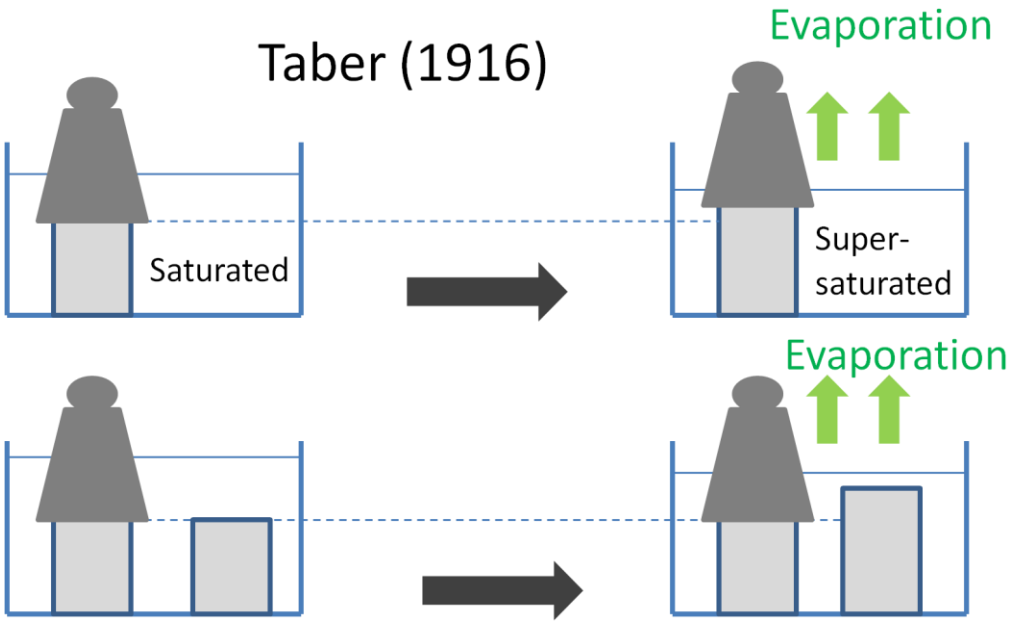


Figure 2.2 Experiments performed by Taber (1916) depicting the role of supersaturation in exerting stress

Supersaturation is the precursor for ettringite to exert stress on surrounding boundaries. Presence of a disjoining pressure between the growing crystals and any confining surface is also essential in addition to supersaturation; otherwise, the crystal will stop growing

when it comes in contact with surrounding wall [Scherer, 2004]. A crystal with curvature, κ_{CL}, is in equilibrium when the solubility product, K, satisfies the following equation [Freundlich, 1926; Cahn, 1980]:

$$\gamma_{CL}\kappa_{CL} = \frac{RT}{v_C}\log\left(\frac{K}{K_S}\right) \qquad \text{Eq. 2–1}$$

where γ_{CL} is the interfacial energy between crystal and liquid, R is the ideal gas constant, T is the absolute temperature and K_s is the equilibrium solubility of macroscopic crystal. It is evident from the above equation that crystals growing in smaller pores are in equilibrium with a solution of higher concentration than a macroscopic crystal. Another way to look at the equation is that a higher supersaturation leads to the growth of crystals in smaller pores, as shown in Figure 2.3. In the case of delayed ettringite formation (DEF), a measurable expansion has been observed before any ettringite crystals could be detected using SEM, which supported the fact that the ettringite growing in smaller pores (undetectable in SEM) resulted in the expansion [Famy, 2001].

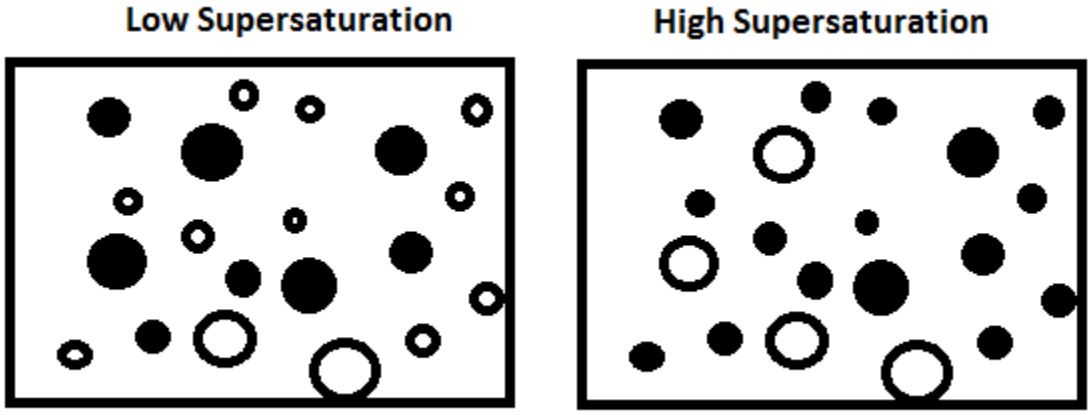
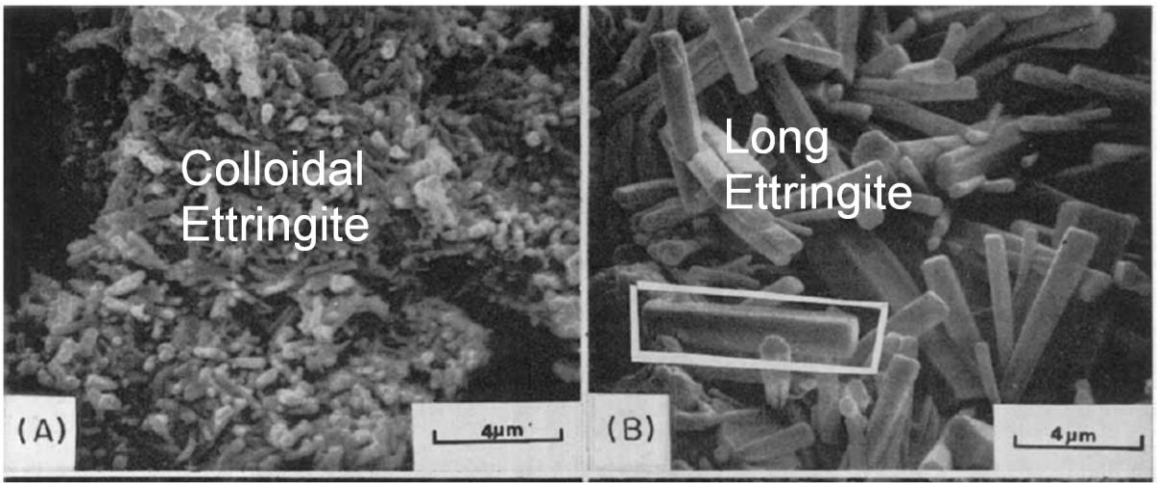


Figure 2.3 A schematic showing the effect of supersaturation on the pore size where crystal formation takes place (Fully-filled circle – supersaturated pores where crystal growth takes place; empty circle – undersaturated pores with pore solution)

- **<u>Swelling Theory</u>** [Mehta, 1973 a; Mehta, 1976; Mehta and Hu, 1978]: Swelling theory emphasizes the swelling behavior of fine ettringite crystals. Mehta and Hu (1978) found a direct relation between the mass gain through adsorption and expansion of paste samples consisting of $C_4A_3\hat{S}$, CH and $C\hat{S}$ in stoichiometric proportions. Mehta (1973 a; 1973 b; 1976) also reported that the morphology of ettringite crystals in presence of calcium hydroxide was finer (colloidal in nature) than in absence of calcium hydroxide (Figure 2.4). The colloidal ettringite tends to adsorb water resulting in swelling and expansion.



(a) (b)

Figure 2.4 SEM micrographs showing ettringite in: (a) $C_4A_3\hat{S}$-$C\hat{S}$ system with lime, (b) $C_4A_3\hat{S}$-$C\hat{S}$ system without lime [Mehta, 1973 b]

In some instances, researchers have attributed expansion to both crystallization stress and water adsorption [Rossetti et al., 1982; Min and Mingshu, 1994]. Odler and Subauste (1999) suggested that wet curing intensifies the expansion due to ettringite formation; however, expansion can still take place in the absence of wet curing. In addition to two theories described earlier, the other proposed mechanism emphasizes expansion due to volume increase [Mather,

1984]. However, there are lack of evidence to link expansion and the total amount of ettringite [Taylor et al., 2001].

2.4 FACTORS AFFECTING EXPANSION OF CSA CEMENT

2.4.1 Supersaturation

In many different cases, supersaturation is often considered as the precursor to crystallization-induced expansion. Ping and Beaudoin (1992) investigated the problem of sulfate attack, and suggested that confined growth of ettringite and supersaturation were two essential factors for crystallization stress. Scherer (2004) emphasized the role of supersaturation in salt-induced damage in stones. The presence of a thin film (1-2 nm) between crystal and surrounding walls was suggested to be essential in order to generate crystallization stress [Scherer, 2004]. In a recent study [Bizzozero et al., 2014], higher supersaturation were found to be related to the increase in unrestrained expansion of CSA cement in presence of a higher dosage of calcium sulfate.

2.4.2 Amount of Ettringite

Even though the expansion is due to the formation of ettringite, presence of any direct relationship between the ettringite content and the expansion is debatable [Famy et al., 2001; Kunther et al., 2013]. Famy et al. (2001) studied the expansion of heat treated cement mortar bars which were subsequently cured in different curing environments. Figure 2.5 compares the expansion with the ettringite content for various curing conditions. The ettringite formed in this case was due to delayed ettringite formation in heat-treated mortar bars. It is noted here that Famy et al. (2001) measured the relative ettringite content using an arbitraty unit (a.u.). It is evident that the relationship between expansion and ettringite content is not straightforward.

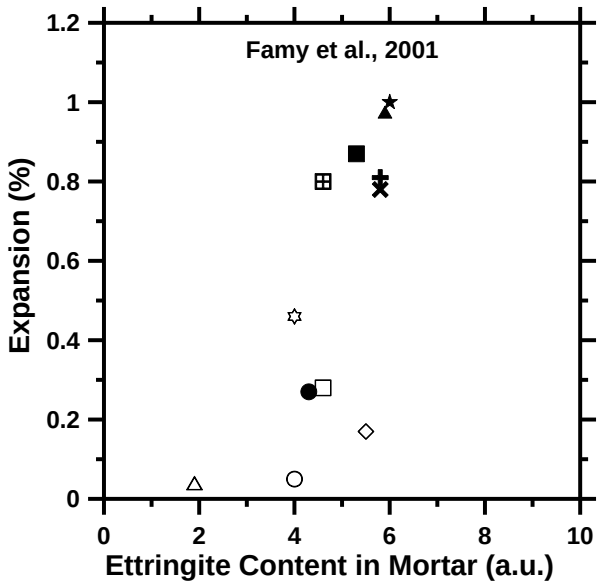


Figure 2.5 Expansion vs. relative ettringite content of heat cured cement mortar bars subsequently stored in different curing environments (adapted from Famy et al., 2001)

In a recent study by Kunther et al. (2013), the cement bars were exposed to various sulfate solutions, and expansion was measured. No direct relation between expansion and predicted volume increase was observed. However, the coexistence of ettringite and gypsum was shown to have resulted in higher expansion. Similarly, Bizzozero et al. (2014) studied the expansion of calcium aluminate cement (CAC) and calcium sulfoaluminate cement (CSA) with varying amounts of gypsum. The authors could not relate the difference in expansion characteristics of CAC and CSA systems to the difference in ettringite content. It is noted here that most studies tend to compare expansion with the total amount of ettringite (by weight), but a more relevant parameter could be the volume of ettringite in given pore volume (more detail on this topic is presented later).

2.4.3 Effect of Calcium Sulfate

The presence of calcium sulfate is critical for the formation of ettringite. In absence of calcium sulfate, monosulfate (AFm) is formed in addition to aluminum hydroxide (AH_3).The

presence of calcium sulfate promotes the formation of AFt (ettringite) instead of AFm [Glasser and Zhang, 2001]. In the study by Glasser and Zhang (2001), varying percentage of gypsum was added to a commercial CSA clicker. It was shown for the particular CSA clinker that 30% or higher gypsum addition is needed to form only AFt phase (Figure 2.6). The addition of calcium sulfate has been shown to increase the expansion of CSA cement [Desbois et al., 2010; Chen and Juenger, 2012; Bizzozero et al., 2014].

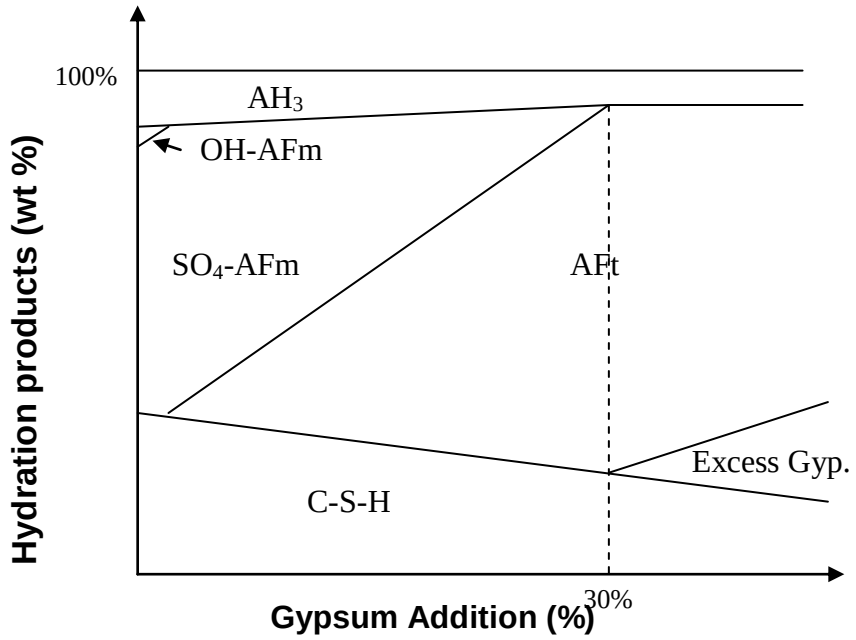


Figure 2.6 The effect of gypsum addition on the phase evolution of CSA-based cement [Glasser and Zhang, 2001]

2.4.4 Effect of Water-to-Cementitious Ratio

The water-to-cementitious ratio (w/cm) has been found to significantly alter the expansion behavior and durability of CSA-based cement. A reduction in w/cm ratio has been shown to increase the expansion [Mather, 1970; Polivka and Willson, 1973; Hoff, 1973; Cohen, 1983; Chen and Juenger, 2012; Bizzozero, 2014]. Furthermore, a low w/cm ratio results in incomplete hydration of ye'elimite, which can lead to delayed expansion in the presence of

moisture [Beretka et al., 1996]. Slow hydration of ye'elimite at low w/b ratio has also been found to affect the rate of expansion [Chaunsali and Mondal, 2014; Chaunsali and Mondal, 2015]. Bizzozero (2014) reported reduction in expansion at higher w/cm ratios due to a decrease in supersaturation and increase in porosity (as increased porosity can accommodate the crystals without development of much crystallization stress).

2.4.5 Effect of Lime

The presence of lime has been reported to affect the expansion of CSA cements. The rate of hydration of ye'elimite in presence of lime was found to be slow during the initial 6 hours, but the expansion was similar to samples without lime at the end of 7 days [Mehta, 1973 b]. The author reported a steady growth of ettringite formation from 6 hours to 7 days although there was initial retardation during the first 6 hours in presence of lime. However, in the absence of lime, ettringite formation completed within 1 day. In another study by Mehta (1973 a), the morphology of ettringite seemed to be affected by the presence of lime. The size of ettringite crystals was small (of colloidal nature) in presence of lime. Mehta (1973 a, 1976, and 1978) postulated that it is the colloidal nature of ettringite which tends to adsorb water and leads to expansion due to swelling mechanism. He argued that just the presence of ettringite is not a sufficient condition for expansion. Particularly, in super-sulfate cements, considerable amount of ettringite does not lead to expansion due to the absence of lime.

Kurdowski and Thiel (1981) studied the influence of free lime on expansion and size of ettringite crystals. The cement with higher free lime content exhibited higher rate of expansion and higher total expansion. However, no significant difference in the crystal size of ettringite was observed in this study. When CSA cement is used with Portland cement, the hydration of C_3S provides lime saturated environment for CSA hydration. Gastaldi et al. (2011) observed lower

shrinkage of the OPC-CSA mixture compared to CSA cement. The lower shrinkage of OPC-CSA mixture was attributed to the higher expansion of ye'elimite in the presence of lime. In a study by Bianchi et al. (2009), the expansion of C_3S-$C_4A_3\hat{S}$-$C\hat{S}$ was monitored with varying $C_3S/C_4A_3\hat{S}$ and $C\hat{S}/C_4A_3\hat{S}$ ratio. Higher amount of $C_4A_3\hat{S}$ together with high $C_3S/C_4A_3\hat{S}$ and $CaSO_4$ amount led to the highest expansion.

2.4.6 Effect of Mineral Admixtures

Mineral admixtures are widely used for enhancing the long-term performance of concrete. The influence of mineral admixtures on expansion characteristics of CSA cements is not fully understood as they not only alter the physical properties but also influence the pore solution chemistry of expansive cement system. At fixed amount of expansive component, the Class F FA replacement was shown to have increased the expansion of expansive mortars [Hoff, 1973]. The reduction in internal restraint (material strength) of fly ash based system due to dilution was found to increase the expansion even though there was not much difference in the amount of expansive component. It is known that the use of mineral admixtures reduces the alkalinity of pore solution due to alkali binding by C-(A)-S-H [Taylor, 1997, Chappex and Scrivener, 2012]. The reduction in alkalinity of pore solution in presence of silica fume was reported to have suppressed the solubility of ye'elimite which resulted in lower expansion [Lobo and Cohen, 1993]. In a study by Folliard et al. (1994), the dilution of CSA cement in the presence of fly ash and silica fume was reported to reduce the extent of expansion. As there are very limited studies on the use of mineral admixtures with CSA cements [Lobo, 1991; Beretka et al., 1993; Folliard et al., 1993, García-Maté et al., 2013], detailed research is warranted in this direction considering the beneficial effect of mineral admixture addition on transport properties of concrete.

2.5 MODELING OF CRYSTALLIZATION STRESS

As per the crystallization stress theory for explaining the expansion mechanism due to ettringite formation, supersaturation is the precursor for crystallization stress. Supersaturation sets the upper bound of crystallization stress which can be estimated by using the following equation [Correns, 1949]:

$$P = \frac{RT}{\nu} \ln\left(\frac{c}{c_s}\right) \qquad \text{Eq. 2–2}$$

where R = 8.314 J/K/mol is the universal gas constant, T is the absolute temperature, and ν_m is the molar volume of the crystal. The supersaturation is described in this equation as the ratio between the actual concentration, c, and saturated concentration, c_s. Now the macroscopic tensile stress developed due to crystallization stress can be calculated by introducing a geometric factor, $f(\phi)$, which depends on the shape and size of pores. Flatt and Scherer (2008) have earlier used a model based on assumptions that all pores are either cylindrical or spherical to assess the damage by delayed ettringite formation (DEF). The macroscopic tensile stress is the average hydrostatic tensile stress which can be calculated as shown below for the two pore geometries (cylindrical and spherical) [Timoshenko and Goodier, 1970]:

Case 1. A cylinder (inner radius, a, and outer radius, b) under internal pressure, p_i

The elastic solution of the given problem (in plane stress) can be expressed in terms of the radial stress, σ_{rr}, and the hoop stress, $\sigma_{\theta\theta}$, as shown below:

$$\sigma_{rr} = \frac{a^2 p_i}{b^2 - a^2}\left(1 - \frac{b^2}{r^2}\right)$$

$$\sigma_{\theta\theta} = \frac{a^2 p_i}{b^2 - a^2}\left(1 + \frac{b^2}{r^2}\right)$$

$$\sigma_{zz} = 0$$

Now the average hydrostatic stress can be written as:

$$\sigma = \frac{1}{3}\left(\sigma_{rr} + \sigma_{\theta\theta} + \sigma_{zz}\right) = \frac{2\left(\frac{a^2}{b^2}\right)p_i}{3\left(1-\frac{a^2}{b^2}\right)}$$

or,
$$\sigma = \frac{2\phi}{3(1-\phi)}p_i \qquad \text{Eq. 2–3}$$

where ϕ is the volume fraction of ettringite exerting stress.

Case 2: A sphere (inner radius, *a*, and outer radius, *b*) under internal pressure, p_i

The elastic solution of the given problem can be expressed in terms of the radial stress, σ_{rr}, and the hoop stresses, $\sigma_{\theta\theta}$ and $\sigma_{\phi\phi}$, as below:

$$\sigma_{rr} = \frac{a^3 p_i}{b^3 - a^3}\left(1-\frac{b^3}{r^3}\right)$$

$$\sigma_{\theta\theta} = \sigma_{\phi\phi} = \frac{a^3 p_i}{b^3 - a^3}\left(1+\frac{b^3}{2r^3}\right)$$

Now average hydrostatic stress can be written as:

$$\sigma = \frac{1}{3}\left(\sigma_{rr} + \sigma_{\theta\theta} + \sigma_{\phi\phi}\right) = \frac{3a^3 p_i}{3(b^3 - a^3)} = \frac{\left(\frac{a^3}{b^3}\right)p_i}{\left(1-\frac{a^3}{b^3}\right)}$$

or,
$$\sigma = \frac{\phi}{(1-\phi)}p_i \qquad \text{Eq. 2–4}$$

where ϕ is the volume fraction of ettringite exerting stress.

As shown in the two expressions mentioned above (Eq. 2–3 and 2–4), the magnitude of tensile stress depends on the volume fraction of ettringite exerting stress and maximum stress

derived from supersaturation. In the studies related to delayed ettringite formation, the precipitation of ettringite in smaller pores was found to be the cause of expansion.

The above-mentioned models are simplistic, and are based on the assumption of spherical and cylindrical pores which do not represent the actual pore structure in cement paste microstructure. In order to compare and get a better estimation of crystallization stress, a model based on poromechanics was also developed [Coussy, 2005; Espinosa-Marzal et al., 2011]. Coussy (2004 & 2005) proposed a relationship between the mean stress and strain in a linear isotropic body subjected to pore pressure and thermal excitation as shown below:

$$\sigma = K\varepsilon - b(S_c p_c + S_L p_L) + 3\alpha K\Delta T \qquad \text{Eq. 2–5}$$

where σ and ε are respectively the mean stress and the mean strain; K and α are respectively the bulk modulus and the thermal volumetric dilation coefficient of the porous solid; b is the Biot coefficient; ΔT is the temperature difference; S_c, S_L, p_c and p_L are saturation level of the crystal, saturation level of the liquid, pressure in the crystal and pressure in the liquid, respectively. The Biot coefficient, b, can be expressed as:

$$b = 1 - \frac{K}{k_s} \qquad \text{Eq. 2–6}$$

where K and k_s are the bulk modulus of the porous and the solid matrix (with zero porosity) respectively.

Now assuming no external stress (i.e., $\sigma = 0$) and no temperature difference ($\Delta T = 0$), the relationship given in Eq. 2–5 under saturated condition ($p_L = 0$) becomes:

$$K\varepsilon = bS_c p_c \qquad \text{Eq. 2–7}$$

Coussy (2005) showed that the local crystallization stress, p_c, can be related to the macroscopic stress, σ^*, by

$$\sigma^* \approx bS_c p_c = K\varepsilon \qquad \text{Eq. 2–8}$$

where S_c in the above relationship can be calculated based on volume fraction of ettringite and total porosity of cement paste. This model has been successfully used in recent years to assess the damage of stone due to salt crystallization [Espinosa et al., 2011; Flatt et al., 2014].

2.6 CONCLUSIONS

The detailed literature review presented in this chapter shows that various factors influence the duration and extent of early-age volume change in CSA cement-based binders. It has been pointed out that both physical and chemical factors must be examined in order to better understand the early-age expansion behavior. It is noted that the influence of material stiffness has not received much attention in studies related to expansion of CSA cement-based binders. Therefore, any study on early-age expansion also needs to monitor the evolution of material stiffness as it evolves rapidly at the early age and is going to influence the deformation characteristics. A modeling methodology has been discussed in order to get an estimate of macroscopic tensile stress developed due to crystallization stress.

CHAPTER 3: MATERIALS, MIXTURE PROPORTIONS AND METHODS

This chapter summarizes the materials, mixture proportions and experimental techniques that were used in this study. A Type I Portland cement[1] and a CSA cement[2] were primarily used. In order to understand the influence of mineral admixtures on early-age volume change, Class C FA (Source: Lafarge), Class F FA (Source: Boral) and silica fume (Source: Norchem) were utilized. In addition to paste mixtures, concrete samples were also prepared in order to understand the influence of restraint (internal and external) on expansion which is always present in large-scale field application such as bridge-deck or slab.

3.1 MATERIALS

The oxide composition of various raw materials utilized in this study is summarized in Table 3.1 and the phase composition is shown in Table 3.2. As shown in Table 3.2, CSA cement had 19.4% ye'elimite ($C_4A_3\hat{S}$), 14.7% gypsum ($C\hat{S}H_2$), 9.4% hemihydrate ($C\hat{S}H_{0.5}$), 16.3% anhydrite ($C\hat{S}$), 35.1% belite (C_2S), and 1.9% ferrite (C_4AF). Class F FA and Class C FA had 62.2% and 87.3% amorphous content respectively as shown in Table 2. Moreover, Class C FA contained 7% C_3A and 1.3% $C\hat{S}$ which were not detected in Class F FA. Silica fume (SF) was mainly composed of amorphous phase.

[1] Manufacturer: Essroc Co.

[2] Product: Komponent; Manufacturer: CTS Co.

Table 3.1 Oxide composition of materials

	OPC	CSA Cement	F FA	C FA	SF
SiO_2	19.7	11.98	59.08	37.76	93.0
Al_2O_3	5.3	7.49	22.43	19.43	0.7
Fe_2O_3	2.4	1.22	8.39	5.33	0.5
CaO	62.8	44.64	1.59	25.56	0.7
MgO	2.6	0.96	1.06	4.09	0.7
SO_3	2.8	27.24	0.20	2.23	--
Total Alkalis	0.28	--	0.64	1.07	1.3
Na_2O_{eq}	0.52	0.56	2.07	1.07	1.00
LOI	1.98	2.10	2.99	0.58	6.0

Table 3.2 Phase composition (% wt.) of raw materials as determined by Rietveld analysis

Phase Composition	OPC	CSA Cement	Class F FA	Class C FA
C_3S	62.2	--	--	--
C_2S	14.1	34.8	--	--
C_3A	9.9	--	--	7.0
C_4AF	5.4	2.1	--	--
Ye'elimite	--	19.3	--	--
Gypsum	1.4	15.0	--	--
Bassanite	1.6	9.4	--	--
Anhydrite	0.8	16.1	--	--
Quartz	--	--	15.8	3.2
Mullite	--	--	21.3	--
Hematite	--	--	0.8	0.2
Anhydrite	--	--	--	1.3
Periclase	1.3	--	--	1.0
Amorphous	--	--	62.2	87.3

3.2 MIXTURE PROPORTIONS

Cement paste samples were prepared at water-to-cementitious material ratios (w/cm) of 0.44. In order to study the influence of CSA cement, various dosages (0%, 7%, 15%, and 30% by weight) of CSA cement were used in OPC-CSA blend. All replacements were based on weight percentage of total cementitious binder. In the current study, mineral admixtures such as Class C FA, Class F FA, and SF were also utilized to investigate their influence on expansion characteristics of CSA-based cement. Class C FA, Class F FA and SF were replaced as 15%, 15%, and 5% of total cementitious binder. For calorimetric studies, additional samples with just OPC and mineral admixtures were also prepared. For gypsum study on Class C FA mixture, external gypsum was added as 0.75%, 2.3%, and 10% (all by wt.) of total cementitious material.

3.3 METHODS

3.3.1 Unrestrained Deformation Using Corrugated Tube and Prism Test

Early-age deformation (within 24 hours) of CSA-based cement pastes was measured in sealed condition using corrugated tube test according to ASTM C1698. Two samples were prepared for each batch, and the test was repeated twice to check the consistency of the data. The standard deviation in length measurements between the two batches was within ±10%. The advantage of using corrugated tube is to be able to capture deformation at very early-age. This test method allows monitoring of the linear deformation by providing increased restraint against lateral deformation, and minimizing the restraint on the fresh paste in the longitudinal direction only. Ettringite begins to form immediately after adding water which triggers the expansion. But the expansive forces cannot begin to manifest themselves until a certain degree of rigidity has been achieved through setting of cement [Bentur and Ish-Shalom, 1975; Mather, 1984]. The

measurement of expansion immediately after casting results in an overestimation of effective expansion, as part of it (expansion occurring before hardening) would not contribute toward the stress development [Chaunsali et al., 2013 a]. In expansive cement mortars, volume stabilization or stiffening of the mixture was found to coincide with the time of final setting [Hoff, 1973]. Similarly, in Portland cement paste, the transition from fluid-to-solid was reported to occur at the time of final setting [Sant et al., 2007]. Therefore, in current study, final set time was adopted as the starting time for estimating the expansion. The final set of the cement paste was determined using Vicat needle apparatus in accordance with ASTM C191. It is noted that Vicat test does not show same variation as do rheological measurements [Struble et al., 2001]; therefore the methods such as Proctor test and ultrasonic wave reflection can be used for better accuracy.

Use of the corrugated tube test was crucial for measuring the deformation at the early-age (within 24 hours). However, one disadvantage of the method is that it cannot isolate the effect of autogenous shrinkage from expansion. Therefore, in addition to the corrugated tube test, prismatic bars of size 1 inch (25 mm) × 1 inch (25 mm) × 11.25 inch (285 mm) were prepared to measure the expansion during saturated lime water curing that prevents the autogenous shrinkage. The samples were demolded after 24 hours, and kept in saturated lime water at 22°C± 2°C. The length changes were monitored at various ages according to ASTM C490. Three samples were prepared for each batch at two different times. The standard deviation in the length measurements was found to be within ±5%. The initial expansion measured through corrugated tube was added to the length measurements of prismatic samples to estimate the total expansion from the final set time (Figure 3.1).

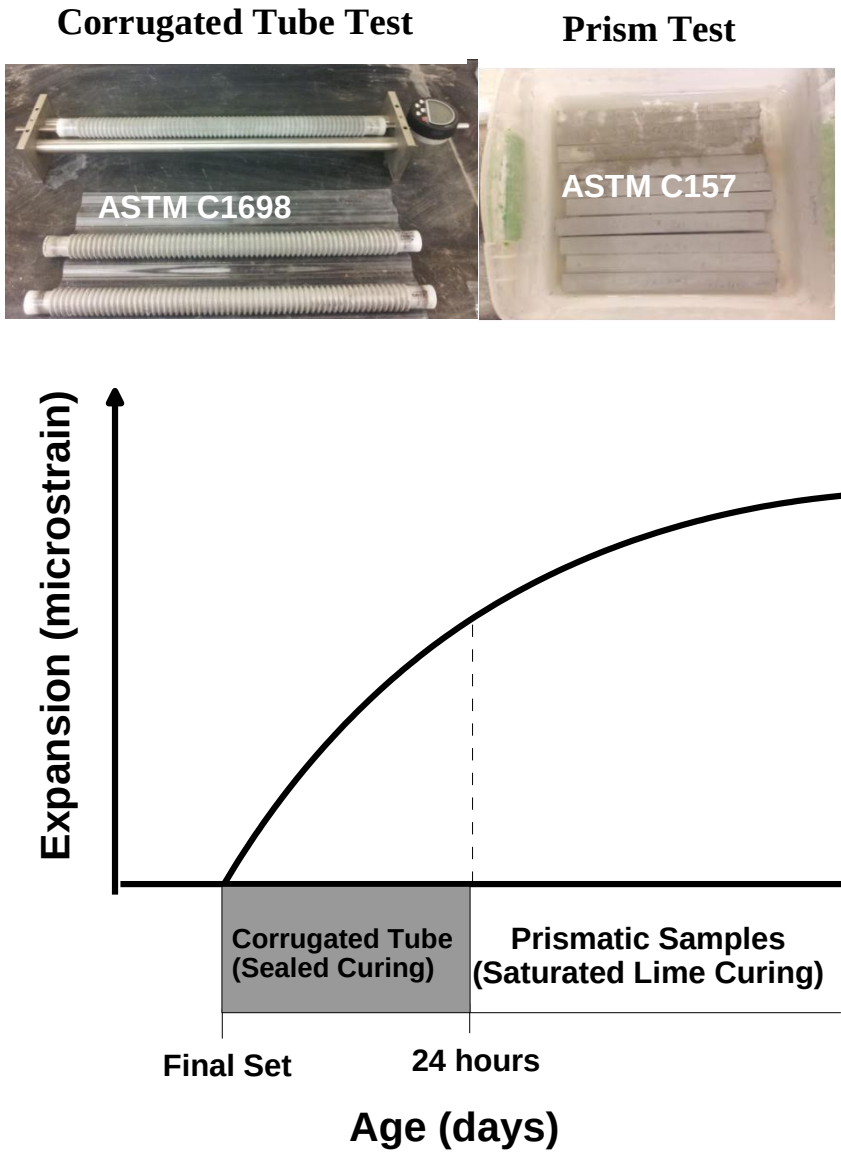


Figure 3.1 A schematic showing the method of measuring expansion from final set using two different test methods (ASTM C1698 and ASTM C157)

3.3.2 Method to Stop Cement Hydration

In this study, it was necessary to track the consumption of ye'elimite and growth of ettringite due to hydration for explaining expansion characteristics. Therefore, hydration of cement was stopped to characterize samples at various ages. A detailed review of various techniques commonly used for stopping hydration can be found in Zhang and Scherer (2011). In this study, solvent exchange method utilizing isopropyl alcohol was used due to its minimum effect on the microstructure. However, it should be noted here that there is a possibility that the method of stopping hydration can cause some dehydration of phases such as ettringite and C-S-H [Zhang and Scherer, 2011]. It is believed that the results should be comparable if the same method is followed for all samples. In the beginning, two different protocols were adopted for solvent exchange. According to first protocol, samples were initially ground in isopropyl alcohol. Subsequently, vacuum filtration was used to remove the alcohol, and this process was repeated 3 times for powdered sample. The collected powdered sample was then kept in vacuum desiccator for at least 24 hours. Second protocol consisted of immersing a 2-3 mm thick sample of 25 mm diameter in isopropyl alcohol for 24 hours before drying it in a vacuum desiccator for at least 24 hours. Both protocols showed similar results as their derivative thermogravimetric plots matched really well. Therefore, the second protocol was adopted for subsequent tests as it was less time consuming.

3.3.3 X-ray Diffraction (XRD)

X-ray diffraction is a powerful technique to identify and quantify crystalline phases present in a material. The application of XRD to cement-based materials has provided valuable information on the progress of hydration. Powdered samples (fineness less than 45 μm) were used for XRD analysis. Initially, qualitative analysis was performed using MDI Jade (2009) in

order to identify crystalline phases. Once all phases were identified, HighScore Plus (Version 3.0 from PANalytical) software was used for quantitative phase analysis using Rietveld method [Rietveld, 1969] which relies on minimization of the difference between the measured and the calculated intensities using non-linear least square fitting algorithm. The powder diffraction file (PDF) of each phase used in Rietveld analysis is shown in Table 3.3. The refined parameters included phase scale factors, background coefficients, zero-shift error, lattice parameters, peak shape parameters, and preferred orientation, if needed. The refinement was carried out until a reasonable match (goodness of fit less than 2) was achieved. Reagent grade TiO_2 (source: Sigma Aldrich) was added to the powdered samples as an internal standard to determine the amorphous content of hydrated cement paste [De La Torre et al., 2001]. The amorphous content was estimated by using following relation (refer to Appendix D for the details):

$$W_{Am} = \frac{1 - \frac{W_{IS}}{W_{RIT}}}{100 - W_{IS}} \times 10^4\% \qquad \text{Eq. 3–1}$$

where W_{Am} is the amorphous content, W_{IS} is the weight percentage of the internal standard and W_{RIT} is the concentration of the internal standard based on Rietveld analysis. In this study, 15% (by weight) of internal standard was used which means $W_{IS} = 15$. Figure 3.2 and Figure 3.3 show the results of Rietveld refinement of the Portland cement and the CSA cement.

Table 3.3 Phases and ICDD PDF codes used for Rietveld analysis

Phase	ICDD Code	Phase	ICDD Code
C_3S	04-014-9801	Periclase	00-004-0829
C_2S	04-013-6291	Gypsum	04-015-4421
C_3A	04-008-8069	Anhydrite	00-037-1496
C_4AF	04-007-5261	Bassanite	00-041-0224
Ettringite	04-011-5267	Ye'elimite	04-009-7268
Portlandite	00-044-1481	Monosulfate	00-045-0221
Calcite	04-007-2808	Monocarbonate	00-041-0219
Rutile	04-015-7316	Hemicarbonate	00-041-0221
Anatase	04-016-2837		

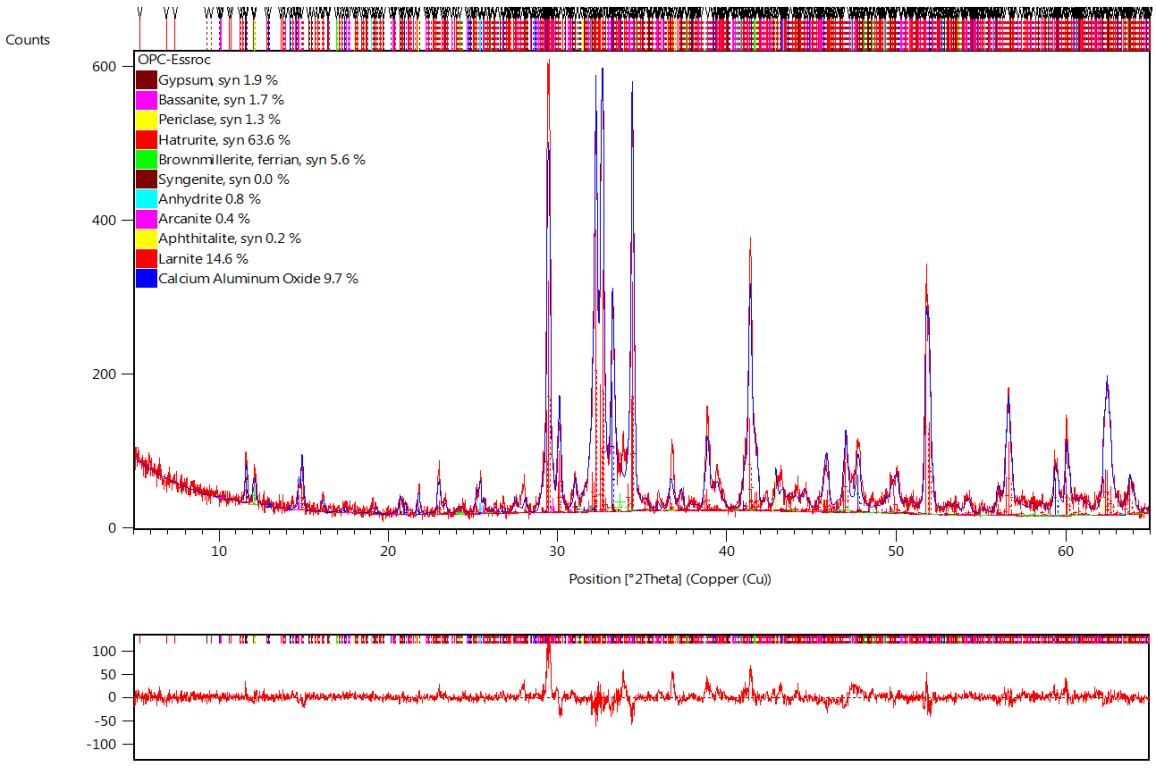


Figure 3.2 Rietveld refinement of the Portland cement used in the current study

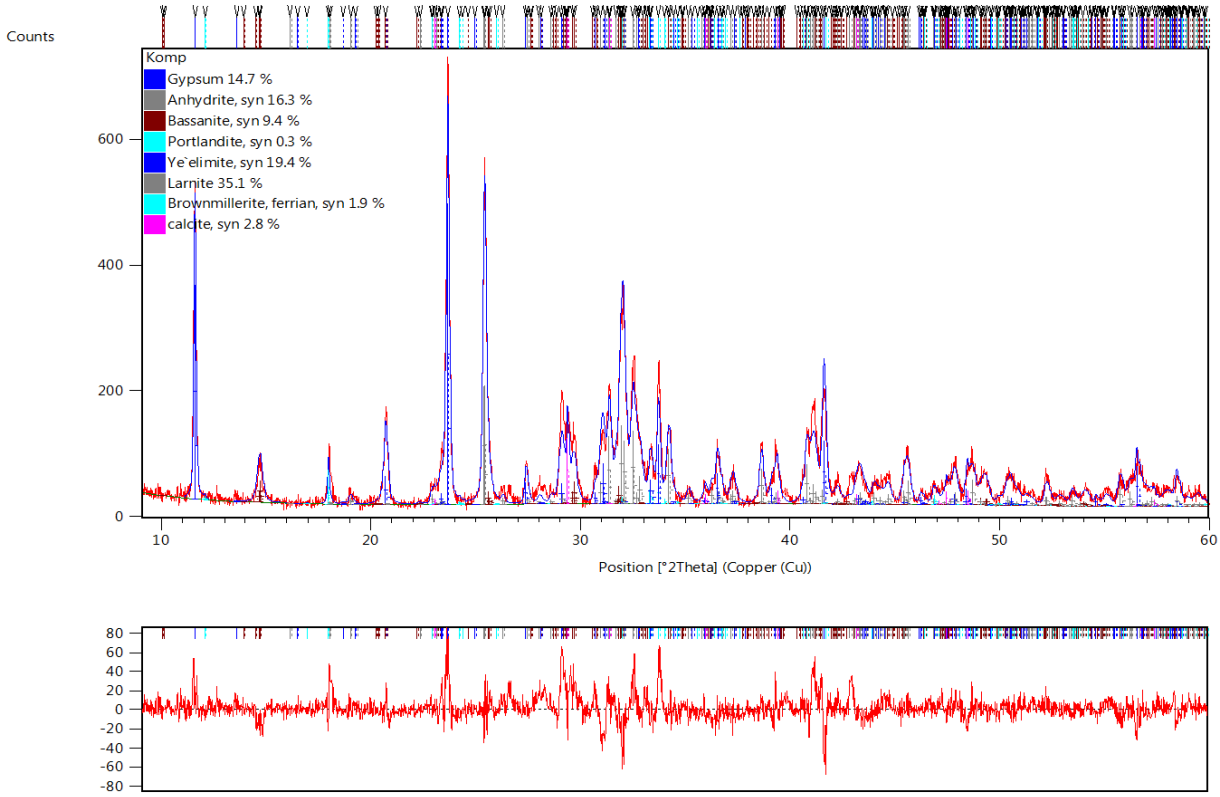


Figure 3.3 Rietveld refinement of the CSA cement used in the current study

3.3.4 Thermogravimetric (TG) Analysis

Thermogravimetric analysis was performed on 25 ± 2 mg of powdered samples passing through 45 µm (325 no.) sieve using a Q50-TA Instrument. The samples were heated in a nitrogen environment (flow: 60 ml/min) up to 900°C at a rate of 15°C per minute.

3.3.5 Scanning Electron Microscopy

Scanning Electron Microscopy (SEM) imaging was performed using a JEOL JSM-6060LV Low Vacuum Scanning Electron Microscope, operating in secondary electron mode. The electron gun was equipped with tungsten filament for generating electron beam. The accelerating voltage and working distance were 15 keV and 10 mm, respectively.

3.3.6 Isothermal Conduction Calorimetry

Isothermal conduction calorimeter was used to monitor the heat evolution in CSA-based cement. TAM air (by TA Instruments) with eight sample ampoules was utilized to determine heat evolution. Small samples for isothermal calorimetry were prepared separately following the mixture proportions mentioned before. The paste samples were mixed manually in glass ampoules for a period of 2 minutes before inserting them in the respective channels. It is noted that the data for the first 45 minutes was not considered for analysis in order to avoid the heat associated with mixing and placing the externally prepared samples and to allow the samples to stabilize at the set temperature of 22°C. The samples were monitored continuously for 72 hours.

3.3.7 Pore Solution Analysis and Thermodynamic Modeling

Pore solution analysis of CSA cements was performed to determine the aqueous phase composition, and therefore, the saturation level of ettringite in presence of the CSA cement. Cement paste samples of size 2 inch (50 mm) in diameter × 3 inch (75 mm) in height were used for pore solution extraction. Samples were prepared using de-ionized (DI) water at w/cm ratio of 0.44. The samples underwent similar curing regime (24 hours of sealed curing followed by saturated lime water curing) as the one used for prismatic samples. The pore solution was extracted after 1 day, 3 days, 7 days and 21 days. The device proposed by Barneyback and Diamond [1981] was used for the extraction. The device used in this study had the upper body made of a single cylinder unlike two cylinders which were used in the device proposed by Barneyback and Diamond (1981). It is noted here that the applied stress has been found to influence the concentration of ions in the pore solution [Chappex and Scrivener, 2012]. However, the concentration has been found to be comparable when a compressive load up to approximately 500 MPa was used [Lothenbach, 2010]. In this study, the applied maximum

pressure ranged from 300 MPa to 400 MPa that was required to extract 5-10 ml of pore solution depending on the age of the sample. Immediately after extraction, the pore solution was filtered using 0.2 μm filter for chemical analysis. One part of the extracted pore solution was treated with 6.3% HNO_3 to prevent carbonation, and was later used for the determination of Ca, Al, Si, S, Na, and K ion concentration using Inductively Coupled Plasma Optical Emission Spectrometry (ICP-OES). The ICP-OES analysis was performed at Microanalysis Laboratory of the University of Illinois. The rest of the pore solution was used for pH measurement. The pH meter was calibrated against known KOH solutions for determining hydroxyl ion concentration.

Using aqueous phase composition of cement pore solution, the hydration process can be monitored by estimating the saturation indices of the solids in contact with the aqueous phase. Saturation index (*SI*) can be expressed as [Rothstein et al., 2002; Damidot et al., 2011]:

$$SI = \ln\left(\frac{K}{K_{sp}}\right) \qquad \text{Eq. 3–2}$$

where K is the ion activity product and K_{sp} is the solubility product of a given phase. If $SI = 0$, the solution is at equilibrium whereas for $SI > 0$ and $SI < 0$, the solution is supersaturated and undersaturated with respect to the given crystal, respectively. The dissolution reaction of ettringite can be expressed in the following form [Rothstein et al., 2002; Lothenbach et al., 2008; Lothenbach, 2010; Damidot et al., 2011]:

$$Ca_6Al_2(SO_4)_3(OH)_{12}.26H_2O \leftrightarrow 6Ca^{2+} + 2Al(OH)_4^- + 3SO_4^{2-} + 4OH^- + 26H_2O \qquad \text{Eq. 3–3}$$

Now considering the ionic species forming ettringite, the ion activity product of ettringite can be written as:

$$K(ettringite) = \{Ca^{2+}\}^6 \{Al(OH)_4^-\}^2 \{OH^-\}^4 \{SO_4^{2-}\}^3 \{H_2O\}^{26} \qquad \text{Eq. 3–4}$$

where $\{Ca^{2+}\}$, $\{Al(OH)_4^-\}$, $\{OH^-\}$, $\{SO_4^{2-}\}$ and $\{H_2O\}$ are the activities of respective ions. The solubility product (K_{sp}) of ettringite at 25°C is $10^{-44.90}$ [Perkins et al., 1999; Warren and Reardon, 1994]. The activity of an ion is the product of ion concentration (m_i), and activity coefficient (γ_i). The activity coefficient which depends on ionic strength of the solution (I), other ionic species and temperature can be calculated using extended Debye-Hückel equation as [Nordstorm and Munoz, 1988]:

$$\log \gamma_i = \frac{-Az_i^2\sqrt{I}}{1+Ba_i\sqrt{I}} + b_i I \qquad \text{Eq. 3–5}$$

where A and B are Debye- Hückel solvent parameters dependent only on temperature, a_i is the Debye-Hückel ion-size parameter, b_i is a semi-empirical parameter (~ 0.064 at 25°C), z_i is the charge of ion, and I is the ionic strength of the solution. Using ion activity product and solubility product of a phase, its saturation level in the pore solution can be determined using Eq. (3). When the aqueous phase is supersaturated with the ions (i.e., SI >0), there is tendency for precipitation of the solid in larger amount until the equilibrium is reached. Similarly, in undersaturated case (SI < 0), the solid tends to dissolve in order to achieve equilibrium. In this study, the thermodynamic calculations to estimate saturation indices were performed by using a geochemical modeling package: GEMS-PSI [Wagner et al., 2012; Kulik et al., 2013] which was supplemented with cement specific thermodynamic database [Matschei et al., 2007].

3.3.8 Capillary Porosity

Quantitative X-ray diffraction as described in the previous section provides information on the weight fraction of various phases. In order to convert the weight fraction to volume fraction, knowledge of the total pore volume and density of each phase is essential. As a first step towards determination of total pore volume, capillary porosity of cement paste was determined by solvent exchange method [Day and Marsh, 1988]. The slices of size 25 mm

(diameter) × 1-2 mm (thickness) were cut and immersed in isopropyl alcohol for 24 hours. Afterwards, the sample volume was determined by buoyancy method using isopropyl alcohol as the liquid medium. Subsequently, samples were dried in a vacuum desiccator. The weight difference due to drying was attributed to the removal of capillary water. Finally, capillary porosity was calculated by dividing capillary pore volume by the sample volume.

3.3.9 Compressive Strength

Cement paste for determining the compressive strength was prepared according to ASTM C305, and cubes of size 2 inch (50 mm) × 2 inch (50 mm) × 2 inch (50 mm) were cast. Triplicate of samples were prepared for each batch. The samples were demolded after 24 hours before curing in saturated lime water. The compressive strength was determined according to ASTM C109.

3.3.10 Tensile Strength

Tensile strength of cylindrical paste samples (diameter: 50 mm; height: 100 mm) was determined according to ASTM C496. The loading rate was maintained within a range between 11 to 15 Kg/sec. Three samples were tested for each batch.

3.3.11 Dynamic Modulus

The stiffness of cement paste samples of size 40 mm × 40 mm × 150 mm was monitored by performing the dynamic modulus test according to ASTM C215. The longitudinal resonant frequency was measured to calculate the dynamic elastic modulus (E) of paste samples according to following relationship:

$$E = DMn^2 \qquad \text{Eq. 3–6}$$

where $D = 4\,L\,/(b \times t)$ for a prismatic sample of size b (in meters) × t (in meters) × L (in meters), M is the mass of the sample (in Kg), and n is the fundamental longitudinal frequency (in Hz). Two samples were prepared for each batch.

CHAPTER 4: EARLY-AGE VOLUME CHANGE OF CSA CEMENT-BASED BINDERS

4.1 INTRODUCTION

This chapter summarizes the observations on early-age expansion of CSA cement-based binders. Unrestrained expansion of CSA cement-based binders was monitored by combining measurements from corrugated tube test in sealed condition for initial 24 hours and from mortar prisms cured in saturated lime water beyond 24 hours (refers to Section 3.3.1 for details). Furthermore, changes in the physical properties such as capillary porosity and dynamic modulus with time were also monitored. The CSA cement-based binders include OPC-CSA and OPC-CSA-MA system (refer to Sec 3.2 for mixture proportions).

4.2 EARLY-AGE VOLUME CHANGE, POROSITY AND DYNAMIC MODULUS

4.2.1 OPC-CSA Binder

Expansion characteristics of OPC-CSA blends are shown in Figure 4.1. It is evident that the expansion of OPC sample was insignificant compared to OPC-CSA blends. Some expansion of OPC paste sample can be attributed to osmotic swelling of calcium silicate hydrate (C-S-H) gel [Brunauer et al., 1958]. With increase in the amount of CSA cement, there was noticeable increase in the expansion. Most of the expansion of OPC-CSA blends was complete in the first 7 days. The expansion of OPC-CSA blend with 15% CSA cement was higher by an order of magnitude than OPC. Similarly, OPC-CSA blend with 30% CSA cement exhibited 4-5% expansion which eventually led to cracking of the samples. Figure 4.2 shows the cracking in the prismatic samples with 30% dosage of CSA cement. As seen at macro-scale, the SEM micrographs (Figure 4.3) also depict the extent of cracking in the sample with 30% CSA cement. The expansion process for mixtures with CSA cement was complete within 7 days.

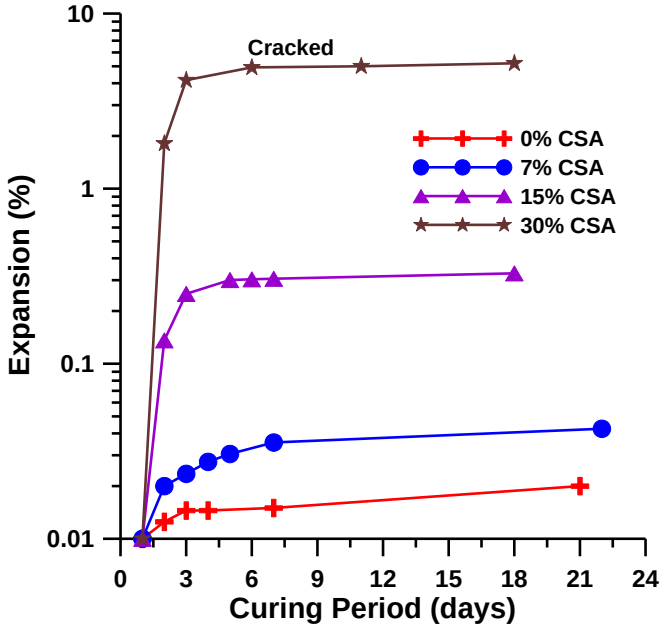


Figure 4.1 Expansion characteristics of OPC and OPC-CSA blends at w/cm – 0.44 (measurement started from 24 hours)



Figure 4.2 Macro-scale cracking of OPC-CSA blend with 30% CSA cement

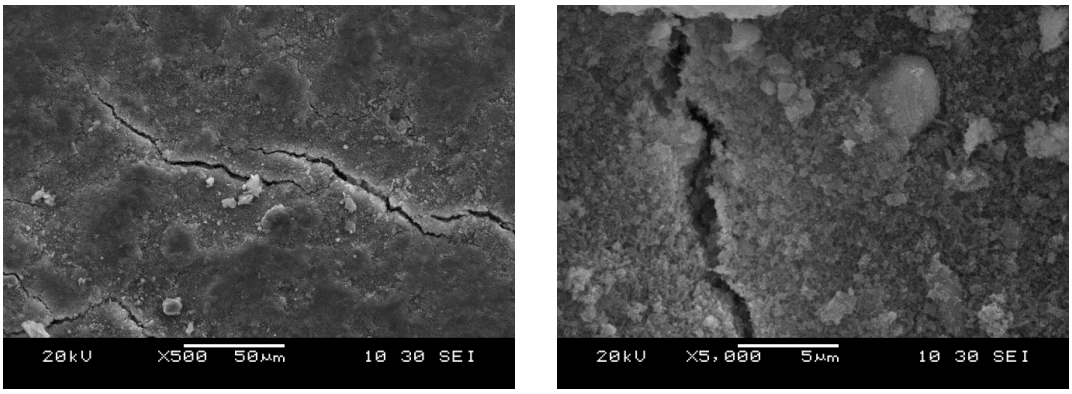


Figure 4.3 SEM micrograph of OPC-CSA sample with 30% CSA cement (Age: 7 days)

The physical properties such as the porosity and dynamic modulus of OPC-CSA blend are expected to influence the expansion characteristics. As expected, porosity of all samples reduced with time due to continued hydration. Porosity of pastes with 0% and 7% CSA cement was similar at all ages, and the paste with 15% CSA cement had little higher porosity at 1 day and little lower at 7 days. Figure 4.4 shows that the higher dosage of CSA cement (i.e., 30%) resulted in an increase in capillary porosity from 1 day to 3 days due to expansion-induced cracking (see Figure 4.2) when all other samples exhibited a reduction in porosity. However, at later age, even 30% CSA cement samples showed lower porosity due to filling of cracks.

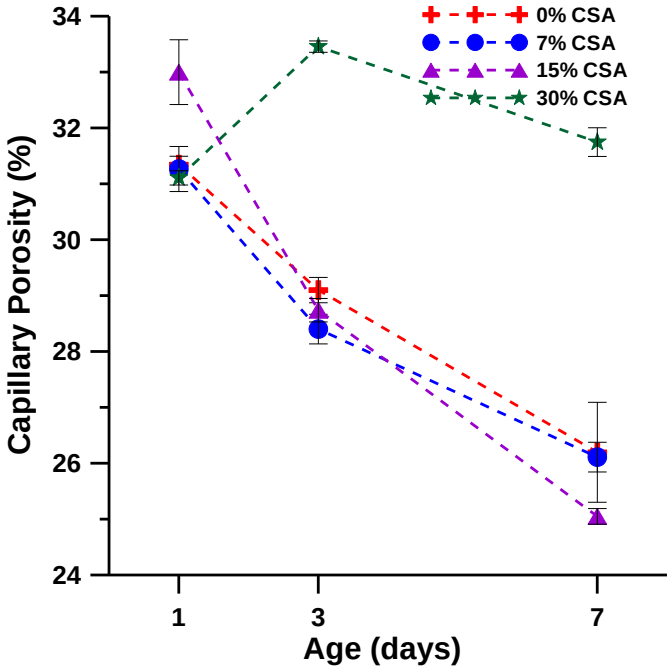


Figure 4.4 Effect of CSA dosage on capillary porosity of OPC-CSA blend

Material stiffness can have considerable influence on the extent of expansion. A material with higher stiffness will show lower expansion due to the same expansion potential. Therefore, evolution of dynamic modulus with time was monitored by measuring resonance frequency in longitudinal direction. Figure 4.5 shows the evolution of dynamic modulus of OPC and OPC-

CSA paste samples. The dynamic modulus of OPC and OPC-CSA blend with 7% CSA cement was similar whereas OPC-CSA blends with 15% and 30% CSA cement exhibited lower modulus at 1 day. Beyond 1 day, there was no significant difference among OPC-CSA blends with 0%, 7% and 15% CSA cement. However, the blend with 30% CSA cement showed lowest modulus at all ages. The drop in modulus was also supported by visual cracking in the samples with 30% CSA cement (Figure 4.2). The dynamic modulus of the blend with 30% CSA decreased from 1 day to 3 days followed by an increase from 3 days onward. Now considering the insignificant difference in modulus values among OPC-CSA blends with 0%, 7% and 15% CSA cement, the expansion characteristics of these samples seemed to have mainly governed by quantity of ettringite and supersaturation w.r.t. ettringite. For OPC-CSA blend with 30% CSA cement, lower modulus appears to have contributed towards the large expansion as shown in Figure 4.1. However, it is possible that the lower modulus is not entirely the cause of the higher expansion but a result of the higher expansion and cracking.

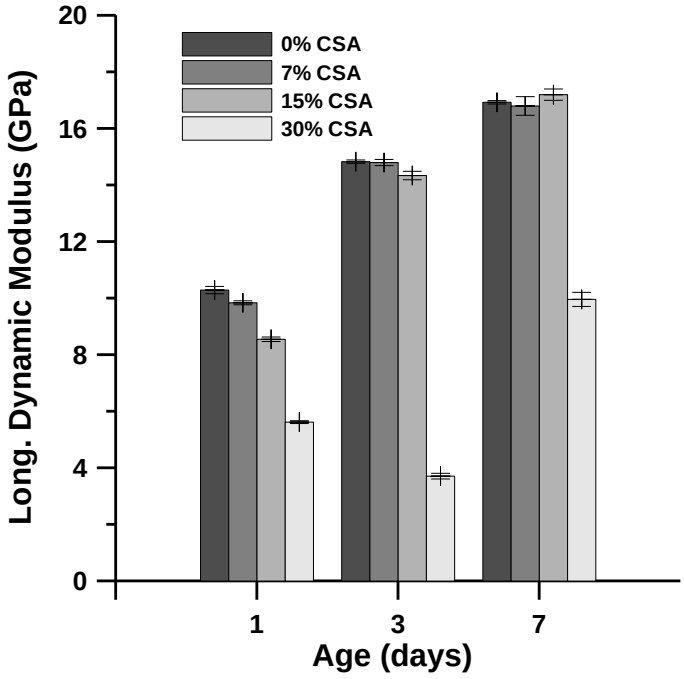


Figure 4.5 Effect of CSA dosage (by weight) on dynamic modulus of OPC-CSA blend

4.2.2 OPC-CSA-MA Binder

Figure 4.6 shows the expansion characteristics of OPC-CSA-MA binder which is compared with OPC-CSA blend. CSA cement content was constant (i.e. 15% by wt. of total cementitious binder) in all mixtures. The Class F FA resulted in highest expansion whereas Class C FA reduced the expansion of OPC-CSA cement paste. Unlike other cement pastes, the OPC-CSA-CFA paste ceased expanding beyond 2 days.

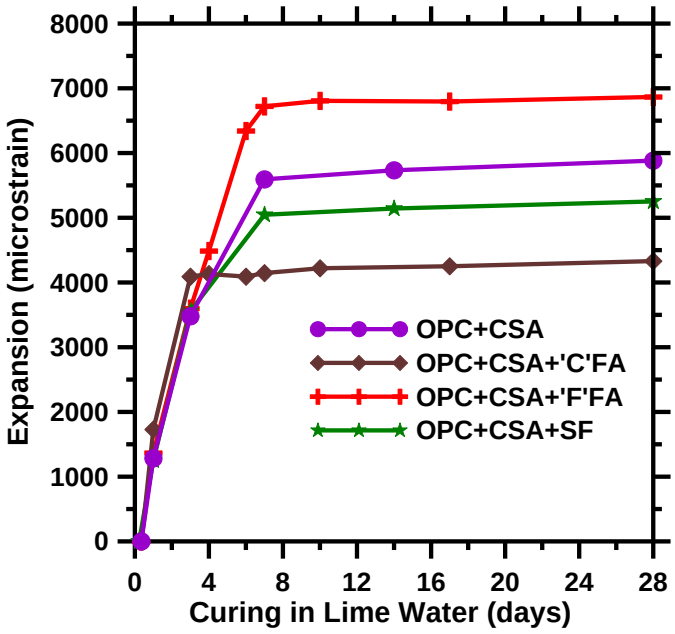


Figure 4.6 Unrestrained deformation of CSA-based cement pastes in saturated lime water curing at w/cm – 0.44 (measurement started from final set time)

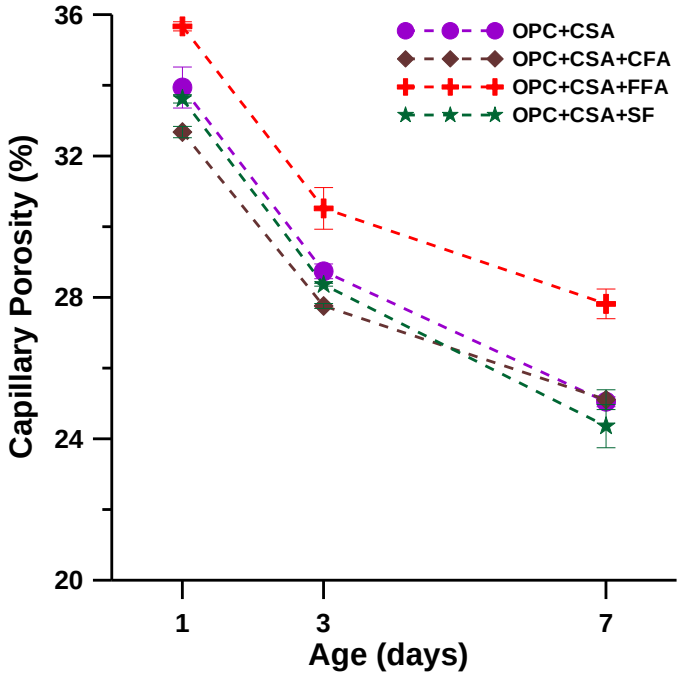


Figure 4.7 Evolution of capillary porosity in OPC-CSA-MA binder

Figure 4.7 shows the evolution of capillary porosity with time in OPC-CSA-MA samples. As none of OPC-CSA-MA samples exhibited cracking, a decrease in porosity was observed in all samples with time. The Class F FA mixture exhibited the highest porosity at all ages whereas SF mixture had the lowest porosity after 7 days. Generally, expansion process can be thought to increase the porosity of the system, but that was not the case here as the continuous hydration of OPC resulted in filling of additional pores created during the expansion process.

Figure 4.8 shows the longitudinal dynamic elastic modulus of OPC-CSA-MA cement pastes. No drop in dynamic modulus of OPC-CSA-MA cement pastes was observed during the time frame of testing which suggests the structural integrity of samples, and was also supported by visual inspection. Class F FA consistently showed the lowest modulus, which means it offered the least resistance against crystallization stress among all mixtures and expanded the most. Silica fume showed the highest modulus at the end of 7 days, indicating the maximum

resistance against expansion. Hence, the modulus test suggests that the expansion would be lower for SF mixture and higher for fly ash mixtures when the crystallization stress is similar among mixtures. At 3 days, the difference between the modulus values of different mixtures was within 1% except the Class F FA which showed 10% lower modulus compared to the OPC-CSA mixture. It should be noted here that the expansion characteristics between mixtures were similar within the first 3 days and began to deviate between 3 days and 7 days. This behavior could be because the paste samples remain relatively less stiff (having low elastic modulus) and have high porosity at early-age (up to 3 days). Effects of different factors in governing the expansion of various mixes are carefully considered and presented in Chapter 6.

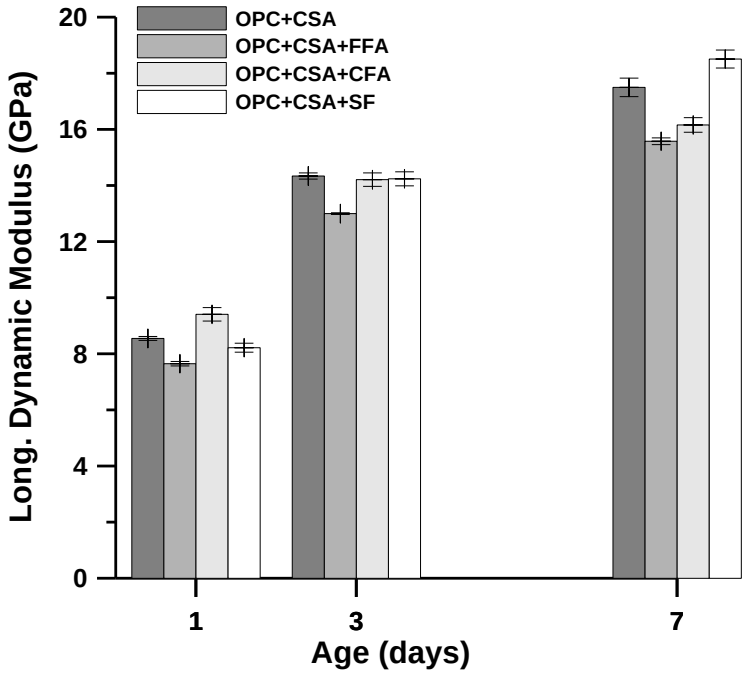


Figure 4.8 Evolution of dynamic modulus in OPC-CSA-MA mixtures

Effect of Gypsum Addition

Among the mineral admixtures used in this study, Class C FA behaved differently in a way that the expansion ceased after the first 2 days unlike other samples which expanded until 5-7 days. The difference in the behavior was hypothesized to be due to the early depletion of

gypsum in the Class C FA mixture (more detail in Chapter 5). Therefore, two additional sets of samples with varying amounts of gypsum were prepared to further investigate the behavior of Class C FA mixture. One set of samples had 2.3% additional gypsum (by weight) of total cementitious material which was equivalent to 15% additional gypsum (by weight) of CSA cement. And the other set of sample contained 10.5% (by weight) gypsum of total cementitious material which was equivalent to 70% gypsum (by weight) of CSA cement. As presented in Figure 4.9, both samples with additional gypsum showed an increase in the expansion. The expansion of the sample with 2.3% gypsum was approximately four-fold higher than that of the sample without any additional gypsum. The sample with 10.5% additional gypsum showed a major increase in the expansion and ultimately cracked whereas the samples with 2.3% gypsum were still intact. It is also noted that the gypsum addition prolonged the duration of the expansion compared to the Class C FA mixture without any additional gypsum.

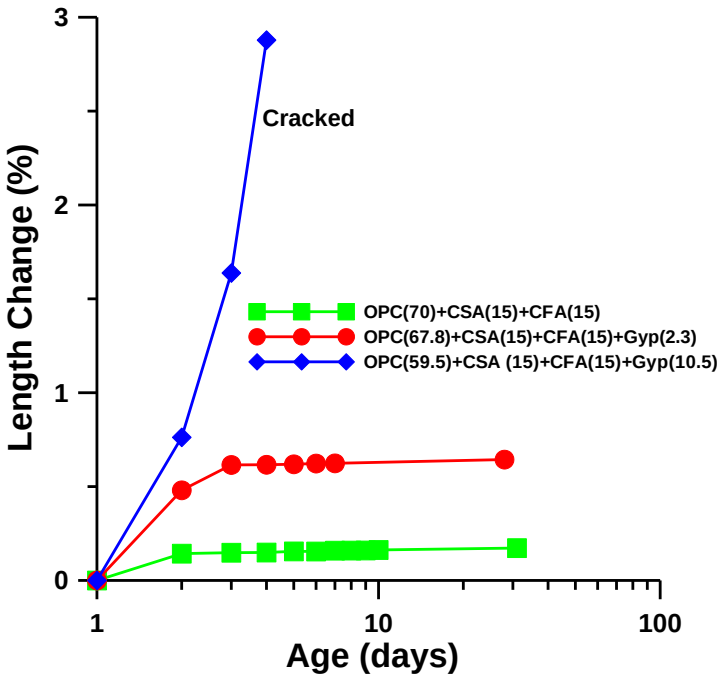


Figure 4.9 Effect of additional gypsum on early-age volume change of OPC-CSA-CFA mixture

Figure 4.10 shows the effect of gypsum addition on the evolution of capillary porosity with time. The capillary porosity was found to be only few percent higher after 1 day in the sample with additional gypsum whereas any effect of gypsum addition on porosity was not observed at later ages. The dynamic modulus of samples with gypsum was lower than those without gypsum, particularly at early age. The decrease in modulus can partly be attributed to the dilution of OPC with gypsum. This decrease in dynamic modulus in the sample with additional gypsum can partially cause an increase in the expansion; however, any changes in the chemical properties that can also influence the expansion will be presented in Chapter 5. It should be noted that the porosity and dynamic modulus measurements on samples with only 2.3% additional gypsum are presented here as the samples with the higher gypsum addition cracked severely.

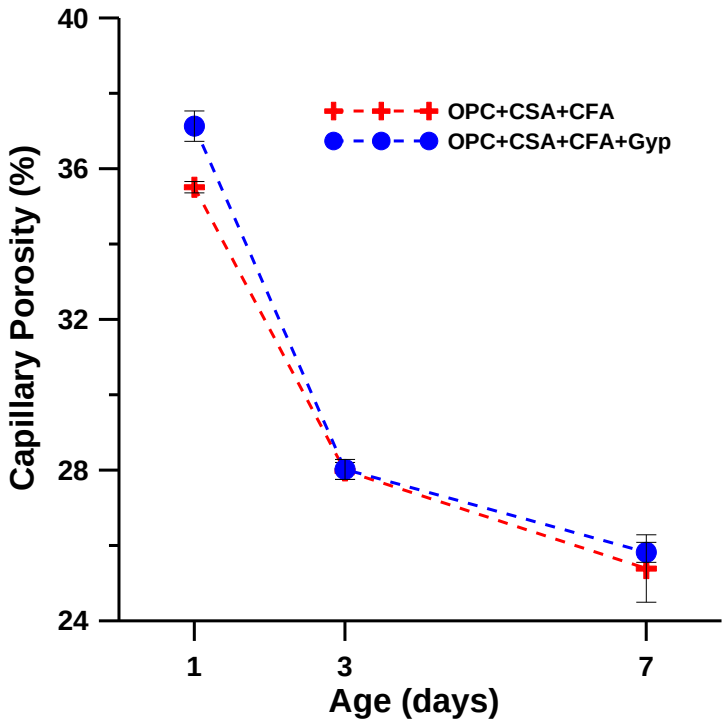


Figure 4.10 Capillary porosity of OPC-CSA-CFA sample with and without gypsum

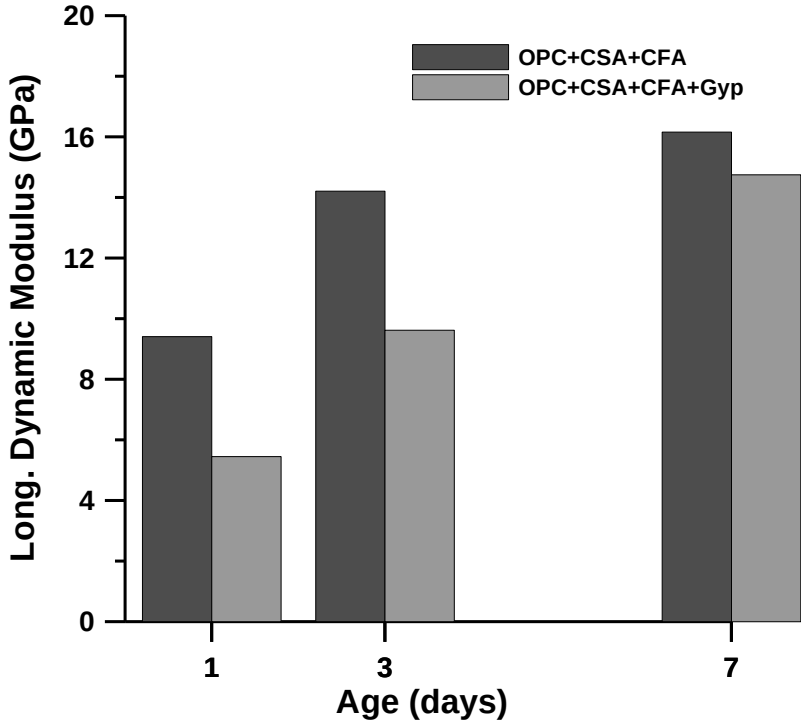


Figure 4.11 Dynamic modulus of OPC-CSA-CFA sample with and without gypsum

4.3 CONCLUSIONS

The main conclusions from this chapter can be summarized as below:

- The unrestrained expansion of OPC-CSA blend increased with an increase in CSA cement content. Elastic modulus of OPC-CSA blend at 1 day was reduced with an increase in the CSA dosage. This reduction could be due to the dilution of Portland cement in the OPC-CSA blend. The reduction in the elastic modulus with the addition of CSA cement indicates that the lower material stiffness could potentially have led to an increase in the expansion. In the 30% CSA mixture, an excessive expansion and cracking resulted in a further reduction in the elastic modulus.
- Mineral admixtures were found to alter the expansion characteristics of the CSA-OPC-MA blends. Class F FA increased the expansion whereas Class C FA and SF reduced it. Unlike other mineral admixtures, the Class C FA ceased expanding

beyond 2 days. The addition of gypsum increased the extent and duration of the expansion in the OPC-CSA-CFA mixture. Elastic moduli of the samples with additional gypsum were lower than that of without gypsum, highlighting the possible contribution of the reduced stiffness in increasing the expansion.

CHAPTER 5: EARLY-AGE HYDRATION OF CSA CEMENT-BASED BINDERS

5.1 INTRODUCTION

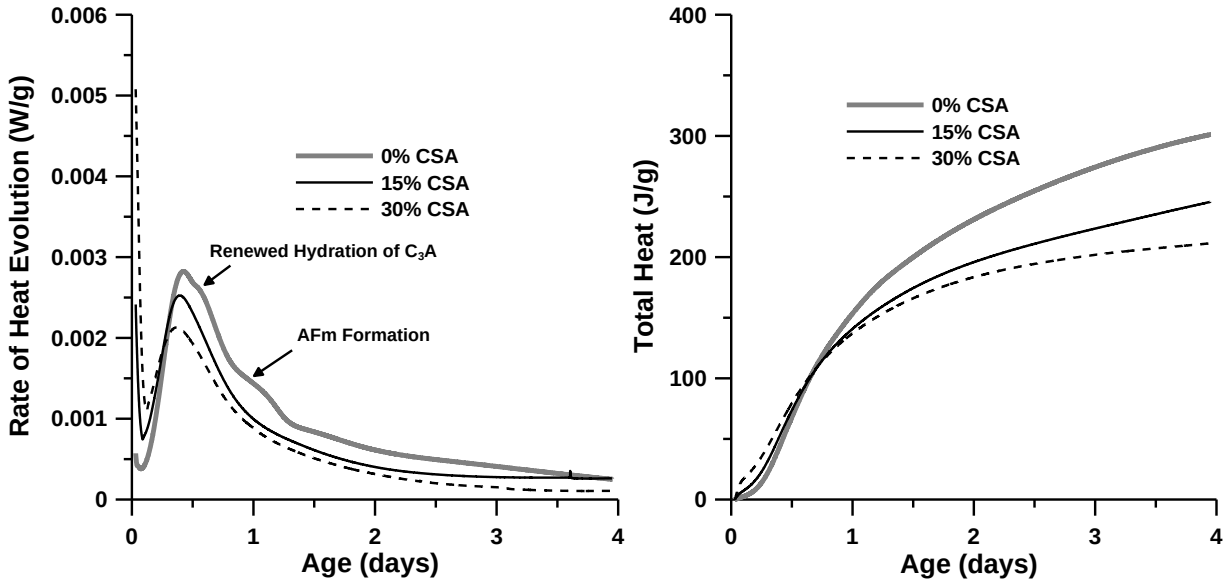
This chapter summarizes the hydration behavior of CSA cement-based binders. Isothermal calorimetric studies were performed to study the hydration kinetics of CSA cement-based binders. Both qualitative and quantitative X-ray diffraction analyses were carried out to monitor the hydration progress. Thermogravimetric studies were performed to validate the quantitative X-ray diffraction results and examine the presence of amorphous AH_3 which cannot be identified though X-ray diffraction. The pore solution analysis was carried out to estimate the saturation levels of ettringite in CSA cement-based binders.

5.2 HEAT OF HYDRATION

5.2.1 OPC-CSA Binder

Figure 5.1 shows the rate of heat evolution and total heat for OPC-CSA blends with various dosages of CSA cement. It is evident that the addition of CSA cement reduced the height of the main peak corresponding to C_3S hydration. The reduction in C_3S peak intensity as observed in this study also agrees with Nocun-Wczelik et al. (2012) who attributed the reduction to dilution effect. During the hydration of OPC cement, a small shoulder after the main C_3S peak and a peak around 24 hours correspond to the renewed hydration of C_3A and the conversion of AFt to AFm, respectively [Bullard et al., 2010]. On the contrary, the AFt to AFm conversion peak was not observed in samples with CSA cement due to the presence of surplus gypsum. G. Le Saoût et al. (2013) also reported the retardation of C_3A hydration when CSA cement was added to OPC. The total heat of OPC-CSA binder was found to be lower than that of the OPC, at

least when the data collected during the initial 45 minutes is not considered due to the effect of external mixing.

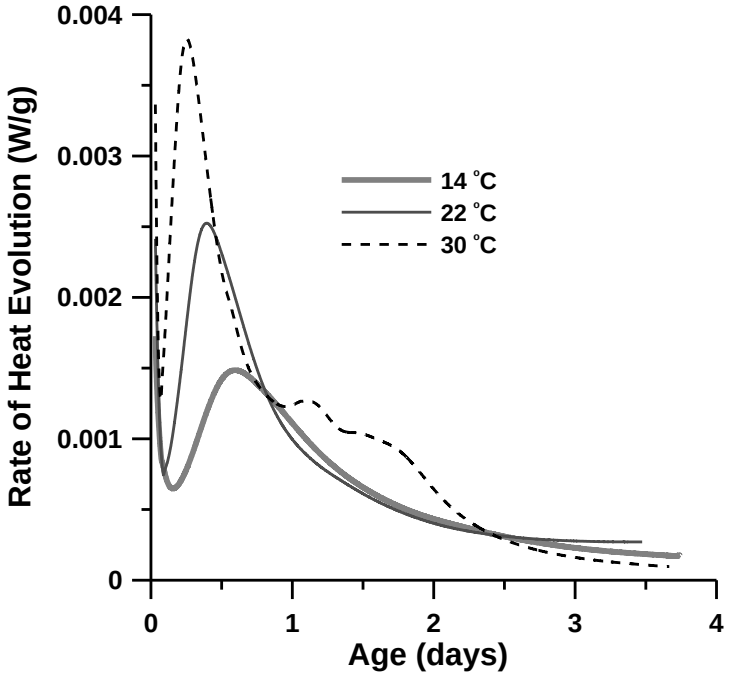


(a) (b)

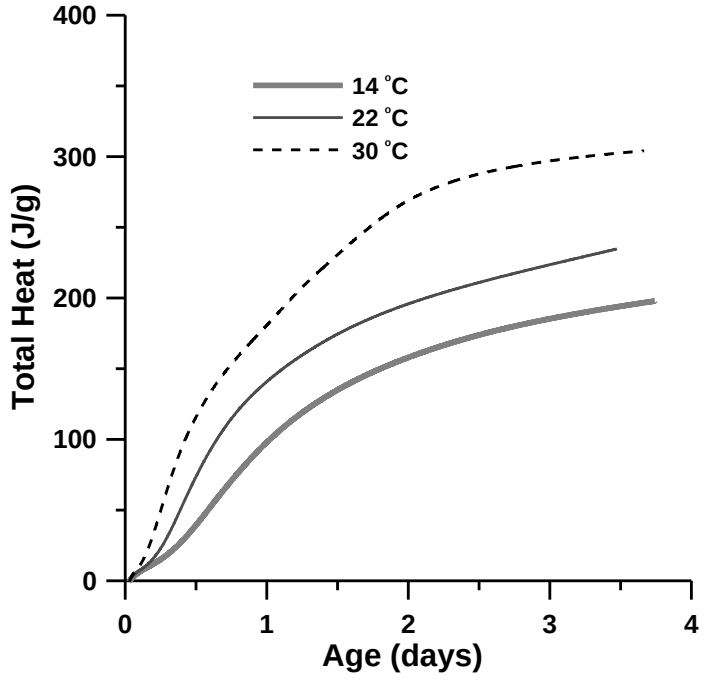
Figure 5.1 Effect of CSA dosage on: a) the rate of heat evolution, and b) total heat release of OPC-CSA cement system

Effect of Temperature

Temperature has been shown to have significant effect on hydration of Portland cement. In this study, binder with 15% CSA cement was utilized to examine the effect of temperature on the hydration of OPC-CSA blend. Figure 5.2 shows the effect of three curing temperatures. As expected, higher curing temperature increased the rate of heat evolution and the total heat of hydration of OPC-CSA binders, which agrees with the results of Chen and Juenger (2011).



(a)

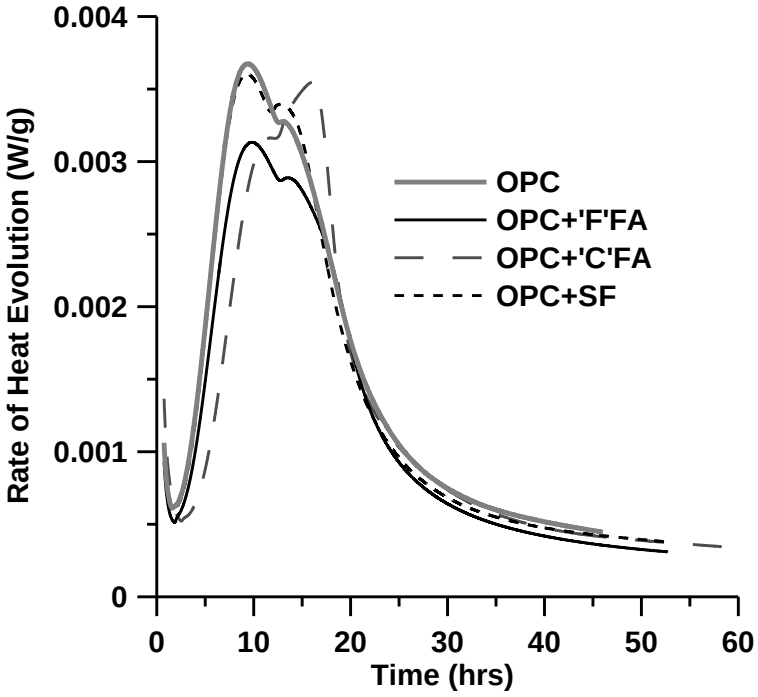


(b)

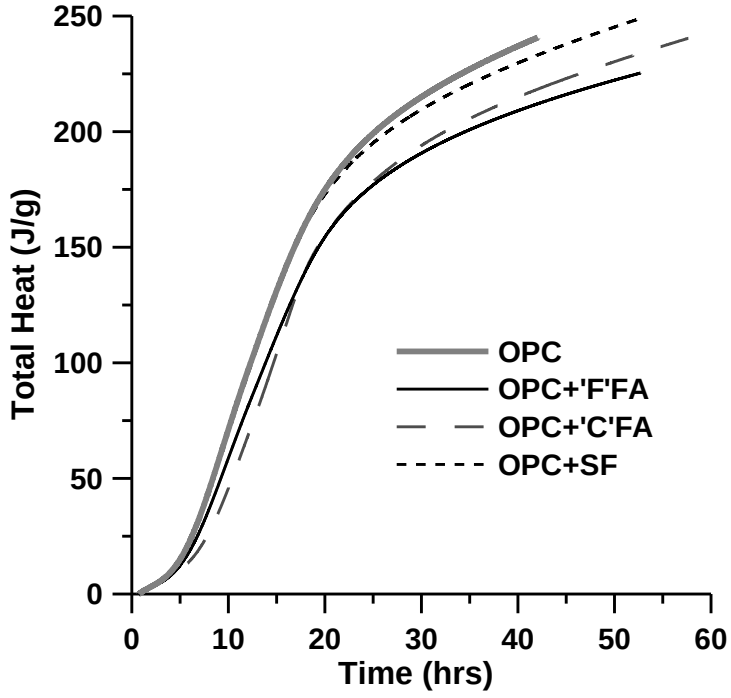
Figure 5.2 Effect of temperature on: a) heat evolution, b) total heat during the hydration of OPC-CSA binder with 15% CSA cement

5.2.2 OPC-CSA-MA Binder

Influence of mineral admixture (MA) addition on the heat of hydration of OPC and OPC-CSA binders was studied and presented in Figure 5.3 and 5.4 respectively. As shown in Figure 5.3, the mineral admixtures reduced the rate of heat evolution and the total heat depending on the percentage of replacement. All admixtures reduced the height of the main peak due to C_3S (alite) hydration. An increase in the height of the C_3A peak was observed in the Class C FA mixture due to the presence of C_3A in the fly ash. The Class C FA was also observed to cause more retardation in the hydration of OPC than the other admixtures. This observation is in agreement with a previous study by Fajun et al. (1985) in which the authors reported more retardation in presence of Class C FA than in Class F FA. Effects of mineral admixture addition on the hydration of OPC-CSA binder were observed to be similar (see Figure 5.4). It is evident that the mineral admixtures further reduce the intensity of the C_3S hydration peak. As seen before, Class C FA caused more retardation of the hydration of the OPC-CSA binders than other admixtures. Only difference is that the Class C FA mixture showed a second peak at around 45 hours possibly due to gypsum depletion and AFt to AFm conversion. This peak only appears in the Class C FA mixture due to the presence of C_3A in the Class C FA. It should be noted that the time of appearance of this addition peak matches well with the time when the OPC-CSA-CFA mixture stopped expanding (Figure 4.6).

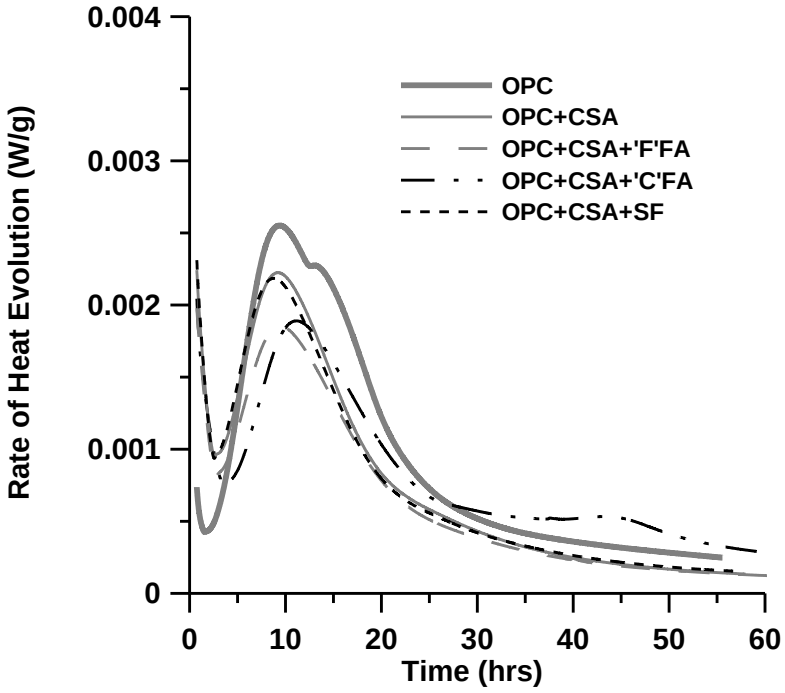


(a)



(b)

Figure 5.3 Effect of mineral admixtures on: a) the rate of heat evolution, b) total heat during the hydration of plain OPC System



(a)

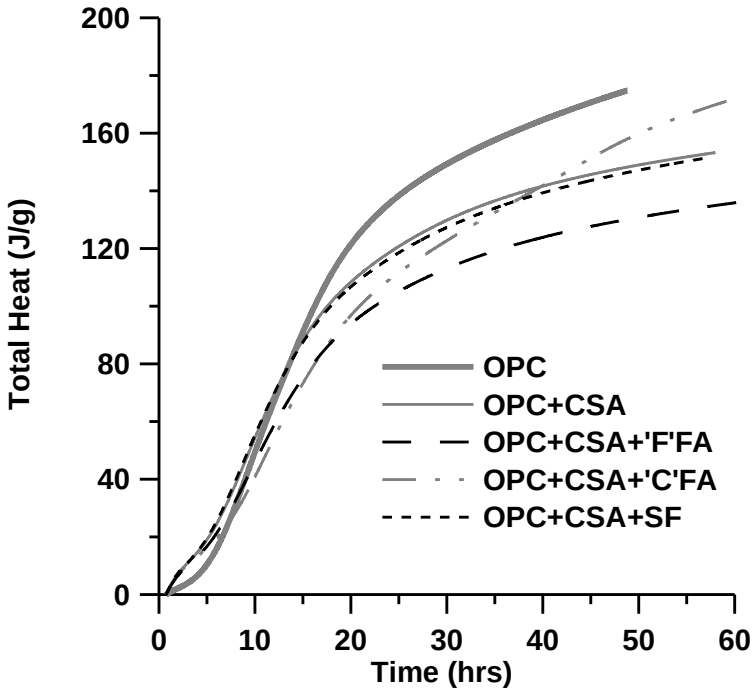


Figure 5.4 (a) Rate of heat evolution, and (b) total heat of OPC, OPC-CSA and OPC-CSA-MA cement pastes

Effect of Gypsum Addition

In order to validate the hypothesis that the additional peak in the Class C FA mixture appears due to the depletion of gypsum, additional gypsum was added into OPC-CSA-CFA blend and calorimetric study was repeated. Gypsum was added as 5% and 15% of CSA cement which corresponds to 0.75% and 2.3% additional gypsum in total cementitious binder. As shown Figure 5.5, with the addition of extra gypsum, the peak shift towards later age. Chen and Juenger (2011) also reported the shift in peak corresponding to rapid dissolution of $C_4A_3\hat{S}$ in calcium sulfoaluminate-belite cement due to the addition of gypsum. As the dosage of gypsum was increased, the peak did not appear within the 72 hours duration of the study.

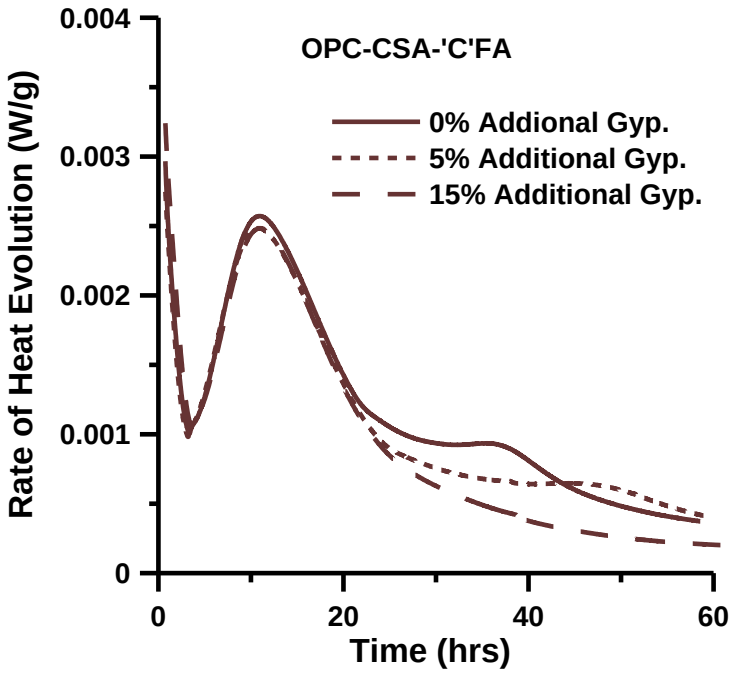


Figure 5.5 Effect of gypsum addition on the hydration of OPC-CSA-C FA paste

5.3 HYDRATION PROGRESS

5.3.1 OPC-CSA Binder

Figure 5.6 shows the X-ray diffraction patterns of OPC-CSA blends with varying CSA cement content at the age of 1, 3, and 7 days. It is evident that OPC-CSA blend with 30% CSA cement had the highest peak intensity for the unhydrated ye'elimite at 1 and 3 days. The intensity of ye'elimite peak decreased with the reduction in CSA cement content in a way that ye'elimite could not be detected in a blend with 7% CSA cement at 3 days. Figure 5.6 shows that the ye'elimite was consumed completely in all OPC-CSA blends at the end of 7 days. For quantitative study, Rietveld analysis was performed on OPC and OPC-CSA cement samples, and the results are shown in Table 5.1 and Figure 5.7. The reader is referred to Appendix A for the refinement plots. The ettringite content in 30% CSA cement sample was higher than that in other mixtures, and the amount increased noticeably with time (Figure 5.8). The amount of ettringite was quite similar beyond 1 day in 15% CSA cement sample whereas, for 0% and 7% CSA cement samples, it decreased due to conversion of ettringite to monosulfate and hemicarbonate. Figure 5.6 (b) shows the trace of monosulfate and hemicarbonate in 0% and 7% CSA sample after 3 days. Moreover, monocarbonate was detected in 0%, 7%, and 15% CSA cement samples at the end of 7 days (Figure 5.6 (c)). mono/hemi carbonate. The difference in ettringite content could be related to the difference in expansion potential between different mixtures. As expected, the amorphous content of 30% CSA samples was the lowest due to the lower amount of OPC present in the system.

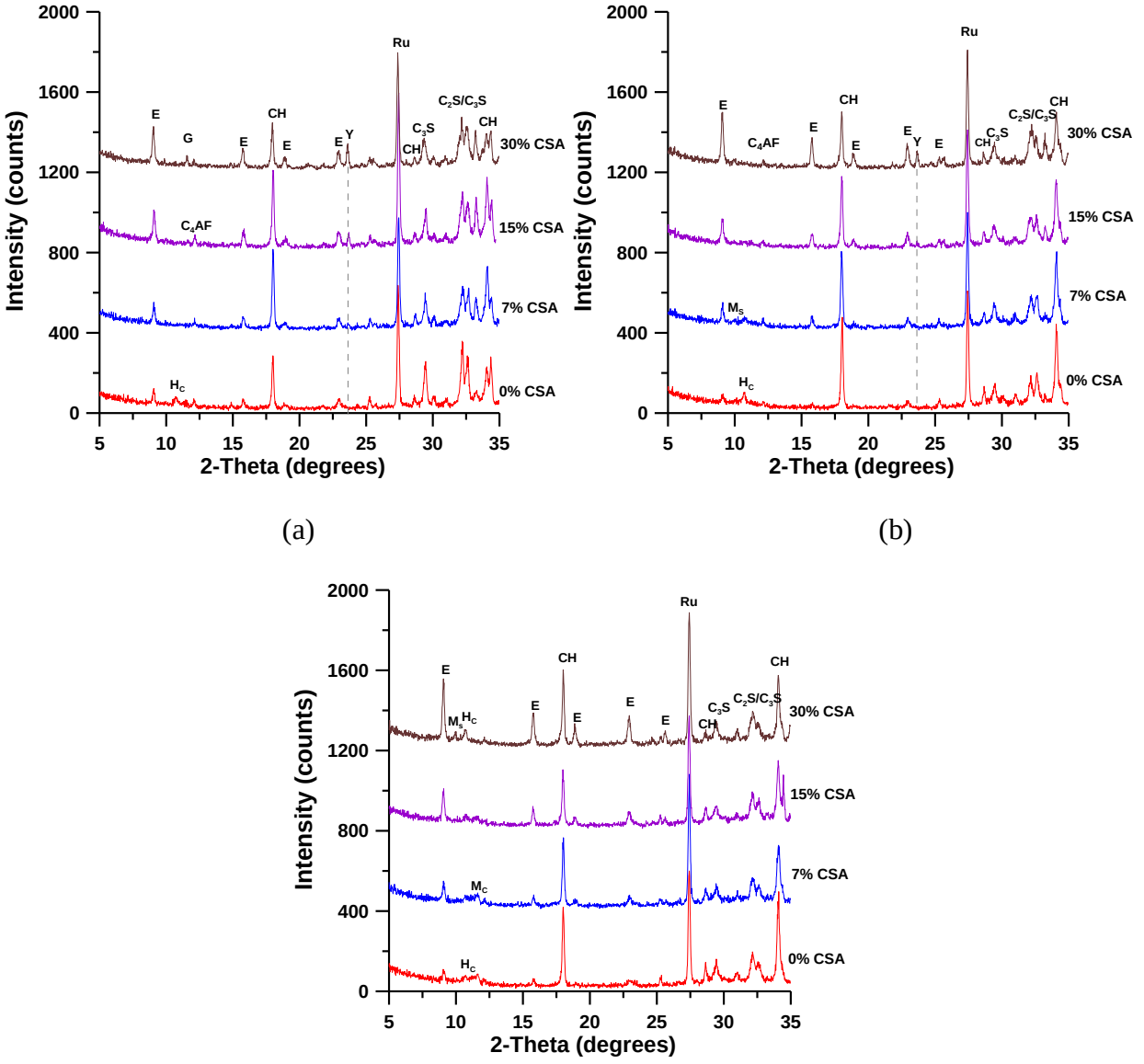


Figure 5.6 X-ray diffraction patterns of OPC and OPC-CSA blends with 15% rutile at the age of: a) 1 day, b) 3 days, and c) 7 days (Note: E – ettringite; Y – ye'elimite; M_s – monosulfate; M_c – monocarbonate; H_c –hemicarbonate; Ru – rutile; C_2S – belite; C_3S – alite; C_4AF –aluminoferrite; CH – portlandite)

Table 5.1 Phase composition (% wt.) of OPC-CSA binder (with 0%, 7%, 15% and 30% CSA cement) at various ages using Rietveld analysis

Phase	Age	C_3S	C_2S	C_3A	C_4AF	$C\hat{S}H_2$ +$C\hat{S}H_{0.5}$	$C_4A_3\hat{S}$	Ett	CH	$C\hat{C}$	Amor
0% CSA	1	22.9	14.4	1.8	1.9	0.1	0.0	5.0	10.8	1.3	39.9
	3	13.3	12.5	0.8	1.2	0.3	0.0	2.9	15.5	0.8	48.5
	7	8.6	14.8	0.3	1.1	0.8	0.0	1.5	18.2	2.0	51.6
7% CSA	1	20.2	11.7	8.1	2.4	-	0.8	9.4	13.1	2.1	30.2
	3	7.5	16.7	1.3	1.3	-	0.0	5.8	15.5	1.8	49.2
	7	5.6	15.4	0.4	0.9	-	0.0	5.6	14.0	1.5	55.0
15% CSA	1	16.4	12.2	7.1	1.9	0.6	1.1	10.6	10.1	2.1	35.2
	3	10.0	14.6	1.3	1.5	0.3	0.4	10.4	11.4	1.5	47.9
	7	11.8	12.5	0.1	0.6	0.6	0.1	10.0	12.8	1.9	49.0
30%CSA	1	19.9	18.9	7.8	1.5	-	3.1	14.9	8.2	0.9	20.7
	3	9.8	16.3	5.4	1.7	-	2.1	17.9	9.6	0.0	32.8
	7	6.3	13.2	0.4	1.0	-	0.0	21.4	11.4	2.9	42.6

$C\hat{S}H_2$ – Gypsum; $C\hat{S}H_{0.5}$ – Bassanite; $C\hat{C}$ – Calcite; Amor – C-S-H

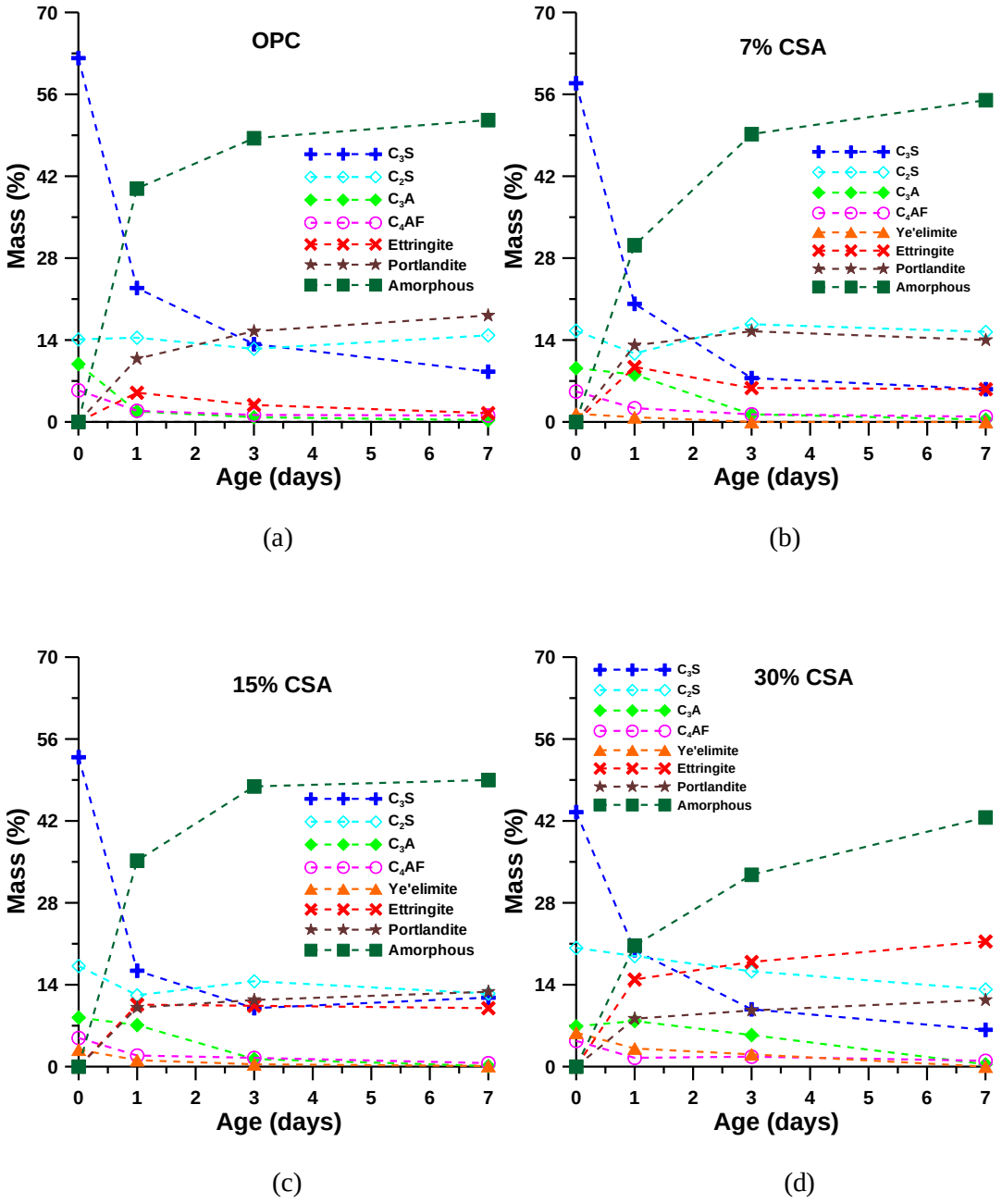


Figure 5.7 Evolution of unhydrated and hydrated phases in OPC-CSA binders with: a) 0% CSA, b) 7% CSA, c) 15% CSA, and 30% CSA cement

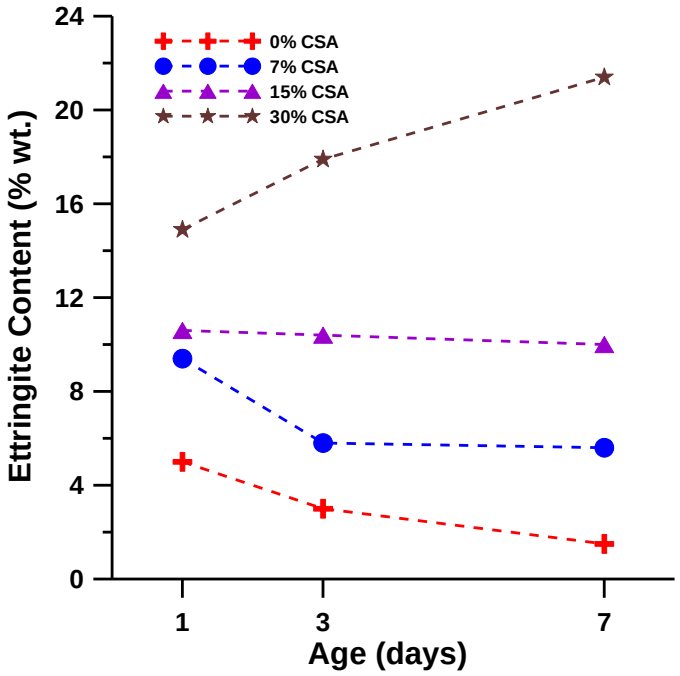


Figure 5.8 Evolution of ettringite content in OPC-CSA binders

Figure 5.9 shows the SEM micrographs of the OPC-CSA binder with 15% CSA cement after 7 days. Ettringite was observed to have a needle-like structure. Ettringite crystals of length up to 5 µm were observed throughout the microstructure. As presented in Figure 5.8, all OPC-CSA binders had portlandite present at all ages that formed due to the hydration of OPC. The presence of small crystals (or colloidal) of ettringite in lime-rich system, as observed by Mehta (1973 a, 1976), was not observed in this study.

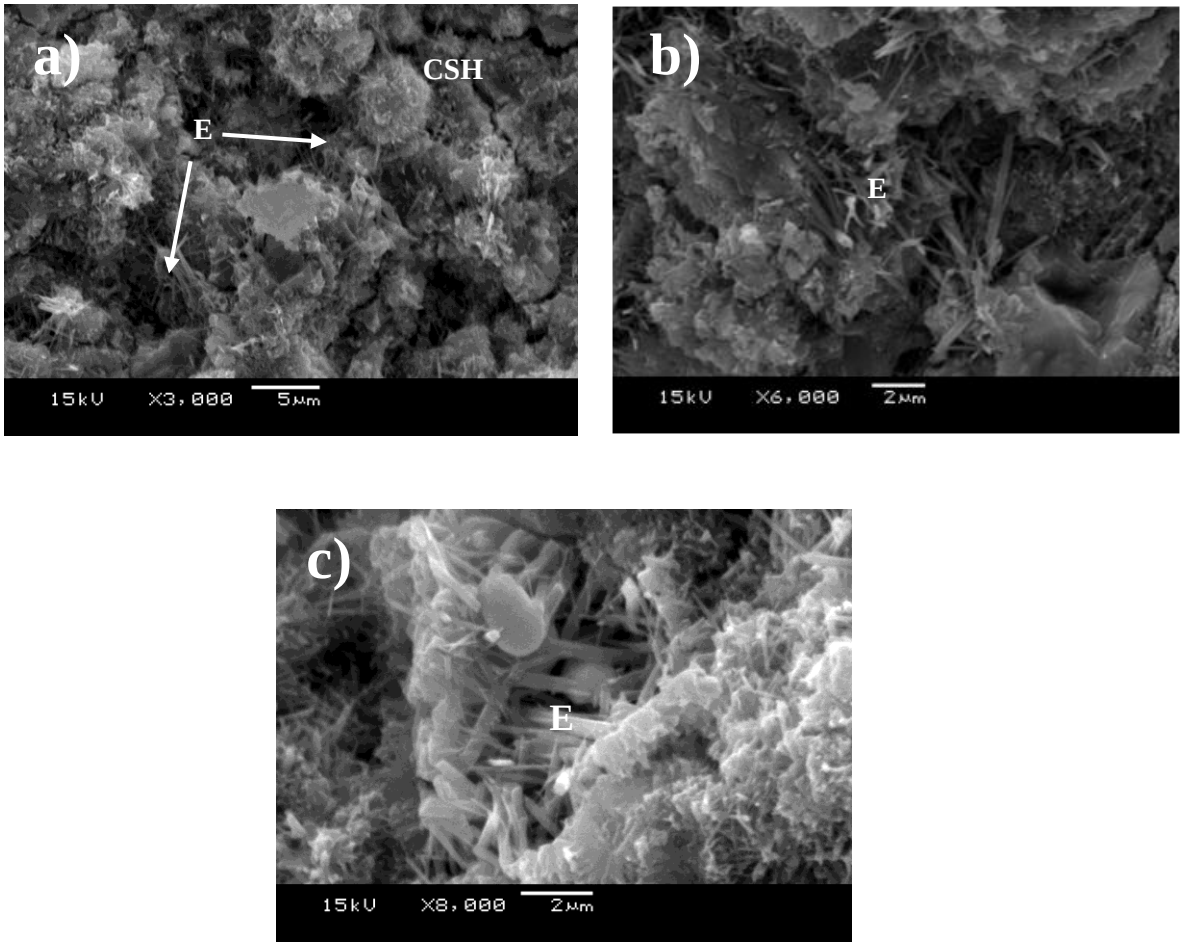
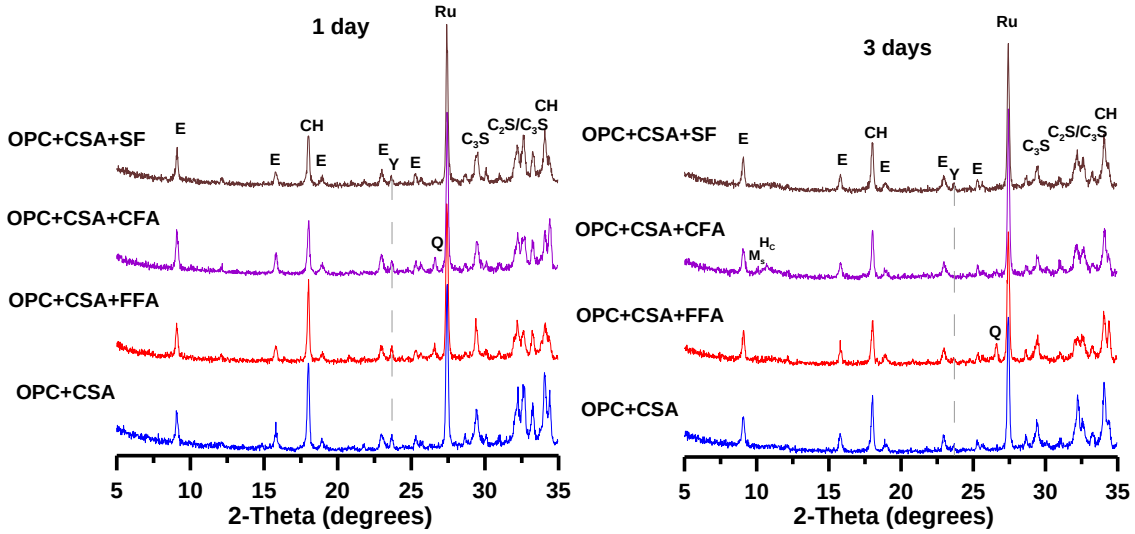


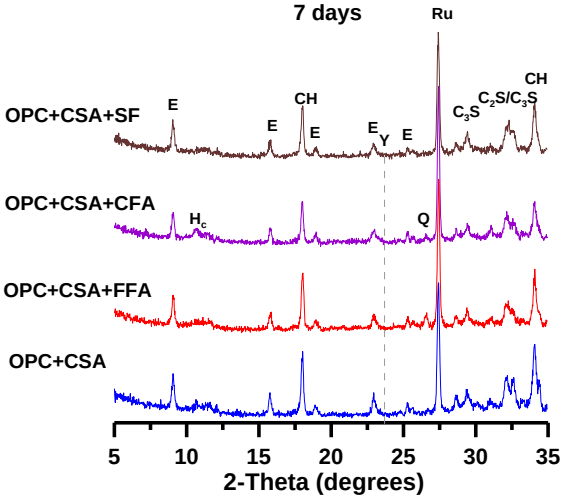
Figure 5.9 SEM micrographs of OPC-CSA binder with 15% CSA cement after 7 days (E – ettringite; C-S-H – calcium silicate hydrate)

5.3.2 OPC-CSA-MA Binder

Figure 5.10 shows the hydration progress of OPC-CSA-MA binders at various ages. As shown in Figure 5.10 (a) and (b), ye'elimite was found to be consumed after 7 days in OPC-CSA and OPC-CSA-F FA binders. The behavior of Class C FA was peculiar in a way that ye'elimite could not be detected at the age of 3 days, suggesting faster consumption of ye'elimite. Since ye'elimite was consumed earlier in Class C FA mixture, the expansion process ceased beyond 2 days, as shown in Figure 4.6.



(a) (b)



(c)

Figure 5.10 X-ray diffraction patterns of OPC-CSA-MA binders at the age of: a) 1 day, b) 3 days, c) 7 days (E – ettringite, CH – portlandite, Y – ye'elimite, Q – quartz, Ru – rutile, C_3S – alite, C_2S – belite)

Rietveld analysis of OPC-CSA-MA binders is presented in Table 5.2, and the phase composition is plotted in Figure 5.11. The reader is referred to Appendix B for the refinement plots. It is very clear that majority of the ettringite formed within the first 24 hours. Furthermore,

ye'elimite was completely consumed at the end of 7 days in samples with mineral admixtures. The amorphous content in all samples increased with age due to continuous formation of C-S-H gel. Figure 5.12 shows the evolution of ettringite content in OPC-CSA-MA binders with time. The ettringite content in OPC-CSA-CFA mixture decreased between 1 and 3 days, due to formation of monosulfate and hemiocarbonate (Figure 5.10 (b)).

Table 5.2 Phase composition (% wt.) of OPC-CSA-MA binders using Rietveld analysis

Phase	Age	C_3S	C_2S	C_3A	C_4AF	$C\hat{S}H_2$ +$C\hat{S}H_{0.5}$	$C_4A_3\hat{S}$	Ett	CH	$C\hat{C}$	Amor
OPC+CSA	1	16.4	12.2	7.1	1.9	0.6	1.1	10.6	10.1	2.1	35.2
	3	10.0	14.6	1.3	1.5	0.3	0.4	10.4	11.4	1.5	47.9
	7	11.8	12.5	0.1	0.6	0.6	0.1	10.0	12.8	1.9	49.0
OPC+CSA+FFA	1	10.6	10.7	5.8	1.4	0.3	1.2	9.2	6.5	0.4	49.8
	3	9.4	10.7	1.4	1.3	0.4	0.3	10.2	9.8	0.9	49.8
	7	5.7	8.5	0.2	0.7	0.5	0.0	9.2	9.3	1.2	60.5
OPC+CSA+CFA	1	14.8	11.1	5.9	1.2	0.4	1.1	10.2	4.5	1.5	46.8
	3	6.8	10.9	0.9	0.9	0.3	0.0	7.9	7.0	0.8	63.3
	7	3.2	12.0	0.6	0.8	0.3	0.0	7.6	7.3	1.2	65.0
OPC+CSA+SF	1	12.5	11.5	6.0	1.0	0.5	1.1	8.5	9.4	0.7	47.9
	3	8.3	12.3	1.8	1.6	0.6	0.6	11.2	10.2	1.4	51.1
	7	6.9	12.3	0.7	1.2	0.5	0.0	10.7	10.0	1.3	55.7

$C\hat{S}H_2$ – Gypsum; $C\hat{S}H_{0.5}$ – Bassanite; $C\hat{C}$ – Calcite; Amor – C-S-H

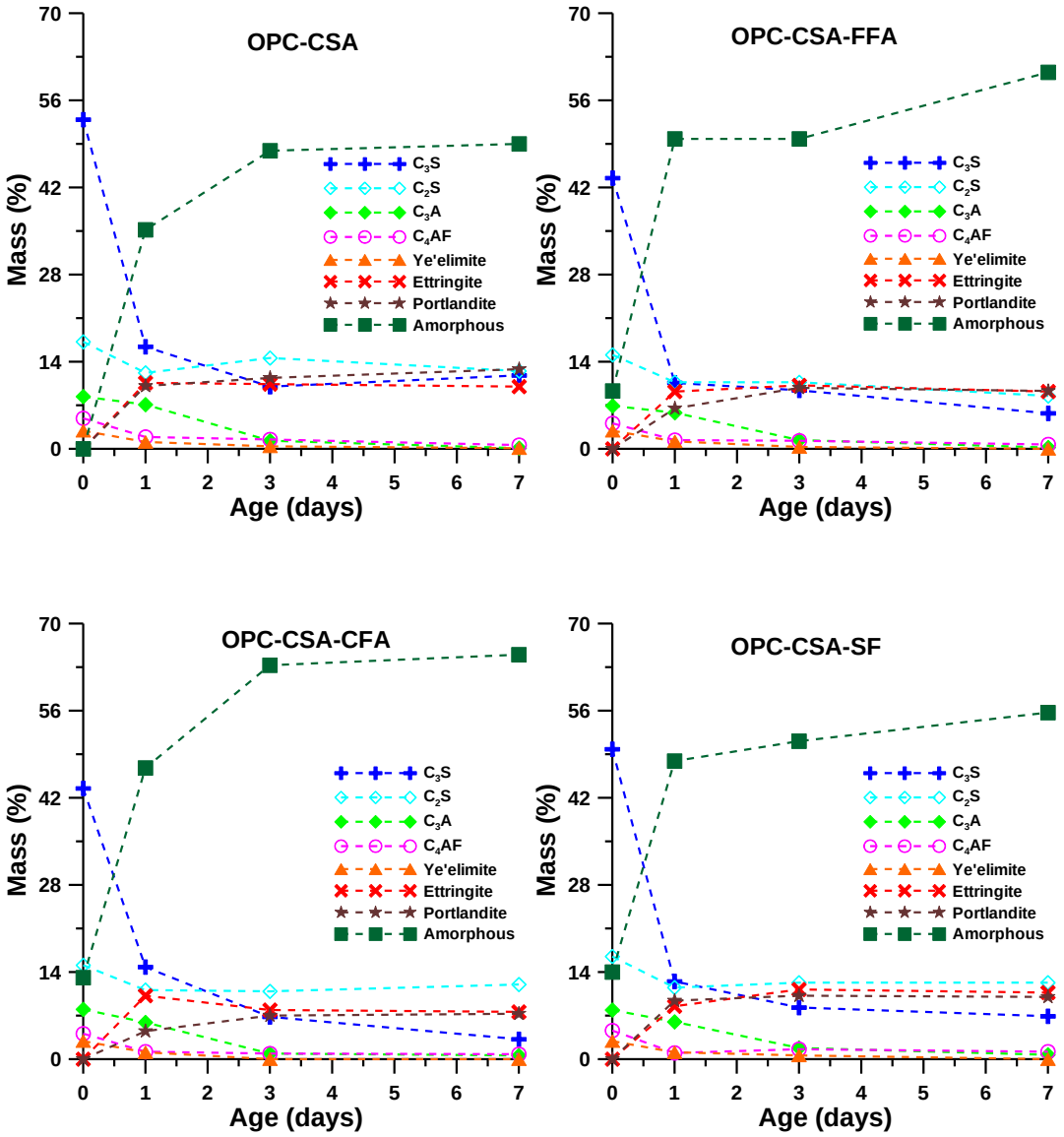


Figure 5.11 Evolution of hydrated and unhydrated phases in OPC-CSA-MA binders with 15% CSA cement

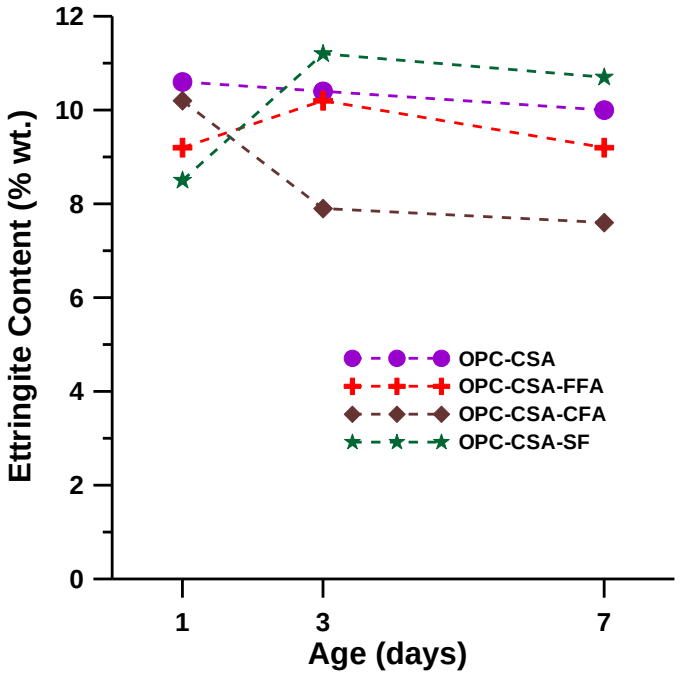


Figure 5.12 Evolution of ettringite in OPC-CSA-MA binders

Effect of Gypsum Addition

It has been shown earlier the 15% additional gypsum (i.e., 2.3% additional gypsum in total cementitious binder) increased the expansion and modified the calorimetric curve for OPC-CSA-CFA mixture (Figure 5.5). In order to understand whether the expansion increased due to increased ettringite formation X-ray diffraction analysis was performed on the samples with 15% additional gypsum. As shown in Figure 5.13, gypsum peak was clearly evident at 1 day in the OPC-CSA-CFA mixture with 15% additional gypsum, and the ye'elimite peak was present until 2 days. Rietveld analysis showed that the amount of ettringite was increased at 3 days in the sample with gypsum, as shown in Table 5.3. The reader is referred to Appendix C for the refinement plots.

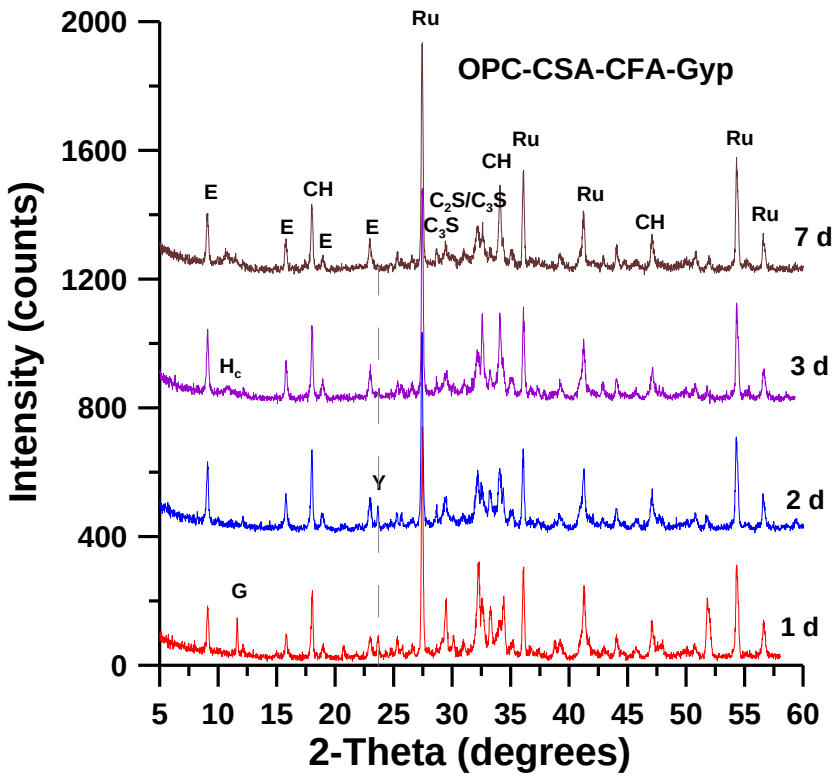


Figure 5.13 X-ray diffraction pattern of OPC-CSA-CFA sample with 15% additional gypsum sample at various ages

Table 5.3 Phase composition (% wt.) of OPC-CSA-CFA binders with and without gypsum

Phase	Age	C_3S	C_2S	C_3A	C_4AF	$C\hat{S}H_2$ +$C\hat{S}H_{0.5}$	$C_4A_3\hat{S}$	Ett	CH	$C\hat{C}$	Amor
OPC+CSA+CFA	1	14.8	11.1	5.9	1.2	0.4	1.1	10.2	4.5	1.5	46.8
	3	6.8	10.9	0.9	0.9	0.3	0.0	7.9	7.0	0.8	63.3
	7	3.2	12.0	0.6	0.8	0.3	0.0	7.6	7.3	1.2	65.0
OPC+CSA+CFA	1	18.5	8.5	6.9	1.2	0.7	1.5	9.4	5.5	0.1	45.6
+15% Gyp	3	6.8	14.0	1.3	1.3	0.3	0.3	13.8	8.5	0.5	51.3
	7	4.8	11.3	0.7	0.2	0.2	0.0	10.0	8.0	0.8	62.3

5.4 THERMOGRAVIMETRIC ANALYSIS

Figure 5.14 compares the amount of portlandite determined from Rietveld analysis and thermogravimetric analysis. A reasonable match between the values estimated from the two independent methods was observed. Figure 5.15 shows the thermogravimetric curves of OPC-CSA-MA binders at 1 and 7 days. Clearly the peak around 100°C can be attributed to the decomposition of ettringite and loss of some water from C-S-H. The difference in intensity of this peak is evident between OPC and OPC-CSA binders due to the presence of higher amount of ettringite in the later. Even though AFm was not detectable through XRD, a small peak corresponding to AFm phase at around 120°C was seen in OPC sample at 1 day, and in OPC-CSA-C FA sample at the end of 7 days. A few studies reported the formation of amorphous AH_3 (DTG peak at around 250°C) which is not detectable in XRD. But even TG analysis did not suggest the presence of AH_3 phase in OPC-CSA binder used in this study. The absence of AH_3 could be due to abundance of portlandite which favors the reaction (3) as described in Section 2.2.2.

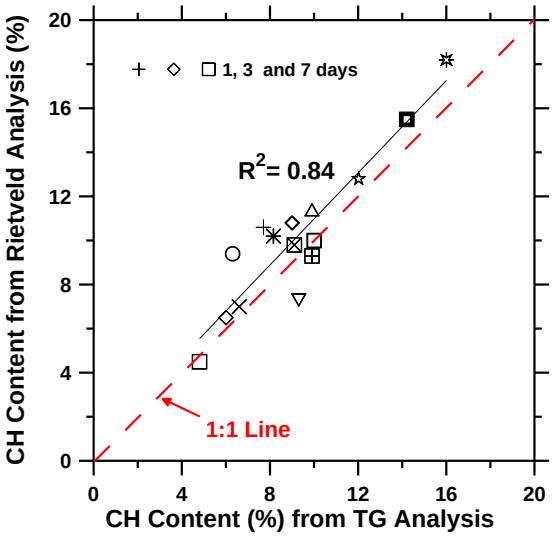
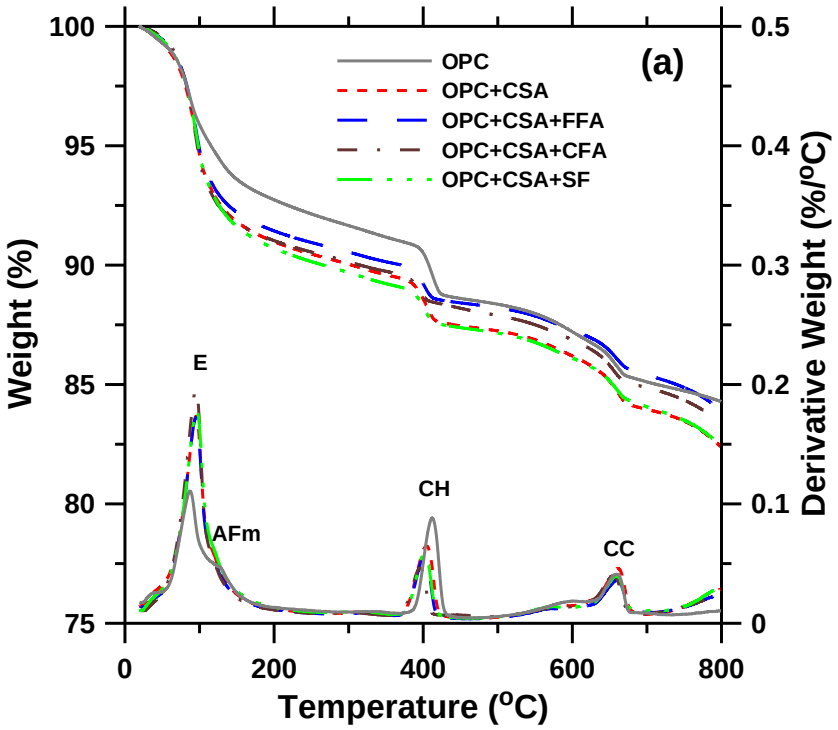
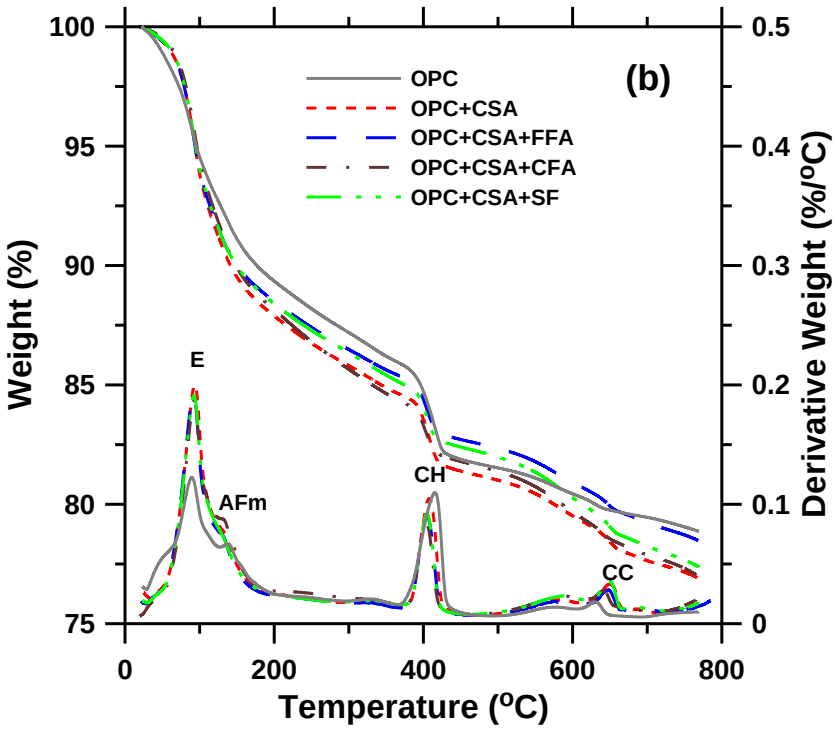


Figure 5.14 Comparison of CH content as determined by Rietveld and TG analyses (Different symbols represent different mixtures)



(a)



b)

Figure 5.15 Thermogravimetric (TG) and derivative thermogravimetric (DTG) plots for CSA-based cement pastes at the end of: a) 1 day and b) 7 days

5.5 PORE SOLUTION CHEMISTRY

5.5.1 OPC-CSA Binder

Figure 5.16 shows the evolution of pH with time in OPC and OPC-CSA binders. As shown in the figure, the pH of the OPC-CSA cement blends was found to be lower than that of the OPC paste, confirming the findings of previous studies [Andac and Glasser, 1999; Winnefeld and Lothenbach, 2010]. Similar to the of the OPC samples, the pH of the OPC-CSA blends with 7% and 15% CSA cement was found to increase with age. The OPC-CSA blend with 30% CSA cement exhibited lowest pH which was around 13 at all ages. However, it should be remembered that the samples containing 30% CSA cement showed excessive cracking. Therefore, ingress of the curing medium (lime saturated water) is expected to contaminate and dilute the pore solution.

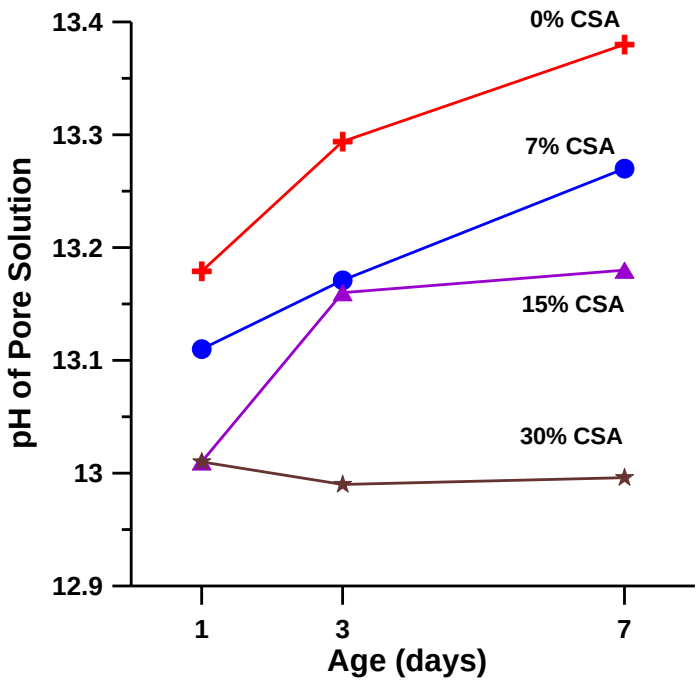


Figure 5.16 Effect of CSA cement content on pH of OPC-CSA blend

The elemental composition of the pore solution extracted at the age of 1, 3 and 7 days is shown in Figure 5.17. The variation in the concentrations of Na, K, Ca, and S ions from two different batches of the same sample was found to be within 20% whereas the variation in Al and Si concentrations was large due to concentration being very low (in micromolar range). A few observations can be drawn from the pore solution analysis data. The sulfur (S) concentration increased with the amount of CSA cement content due to the dissolution of gypsum/anhydrite and ye'elimite present in the CSA cement. The calcium (Ca) concentration also increased in the mixtures with higher amounts of the CSA cement due to continuous dissolution of ye'elimite. This trend is clearly evident at 1 day. It is important to mention here that the cracking of 30% CSA cement samples may have some influence on the pore solution analysis as cracked surfaces will have more excess to the curing medium (i.e., saturated lime water). It is known that the alkalis are released during the cement hydration which increases the total alkali (Na+K) content of the pore solution [Diamond, 1981]. In order to maintain electroneutrality, hydroxyl ion concentration also goes up, which is reflected by an increase in the pH. Figure 5.18 shows a direct relation between hydroxyl ion concentration and alkali concentration, confirming electroneutrality.

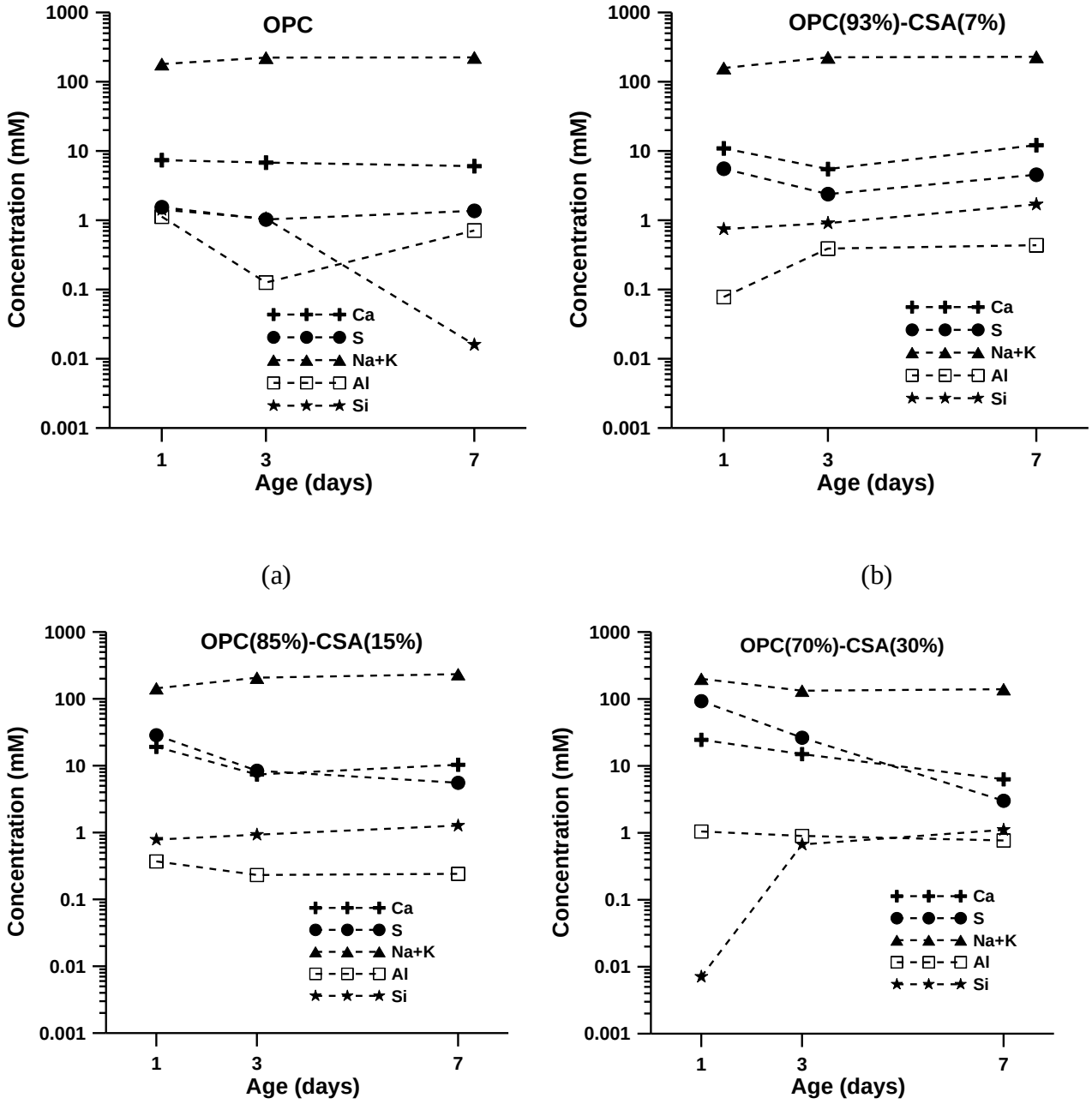


Figure 5.17 Elemental composition of pore solution for: a) 0% CSA, b) 7% CSA, c) 15% CSA, and d) 30% CSA

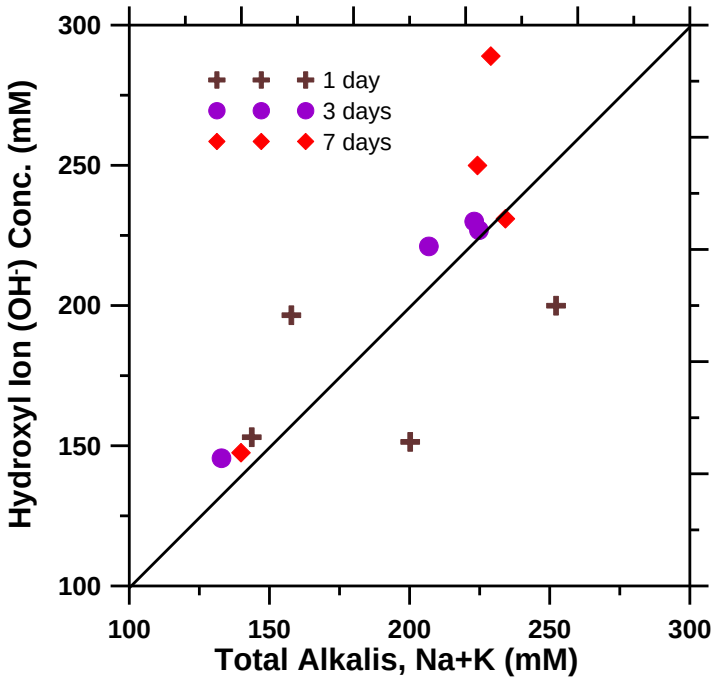


Figure 5.18 Comparison plot between total alkali content and hydroxyl ion concentration of the pore solution

Figure 5.19 shows the saturation levels of ettringite in OPC and OPC-CSA blends as calculated based on the ionic concentration of different species using GEMS-PSI program. In comparison to OPC, the blends containing CSA cement had significantly higher supersaturation with respect to ettringite. With increasing CSA content, a marked increase in supersaturation was also observed. Furthermore, supersaturation level decreased beyond 1 day. As reported in earlier studies [Bizzozero et al., 2014], supersaturation was found to be a key factor in governing expansion. The expansion trend observed for different OPC-CSA blends in this study matches well with the calculated supersaturation level.

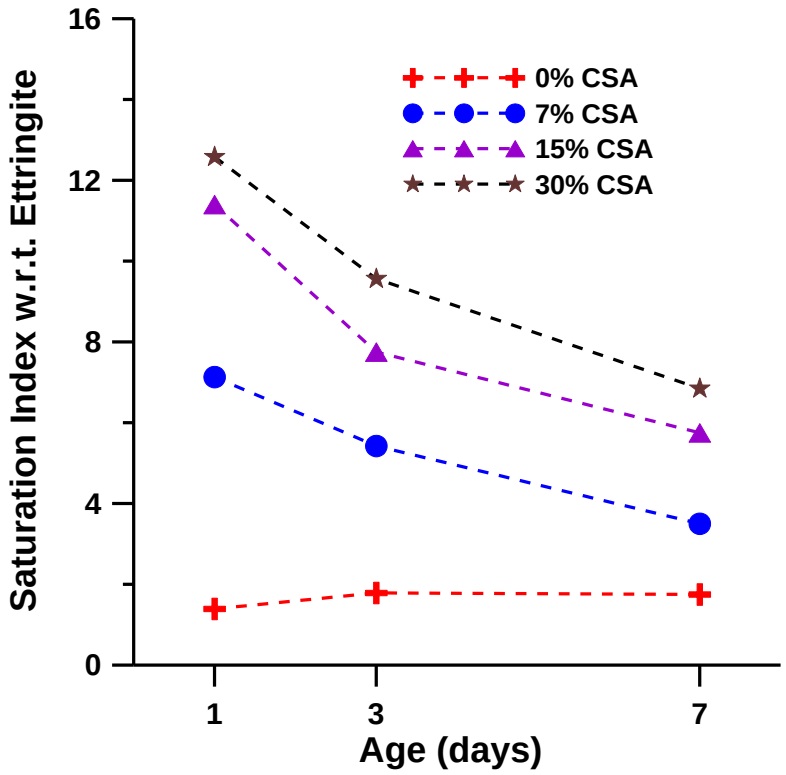


Figure 5.19 Effect of CSA dosage on saturation index of ettringite in OPC-CSA blend

5.5.2 OPC-CSA-MA Binder

The pH of the OPC-CSA-MA system was found to be in range of 12.6-13.1 (Figure 5.20). Alkali concentration in the pore solution increased from 1 day to 7 days due to continuous release of alkalis during the hydration process causing an increase in pH. There was a marked decrease in total alkali concentration and pH of the pore solution of the OPC-CSA-FFA and OPC-CSA-SF cement paste. It has been suggested that C-S-H with a low Ca/Si ratio formed due to a pozzolanic reaction tends to adsorb the alkalis, especially K^+ ions [Chappex and Scrivener, 2012] lowering the alkali concentration. Therefore, in mixtures incorporating Class F FA and SF, the C-(A)-S-H formed due to a pozzolanic reaction is expected to bind alkalis at later ages [Taylor, 1997]. The pH of SF paste was found to be the lowest among all mixtures at the end of 21 days, suggesting the alkali-binding.

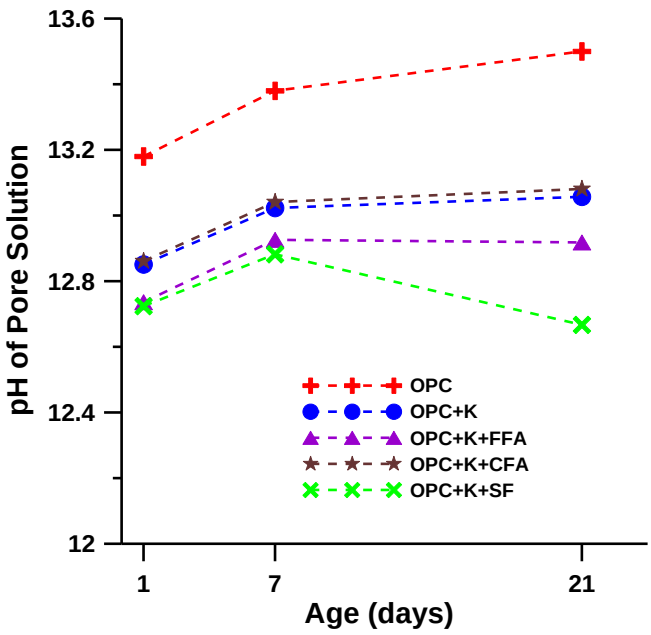


Figure 5.20 Effect of mineral admixtures on pH of OPC-CSA cement system at w/cm – 0.44

Figure 5.21 presents the evolution of concentration of various elements in the pore solution of OPC-CSA-MA cement pastes. Data for the OPC-CSA with 15% CSA cement is presented once again for comparison purpose. Overall, the concentration of various elements was found to be in agreement with available data from literature on CSA cement [Rothstein et al., 2002; Andac and Glasser, 1999; Winnefeld and Lothenbach, 2010]. Total alkali concentration was found to be in good agreement with total hydroxyl concentration, suggesting electro neutrality of the pore solution. As before, the dissolution of ye'elimite and Portland cement phases increases the Ca ion concentration in pore solution during the first 24 hours. At later ages, the formation of ettringite, portlandite, and C-S-H lead to a reduction in Ca ion concentration. Aluminum and silica concentration in the pore solution was found to be lower than 1 mM at all times. The sulfur concentration decreased beyond 1 day as the dissolution of ye'elimite and calcium sulfate is more prominent during the first 24 hours. Later, the formation of ettringite resulted in a decrease in S ion concentration by consuming the sulfates from the pore solution.

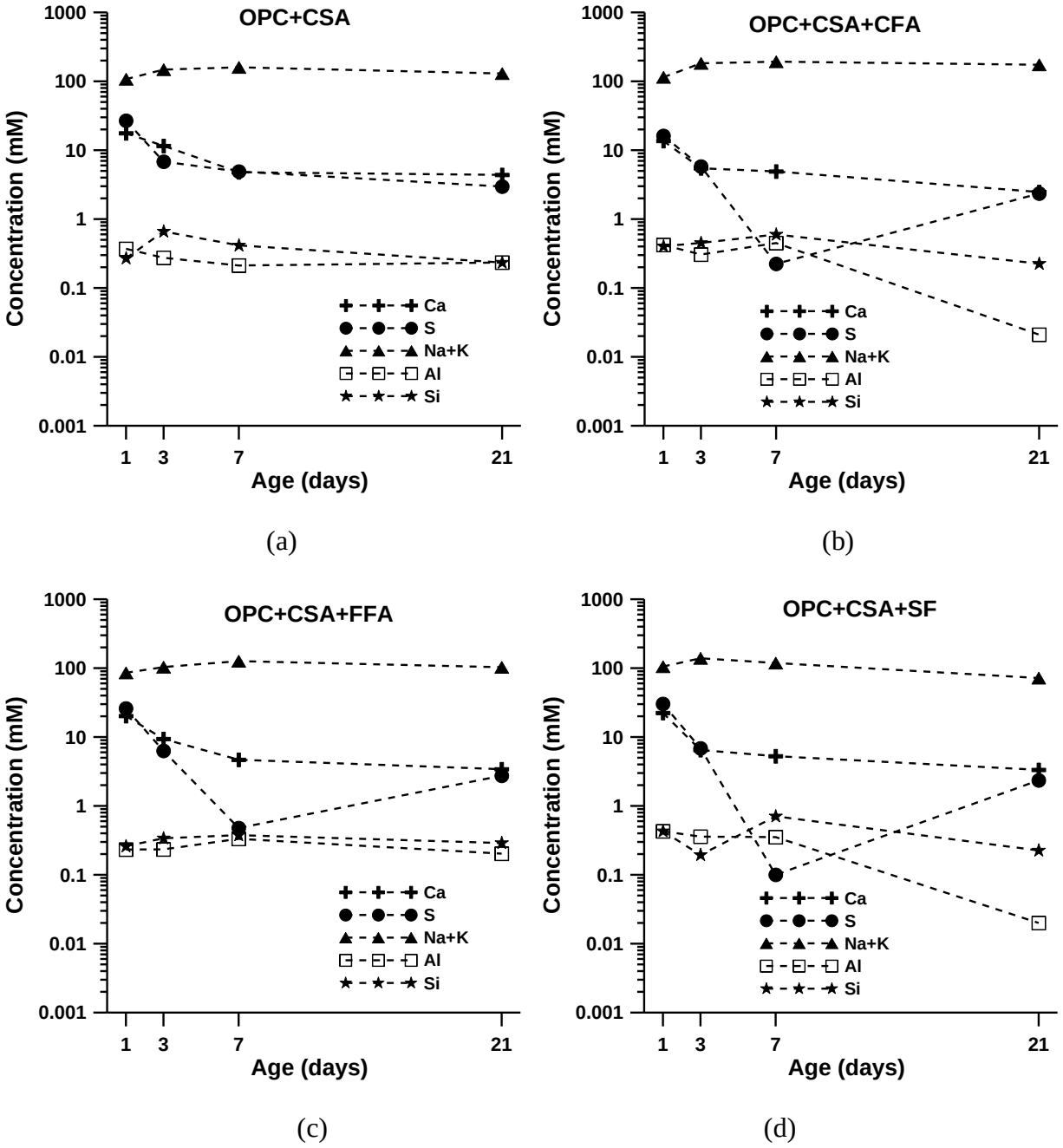


Figure 5.21 Elemental composition of the pore solution of OPC-CSA-MA binders at various ages

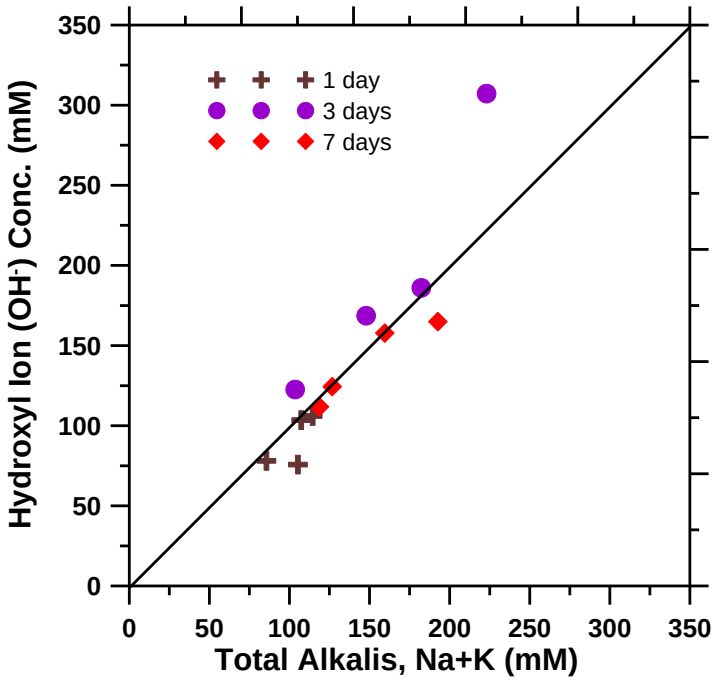


Figure 5.22 Comparison plot between total alkali content and hydroxyl ion concentration of the pore solution

Figure 5.23 shows the saturation index of ettringite for OPC-CSA-MA binders at 1, 3, and 7 days. Data for OPC and OPC-CSA samples without any mineral admixture are included for comparison purpose. The ionic concentration of Ca, Na, K, S, Al, and Si were used as an input for calculating saturation indices using GEMS-PSI. The saturation index with respect to ettringite was high for OPC-CSA-MA samples after 1 day, emphasizing the influence of supersaturation on expansion [Bizzozero et al., 2014]. The incorporation of mineral admixtures did not seem to result in any significant difference in SI at 1 day; however, SI of ettringite was reduced in the presence of mineral admixture at later ages. Similar to the OPC-CSA paste, the degree of supersaturation of ettringite in OPC-CSA-MA cement pastes decreased with time.

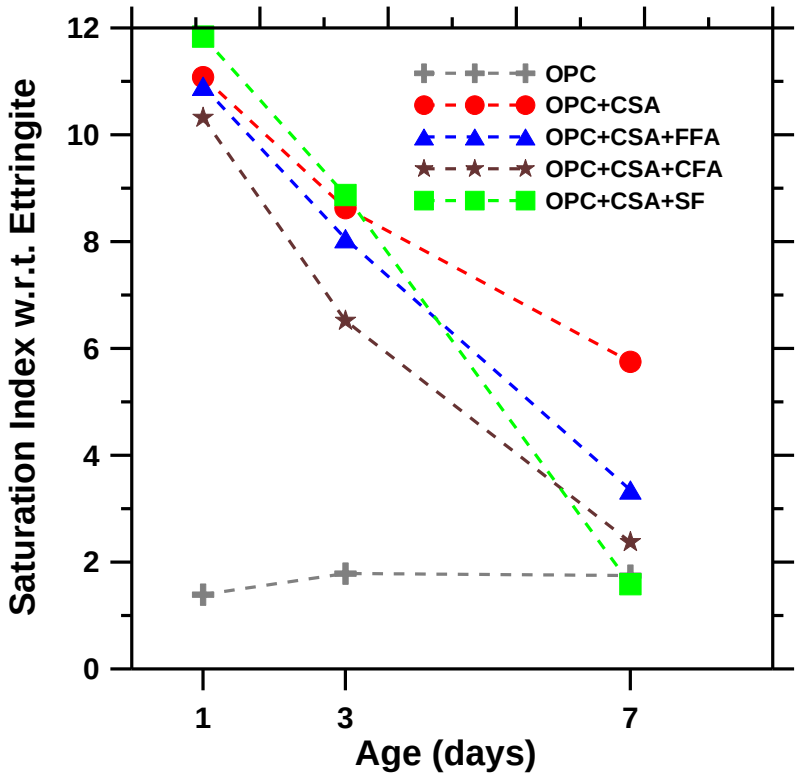


Figure 5.23 Saturation index of ettringite in CSA-based binders

Effect of Gypsum Addition

As we have seen before that the addition of gypsum led to an increase in expansion, therefore pore solution analysis was performed to estimate the saturation levels of ettringite in the presence of 15% additional gypsum of CSA cement (or 2.3% additional gypsum of total cementitious binder). The pH of the pore solution in the presence of gypsum was found to be lower, as shown in Figure 5.24. Figure 5.25 shows the pore solution composition of the CSA cement-based mixtures (OPC-CSA-CFA) with and without gypsum. The presence of gypsum led to an increase in Ca and S ion concentrations due to fast dissolution kinetics of gypsum. Both Ca and S ion concentrations decreased with time upon the formation of ettringite. Figure 5.26 shows the effect of gypsum addition on the supersaturation level with respect to ettringite in the OPC-CSA-CFA binder. The addition of gypsum increased the supersaturation w.r.t. ettringite and

gypsum. At all ages, the supersaturation was higher in samples with additional gypsum. It seems that the higher amount of ettringite (as reported in Table 5.3) and higher supersaturation w.r.t. ettringite resulted in the increased expansion in the OPC-CSA-CFA mixture in presence of additional gypsum.

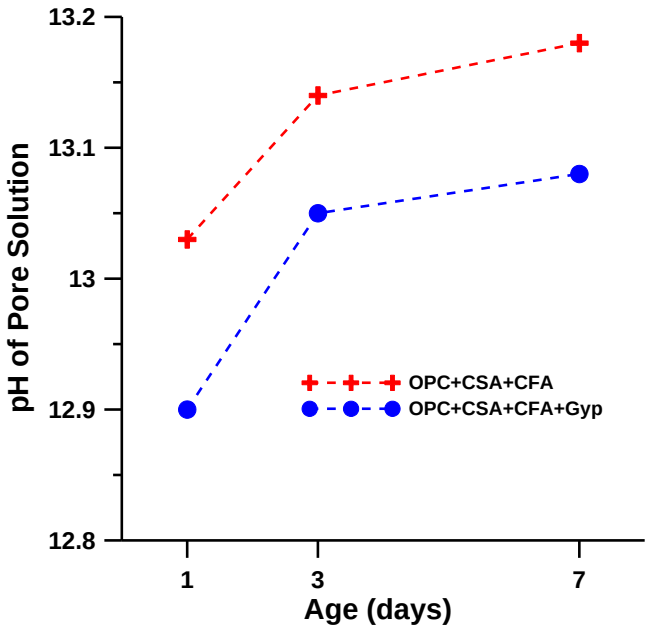


Figure 5.24 The effect of gypsum addition on the evolution of pH

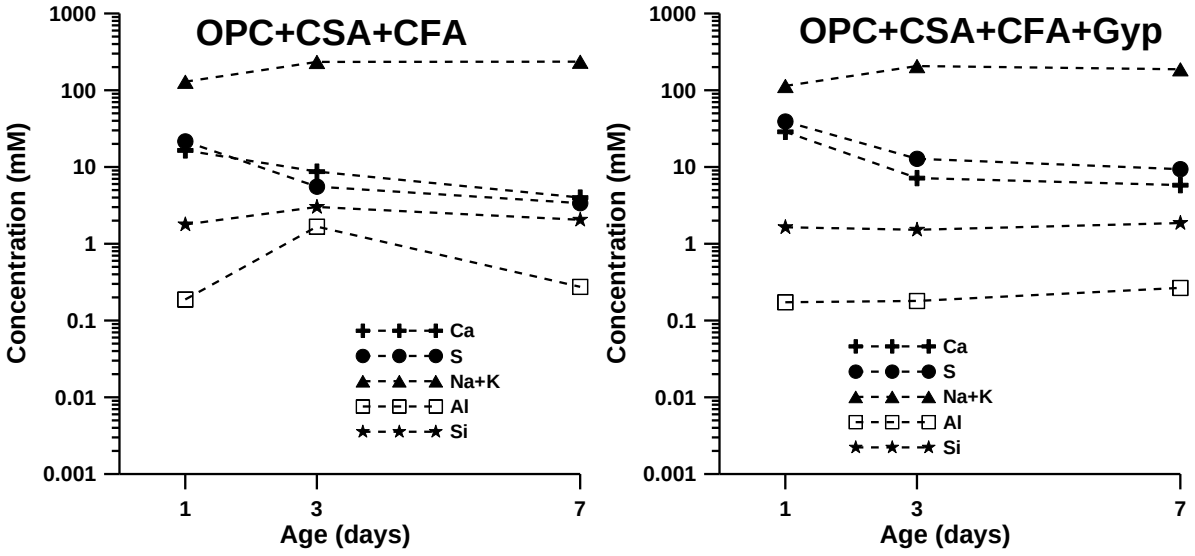
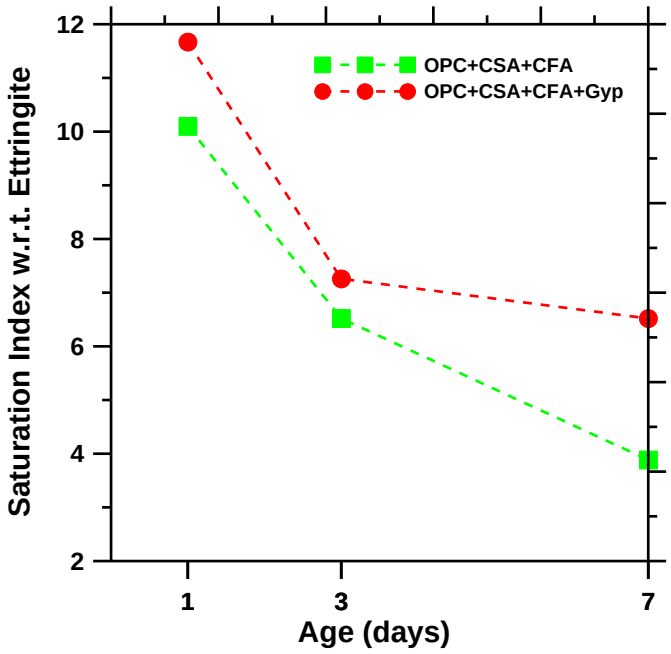
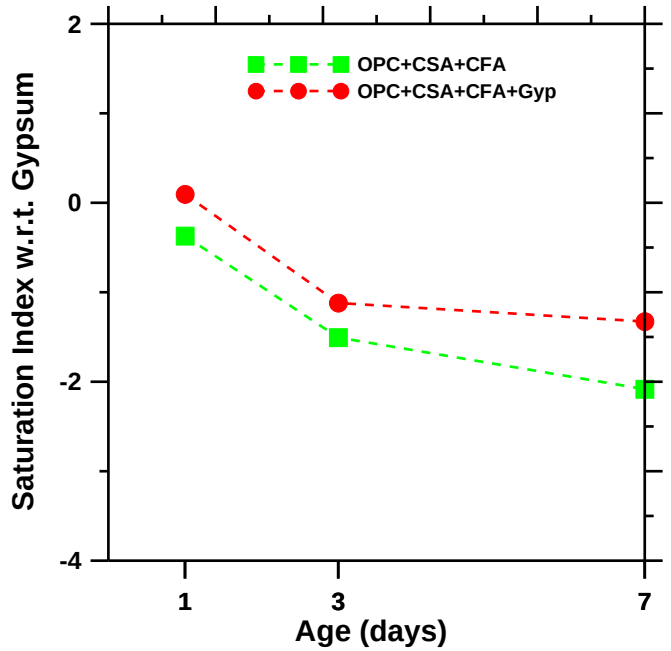


Figure 5.25 Effect of gypsum addition on the pore solution composition of OPC-CSA-CFA mixture



(a)



(b)

Figure 5.26 Effect of gypsum (15% by weight of CSA cement) addition on supersaturation indices w.r.t.: a) ettringite, and b) gypsum in sample containing Class C FA

5.6 CONCLUSIONS

The main conclusions of this chapter can be summarized as below:

- The hydration kinetics of OPC-CSA blend was influenced by the amount of CSA cement. The addition of CSA cement in OPC-CSA blend decreased the height of the main C_3S hydration peak due to dilution effect. An increase in temperature was found to increase the rate of OPC-CSA hydration. The calorimetric study on the influence of mineral admixtures revealed the retardation effect of Class C FA and increase in the height of C_3A hydration peak. The Class C FA used in this study exhibited an additional peak at around 44-45 hours indicating the early consumption of gypsum. Upon addition of extra gypsum, the onset of this peak was delayed, and it was eventually disappeared at high dosage of gypsum (15% by wt. of CSA cement).
- Quantitative XRD analysis showed that the amount of ettringite increased with the amount of CSA cement. In OPC-CSA-MA binders, the presence of MAs did not change the ettringite content significantly. Furthermore, gypsum addition increased the ettringite content at the age of 3 days substantially in OPC-CSA-CFA mixture.
- The pore solution analysis showed that the pH of CSA cement-based binders was lower than that of the OPC cement, validating the findings from previous studies. The calculations from a geochemical modeling program showed an increased saturation level of ettringite in CSA cement-based binders. An increase in the CSA cement and gypsum content increased the saturation index w.r.t. ettringite. The saturation index w.r.t. ettringite were significantly higher in CSA cement-based binders than that of the OPC. The supersaturation w.r.t. ettringite was found to be the precursor for crystallization stress.

CHAPTER 6: FACTORS INFLUENCING EARLY-AGE EXPANSION

This chapter summarizes the effects of various factors which influenced the early-age behavior of CSA cement-based binders examined in this study. Following factors were found to affect the early-age expansion of CSA cement-based binders:

6.1 RATE OF YE'ELIMITE HYDRATION

Hydration of ye'elimite in the presence of gypsum results in the formation of ettringite. Therefore, the hydration rate of ye'elimite is also expected to affect the early-age expansion. Expansion behavior of the Class C FA was found to be influenced by the rate at which ye'elimite was consumed. The XRD results showed the early consumption of ye'elimite in Class C FA mixtures due to early depletion of gypsum. The aluminate content (C_3A) of Class C FA appeared to have resulted in early consumption of gypsum.

Figure 6.1 compares the ettringite content at 1 day against total $C\hat{S}$ and ye'elimite content in the mixtures at t=0. A strong correlation is evident from Figure 6.1. Similarly, total $C\hat{S}$ and ye'elimite content in the mixtures at t=0 were strongly related to expansion at 1 day as shown in Figure 6.2.

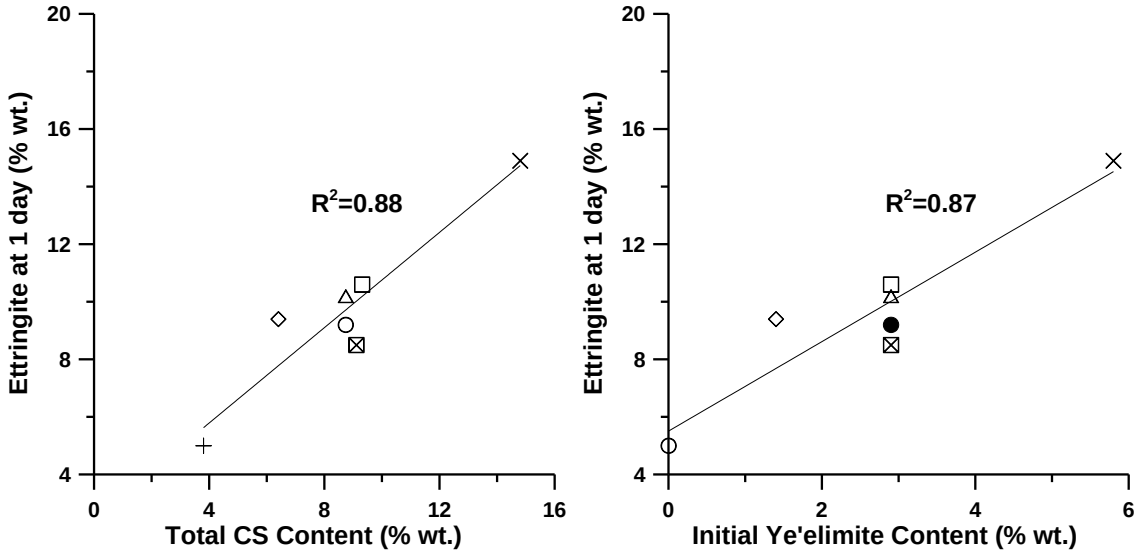


Figure 6.1 Ettringite content at 1 day vs. : a) total CŜ content at t=0, and b) initial ye'elimite content (Note – Different symbols represent different mixtures)

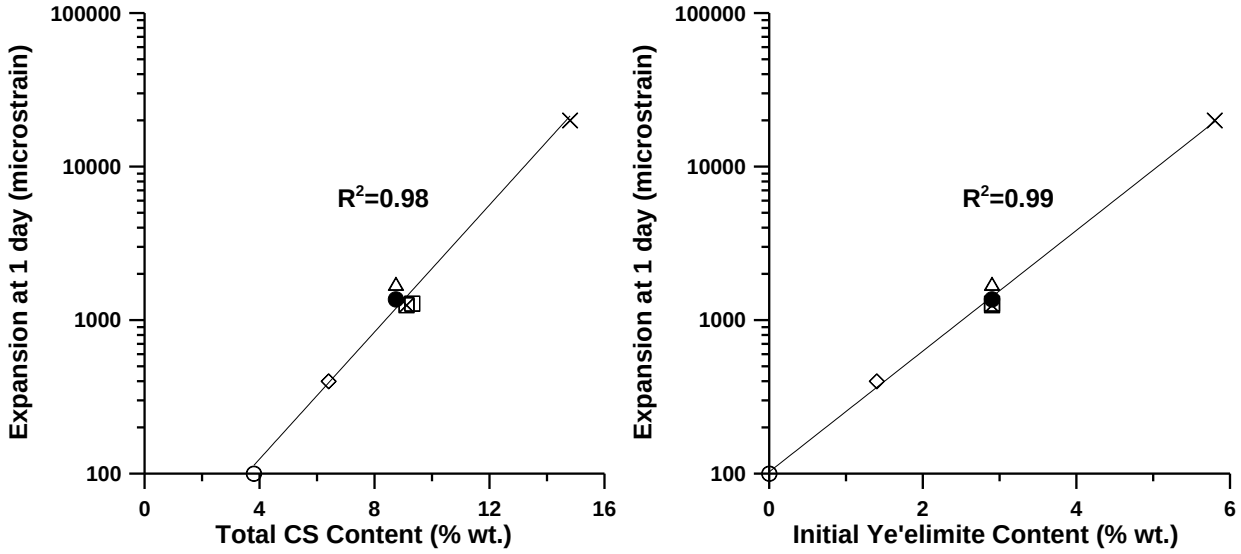
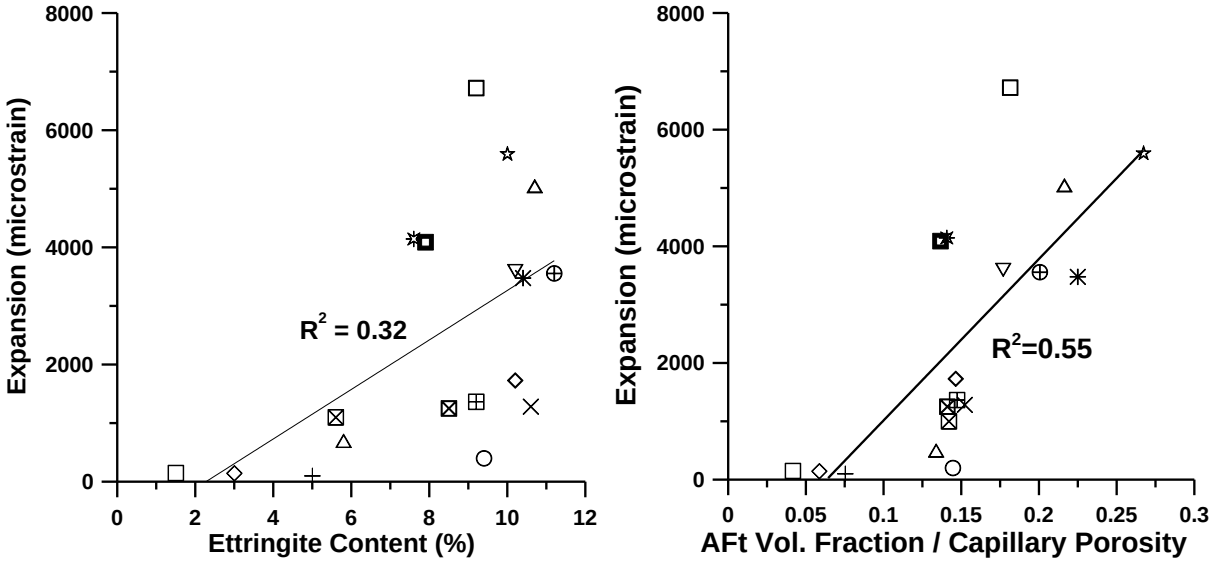


Figure 6.2 Expansion at 1 day vs.: a) total CŜ content at t=0, and b) initial ye'elimite content (different symbols represent different mixtures)

6.2 AMOUNT OF ETTRINGITE IN PORE VOLUME

In many studies in the past, effort was made to relate the total ettringite content with the early-age expansion. However, no simple relationship has been observed. A more relevant parameter of interest could be the ratio of the volume of ettringite in the total pore volume (S_c).

The macroscopic tensile stress due to crystallization has been shown to depend strongly on S_c (refer to Section 2.5). An increase in S_c means an increase in volume of crystals exerting stress in a given pore volume, thereby increasing the tensile stress. The volume fraction of ettringite could be estimated once total porosity was determined. Figure 6.3 (a) shows the correlation between the ettringite content and expansion, and Figure 6.3 (b) shows how the correlation factor improves when expansion is plotted against volume fraction of ettringite in the total pore volume. It is clear that the parameter defined as volume fraction of ettringite in total pore volume (S_c) is a better representation of the confined volume of ettringite responsible for exerting stress and causing expansion than the total weight fraction of ettringite.



a) b)

Figure 6.3 a) Expansion vs. ettringite content (% wt.), and b) expansion vs. ettringite volume fraction in pore volume (Different symbols represent different mixtures)

6.3 SUPERSATURATION

We have seen earlier that supersaturation w.r.t. ettringite was higher in CSA cement-based binders. Expansion at 1 day was found to have a good correlation with saturation index (SI) at 1 day, as shown in Figure 6.4. Higher supersaturation at the end of 1 day would also mean higher potential for expansion as depicted clearly in Figure 6.4. Due to continuous hydration of ye'elimite and subsequent formation of ettringite, the supersaturation in the pore solution starts dropping beyond 1 day. The influence of saturation index (SI) on the incremental length change after day 1 is plotted and presented in Figure 6.5. At first, all mixtures were considered to plot the incremental length change against SI. The correlation factors increased significantly when only OPC-CSA binders were considered. Therefore, it can be inferred that the supersaturation was a predominant factor governing expansion behavior of the OPC-CSA binders.

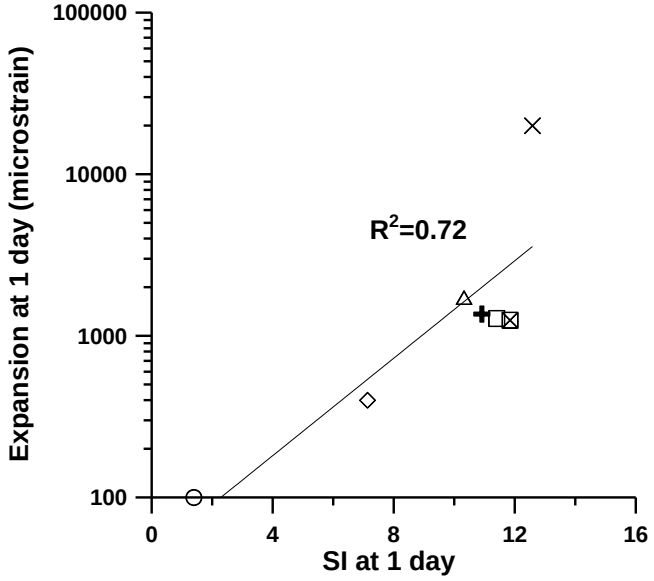
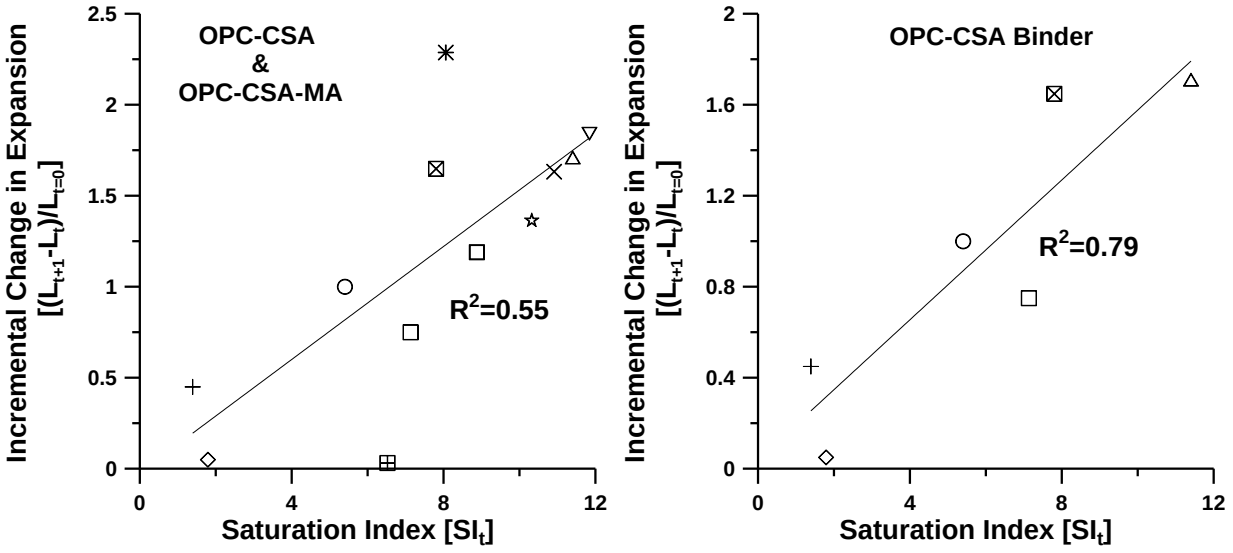


Figure 6.4 Expansion at 1 day vs. SI at 1 day
(Note – Different symbols represent different mixtures)



a) b)

Figure 6.5 Incremental change in expansion vs. saturation index for: a) all mixtures (OPC-CSA & OPC-CSA-MA), and b) only OPC-CSA mixtures

6.4 DYNAMIC MODULUS

This study shows that dynamic modulus is also one of the factors governing expansion. Very few studies have highlighted the importance of dynamic modulus [Hoff, 1973; Ping and Beaudoin, 1992]. Figure 6.6 compares the incremental change in expansion after 1 day against elastic modulus as the modulus is expected to influence the expansion characteristics. As shown in Figure 6.6, the increase in dynamic modulus seemed to have reduced the extent of expansion, particularly after day 1. It is noted that the Class C FA mixture (age: 3 day) was excluded from curve fitting as the expansion of Class C FA mix stopped beyond 2 days.

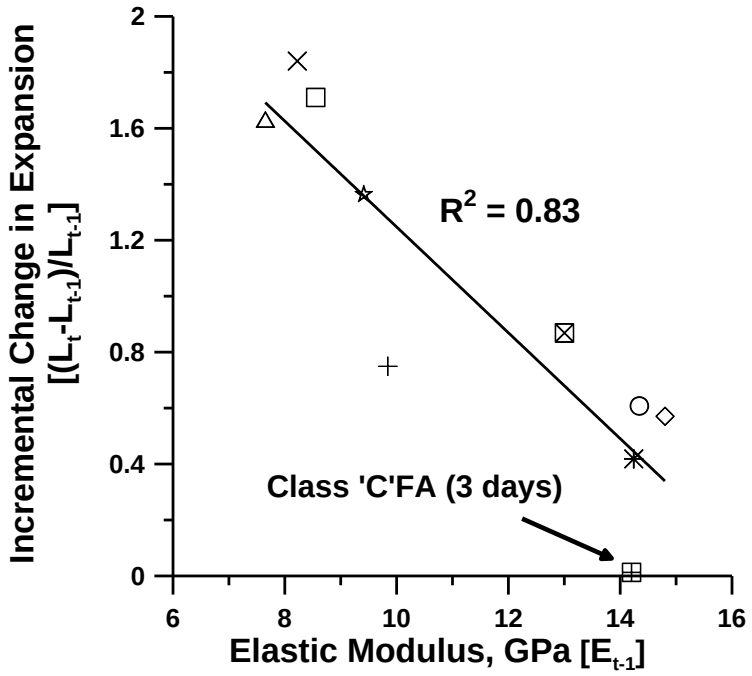


Figure 6.6 Incremental change in expansion vs. elastic modulus for OPC-CSA and OPC-CSA-MA binders (Arrow shows the 3 day old CFA sample which was excluded from curve fitting)

6.5 CONCLUSIONS

This chapter highlights the importance of five main factors which need to be considered to better understand the early-age volume change of CSA cement-based binders. The initial ye'elimite content, total CŜ amount, volume fraction of ettringite w.r.t. total pore volume, supersaturation w.r.t. ettringite, and dynamic modulus were found to govern the expansion characteristics of CSA binders. However, the dominance of one factor over others depends on cement system. The influence of dynamic modulus seemed to be more pronounced beyond 1 day whereas SI appeared to have a good correlation with expansion at 1 day.

CHAPTER 7: ESTIMATION OF CRYSTALLIZATION STRESS AND ITS INFLUENCE ON EXPANSION

As supersaturation was found to be an important factor governing the expansion, this chapter attempts at estimating the crystallization stress which is derived from supersaturation. Various models were used to calculate the crystallization stress. Furthermore, the calculated stress was compared with tensile strength of paste samples in order to predict tensile failure (cracking) due to excessive expansion. Eventually, the strains due to crystallization stresses were calculated and compared with observed strains.

7.1 ESTIMATION OF CRYSTALLIZATION STRESS

7.1.1 OPC-CSA Binder

The estimation of crystallization stress using models based on an assumption of spherical or cylindrical pores as described in Eq. 2-2 and 2-3 requires the information on the volume fraction of ettringite crystals (ϕ) exerting stress. For OPC-CSA binders, the total amount of ettringite, as shown in Table 5.1, was used to calculate the upper bound of crystallization stress. The volume fraction of ettringite was derived from the weight fraction by considering the individual phase densities and the measured capillary porosity of samples. Densities of various phases were adopted from a complied database by Balonis and Glasser (2009). In the absence of pore size distribution for given mixtures, the upper bound of crystallization stress was estimated considering the total volume fraction of ettringite. In addition to the two models mentioned above, the crystallization stress was also estimated using poromechanics in accordance to Eq. 2-7. The Biot coefficient, i.e., b, was assumed to be 0.6 for cement paste [Ghabezloo et al., 2008], and S_c was calculated by dividing the volume fraction of ettringite with total porosity. The total porosity was calculated by adding the volume fraction of ettringite to the measured capillary

porosity as ettringite is assumed to form in the pores and partially fill them. Figure 7.1 shows the crystallization stress estimated by three models, and its comparison with tensile strength of paste samples. Among three models, the model based on cylindrical pores predicted the lowest stress at all ages. The difference in the crystallization stress between the OPC and OPC-CSA system is also evident from Figure 7.1. All three models were able to predict the higher crystallization stress in CSA-based mixtures, and the difference between OPC and OPC-CSA system is significant which explains the observed difference in expansion behavior (Figure 4.1). At 1 day, the models predicted higher crystallization stresses than the tensile strengths of the 15% and 30 % CSA blends. Of course, the tensile creep is expected to be high as the cement paste is relatively less stiff at 1 day, and therefore, will result in some stress relaxation. Considering stress relaxation at 1 day, it is reasonable to assume that the crystallization stress will be similar or lower than tensile strength for 0%, 7% and 15% CSA blends. Furthermore, the crystallization stress was found to be lower or similar than the tensile strength for blends containing 0%, 7%, and 15% CSA cement at 3 days. Again stress relaxation due to the tensile creep will lower the extent of the macroscopic tensile stress developed due to crystallization. The prediction suggests that the blends containing CSA cement up to 15% are unlikely to crack. However, the stress increased significantly as the CSA cement content increased to 30%, causing cracking. Though there were differences in the predicted macroscopic stresses using different models, all models were able to predict the failure of 30% CSA cement sample.

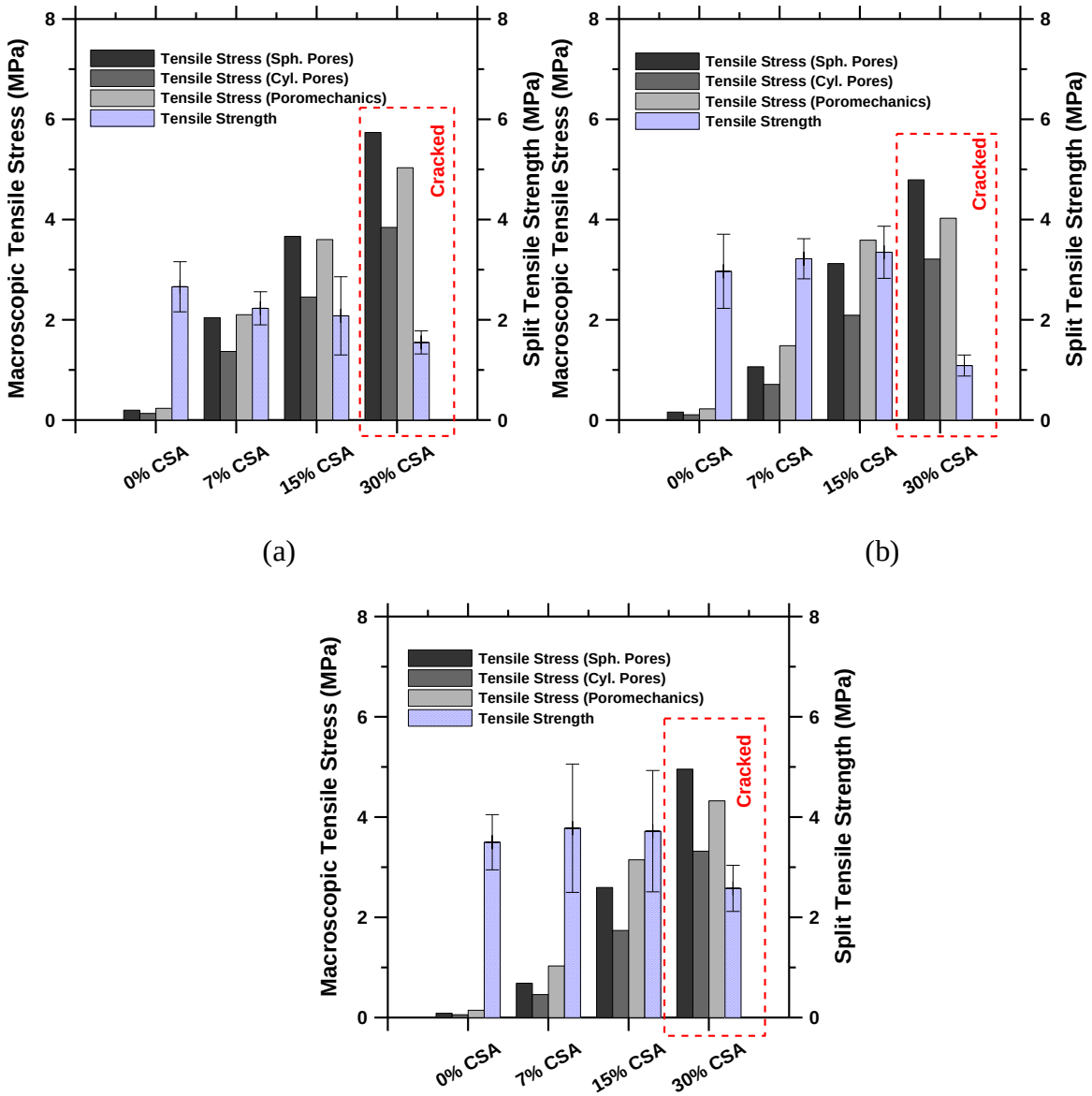


Figure 7.1 Crystallization stress as calculated from three models and its comparison with tensile strength at the age of: a) 1 day, b) 3 days and c) 7 days

7.1.2 OPC-CSA-MA Binder

Figure 7.2 shows the upper bound of crystallization stress in OPC-CSA-MA cement pastes at 1, 3 and 7 days. All tensile stresses were found to be less than 4 MPa. At 1 day, tensile stress in OPC-CSA-MA binder was a bit lower than that in OPC-CSA binder, but this tensile

stress was higher than the tensile strength. Obviously this stress is the upper bound of stress which accounted for the total amount of ettringite. Also, early-age creep would reduce the stress level which means that the stress may be similar or even lower than the tensile strength. A few changes were observed at 3 days. Class C FA mixture experienced the lowest stress which also supports the length change measurement indicating early completion of expansion process (Figure 4.6). The level of tensile stress was similar or lower than tensile strength in OPC-CSA-MA binders. Furthermore, the tensile stress in OPC-CSA-MA binders at the age of 7 days was significantly lower than OPC-CSA binder which can be related to lower SI w.r.t. ettringite in OPC-CSA-MA binders. It is noted that the difference in pore size distribution can introduce some variation in the calculated crystallization stress which was not considered in this study.

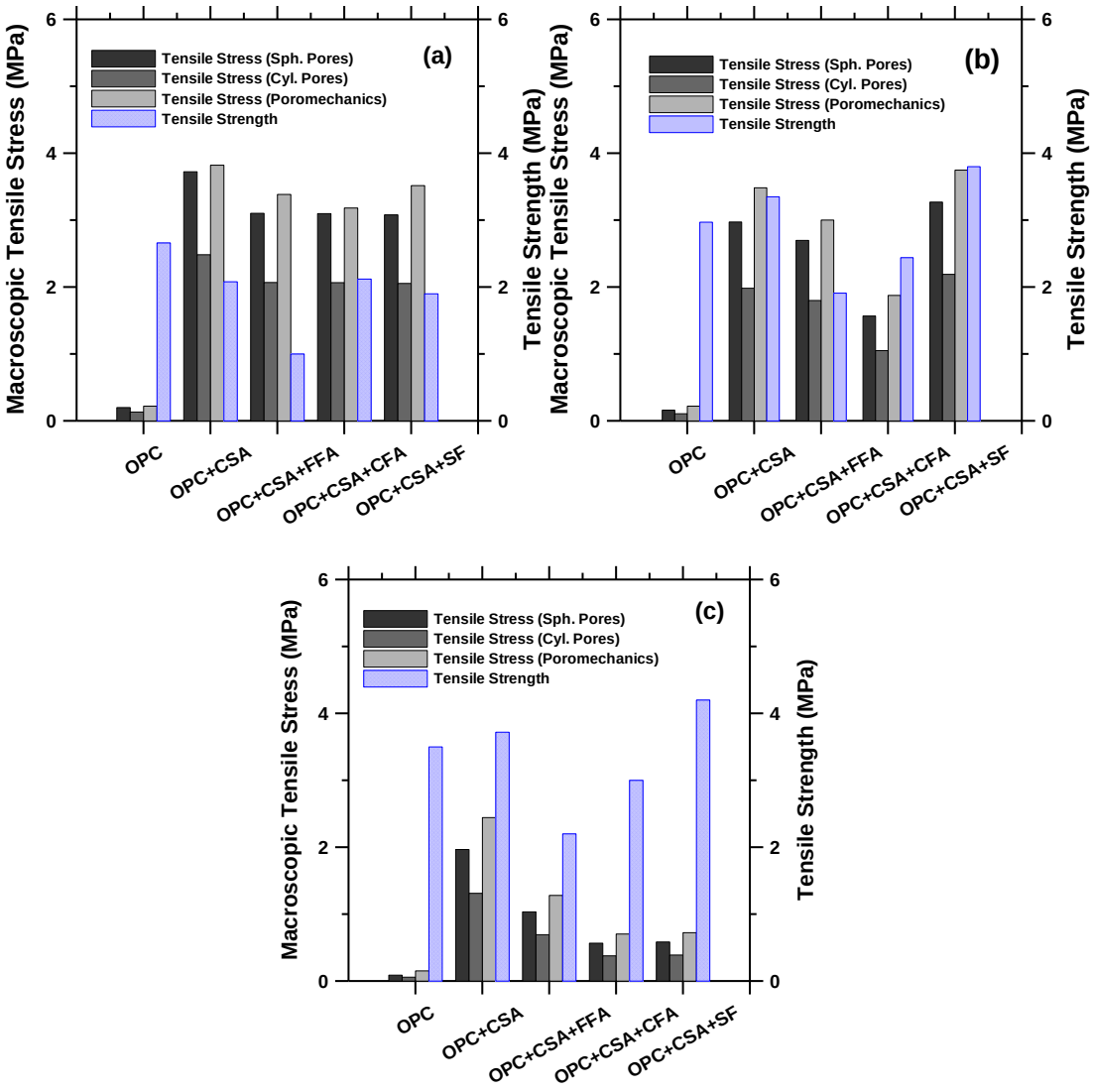


Figure 7.2 Calculation of crystallization stress in OPC-CSA-MA binders using three models and its comparison with tensile strength at the age of: a) 1 day, b) 3 days and c) 7 days

Effect of Gypsum Addition

As we have seen in earlier Chapter 5 that the gypsum addition led to an increase in the supersaturation w.r.t. ettringite, the crystallization stress was higher in samples with additional gypsum as shown in Figure 7.3. The difference in crystallization stress is evident both at 3 and 7 days but not so evident at 1 day.

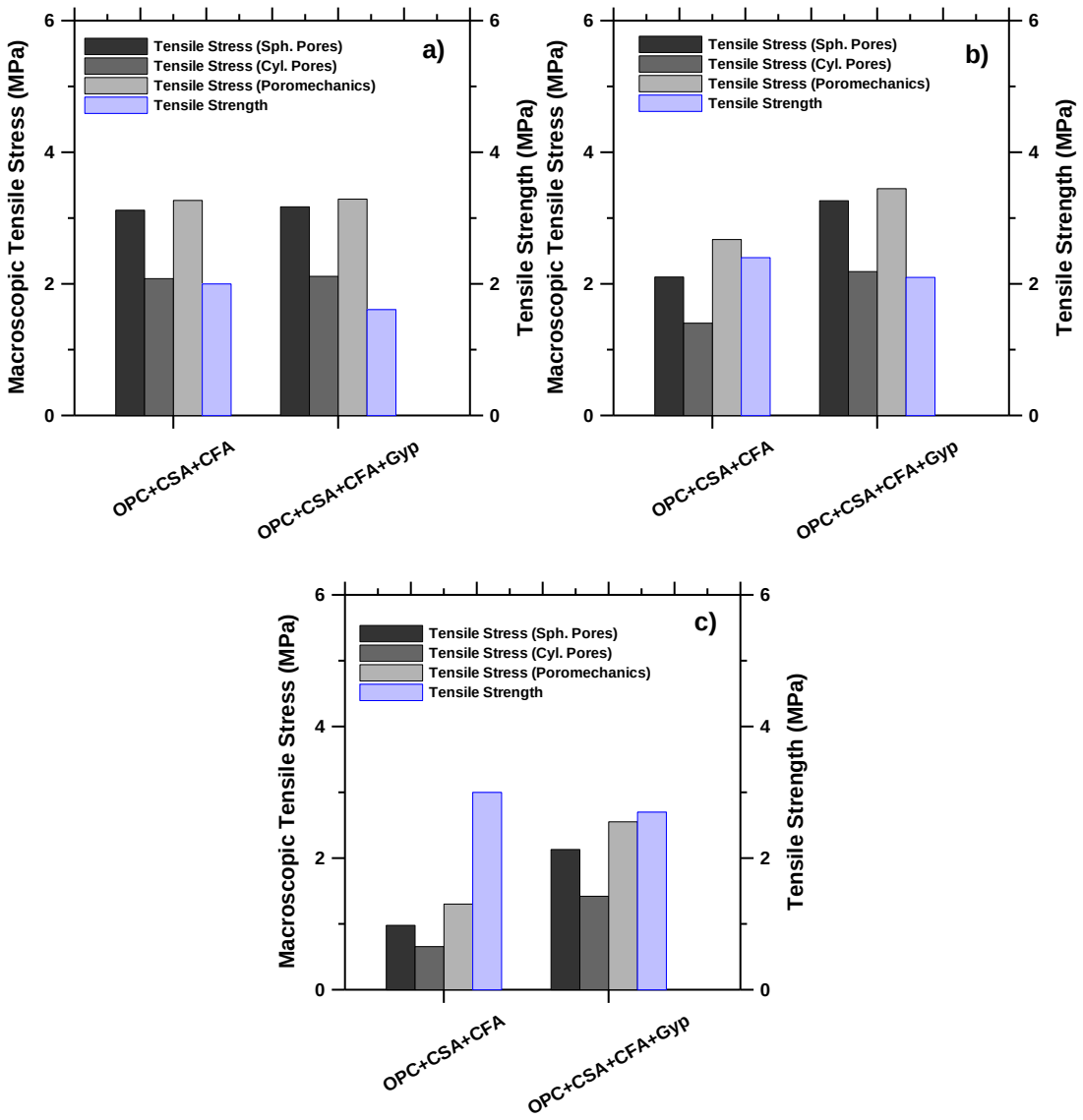


Figure 7.3 Calculation of crystallization stress in OPC-CSA-CFA binder with and without gypsum using three models at the age of: a) 1 day, b) 3 days and c) 7 days

7.2 COMPARISON BETWEEN MEASURED AND CALCULATED STRAIN

In order to compare the measured strains with the calculated strains based on the predicted crystallization stresses, a simple elastic approach was undertaken. The strain due to crystallization stress was calculated under the assumption of isotropic and homogenous material.

The longitudinal strain can be related to the crystallization stress, σ_c, according to the following equation [Mackenzie, 1950]:

$$\varepsilon = \frac{\sigma_c}{3}\left(\frac{1}{K} - \frac{1}{K_s}\right) \qquad \text{Eq. 7–1}$$

where K and K_s are the bulk modulus of a porous solid and the solid skeleton forming the porous solid, respectively. The bulk modulus (K) was calculated from dynamic modulus (E) considering Poisson's ratio of 0.2 and K_s was assumed to be 48 GPa [Grasley et al., 2007]. Figure 8 compares the measured strains with the calculated strains from 1 day through 7 days for CSA-based mixtures. It is evident that the observed strains are 3-4 times larger than the calculated elastic strains. One reason for such mismatch could be due to the assumptions made in the calculation that the strain due to crystallization is elastic. Since the expansion takes place at early-age when the cementitious matrix is still soft, the influence of early-age creep is expected to be high [Altoubat, 2000; Altoubat and Lange, 2001 a; Altoubat and Lange, 2001 b; Østergaard et al., 2001]. As evident from the Figure 7.4, the trend of calculated expansion for the Class C FA mixture matched reasonably well with the observed expansion. Furthermore, both the calculated and the measured strains for the Class C FA mixture were found to be lower than that of the other mixtures. Although the observed expansion was similar for all mixtures till 3 days, the calculated expansion of the OPC-CSA, OPC-CSA-FFA and OPC-CSA-SF mixtures were higher than that of the Class C FA mixture. Additionally, there was not much increase in the expansion the mixtures beyond 3 days based on the elastic strain calculation, however, the measured expansion was observed to increase until 7 days; particularly for the Class F FA mixture the increase was almost linear.

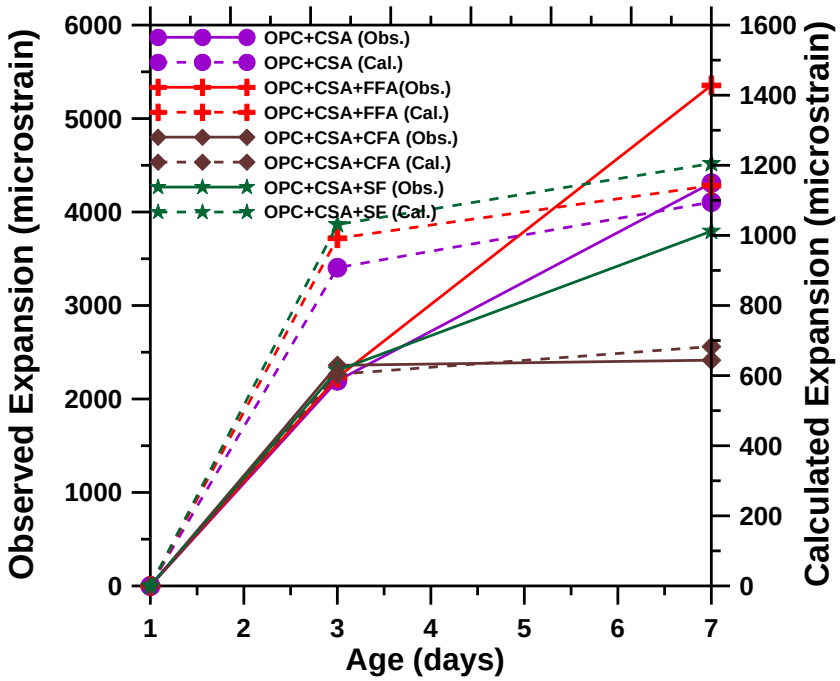


Figure 7.4 Comparison between experimental and calculated elastic strain for various OPC-CSA mixtures (bold and dashed lines represent experimental and calculated strains, respectively)

7.3 CONCLUSIONS

The main findings of this chapter can be summarized as below:

- The supersaturation w.r.t. ettringite was found to give rise to significant crystallization stress in CSA cement-based binders. At a high dosage of CSA cement, the crystallization stress exceeded the tensile strength of the OPC-CSA binder, leading to excessive cracking. Three models utilized in this study enabled a reasonable prediction of the tensile failure of the OPC-CSA binder with 30% CSA cement. The crystallization stress decreased with time due to the decrease in the supersaturation w.r.t. ettringite in the pore solution.
- A comparison between the observed and the calculated expansion showed a reasonable match in the trend however a mismatch in the magnitude of the two when the viscoelastic effects were not considered.

CHAPTER 8: EARLY-AGE BEHAVIOR OF CONCRETE

8.1 INTRODUCTION

Most experiments in this study were performed on cement paste samples which were not restrained. However, expansion of concrete in any practical application is always restrained either by internal restraint (reinforcing bars) or by external restraint (support, shear studs etc.). When expansion of expansive concrete is prevented by the presence of restraint, compressive stress, and creep under the compressive stress develop. Therefore, it is pertinent to examine the restrained expansion characteristics in order to understand the performance of expansive concretes. This chapter discusses the background and current work on restrained expansion characteristics and mechanical properties of CSA-based concrete.

8.2 BACKGROUND

8.2.1 Restrained Expansion of Concretes

The main advantage of early-age expansion occurring in expansive concrete is to induce compressive stress which counteracts the tensile stress developed due to shrinkage (Figure 1.2). The net shrinkage after a drying period is significantly smaller than that of Portland cement concrete although drying shrinkage characteristics of CSA concrete are similar to Portland cement concrete. Restraint plays a key role in effectively utilizing the CSA cements for shrinkage-compensation. Typically, there are two kinds of restraint: internal and external. Internal restraint includes the restraint offered by the reinforcement and aggregate whereas the support conditions offer the external restraint. A minimum reinforcement (0.15%) is suggested by ACI 223R-10 guide when expansive cements are utilized for shrinkage-compensation. The increase in percentage reinforcement was found to reduce the expansion with an increase in induced compressive stress [Russell, 1973; Nagataki and Yoneyama, 1973; Keeton 1973]. When

the expansion is completely prevented due to external restraint, the maximum compressive stress is induced in concrete [Russell, 1973]. In externally-restrained concrete, the rate of change in induced stress (i.e., from compressive to tensile due to shrinkage) was higher than that for internally-restrained concrete. Better shrinkage-compensation is achieved when the concrete is restrained internally, and allowed to expand [Polivka, 1973].

8.2.2 Mechanical Properties and Long-Term Creep

Compressive Strength

The strength development of CSA-based concretes has been found to be comparable to Portland cement concretes. Polivka and Willson (1973) showed that the strength of expansive concretes was higher than that of Portland cement concrete for w/cm ratio below 0.65 whereas Portland cement concretes exhibited higher strength for w/cm ratio above 0.65. In a study by Hoff (1973), the compressive strength of mortars was found to increase with increasing expansive component. Optimum performance was achieved when the expansive component was in range of 10-20%.

Long-Term Creep

There is limited data available on long-term creep of OPC-CSA concrete. Some studies have reported that the creep of OPC-CSA concrete is higher than that of the Portland cement concrete [Nagataki and Goto, 1972; Russell, 1980]. Nagataki and Goto (1972) reported an increase in creep strain with increasing expansive component under constant stress/strength ratio. Similarly, a study by Russell (1980) showed that the creep of OPC-CSA concrete was higher than that of the Portland cement concrete, although the creep test in this study was performed under constant stress condition (Figure 8.1). On the contrary, Li and Ramakrishnan (1978) reported a decrease in creep of OPC-CSA concrete compared to the Portland cement concrete.

This study was primarily focused on gap-graded concrete. Keeton (1973) also observed lower post-expansion creep and shrinkage of OPC-CSA concrete than that of the Portland cement concrete.

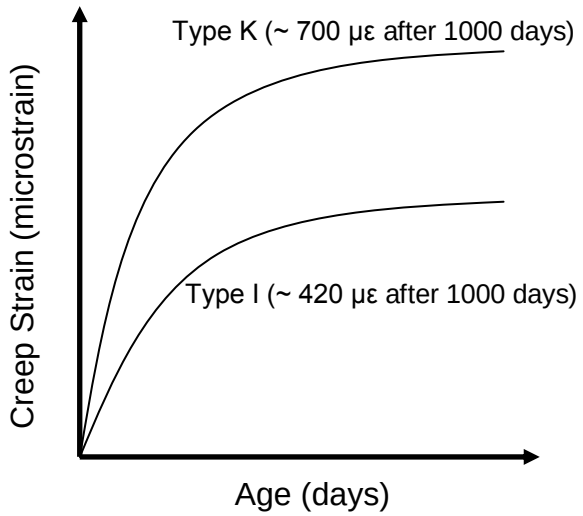


Figure 8.1 Creep properties of unreinforced specimens for 1000 days (adapted from Russell, 1980)

8.3 MIXTURE PROPORTIONS

The mixture proportions of concrete used in this study are shown in Table 8.1. All concrete mixtures had 610 lb/yd^3 of cementitious material. Fine aggregate (FA-01) and coarse aggregates (CA-07) confirming to Illinois Department of Transportation specification were utilized in the proportioning of concrete mixtures. Air entraining admixture (Micro Air from BASF) was used to maintain air content within 4-7% range.

Table 8.1 Mixture proportions of concrete

	Mix-1	Mix-2	Mix-3	Mix-4	Mix-5
Water*	268	268	268	268	268
OPC*	610	518.5	427	427	488
F FA*	0	0	91.5	0	0
C FA*	0	0	0	91.5	0
SF*	0	0	0	0	30.5
CSA Cement*	0	91.5	91.5	91.5	91.5
Fine Agg*	1130	1130	1130	1130	1130
Coarse Agg*	1826	1826	1826	1826	1826
w/cm	0.44	0.44	0.44	0.44	0.44
AEA (fl oz/cwt)**	2.0	3.2	4.1	4.3	3.7
Slump (in)	3.5	3.0	4.0	6.5	2.0
Air Content (%)	5.5	6.2	4.2	6.6	4.7

* Quantities are in lb/yd^3

** AEA – Micro Air (BASF)

8.4 METHODS

8.4.1 Restrained Expansion

Restrained expansion of expansive concrete was monitored according to ASTM C878. Concrete samples of size: 75 mm × 75 mm × 254 mm were prepared and cast in a mold shown in Figure 8.2. The steel rod placed at the center with attached end plates provides a restraint for the concrete. The samples were demolded after 6 hours, and immersed in saturated lime water for a period of 7 days. Length measurements were taken after 6 hours of casting (at demolding time) and after 7 days of saturated lime water curing. The 7-day expansion value provides useful information as it can be related to the maximum expansion experienced by a structural member in the field (as per ACI 223R-10). The test procedure was further modified to understand the drying shrinkage behavior of expansive concrete. Hence, the concrete prisms were exposed to a

drying environment of 23±2°C and 50% RH after the saturated lime water curing for 7 days. The length measurements were taken at regular intervals after exposing concrete samples to drying.

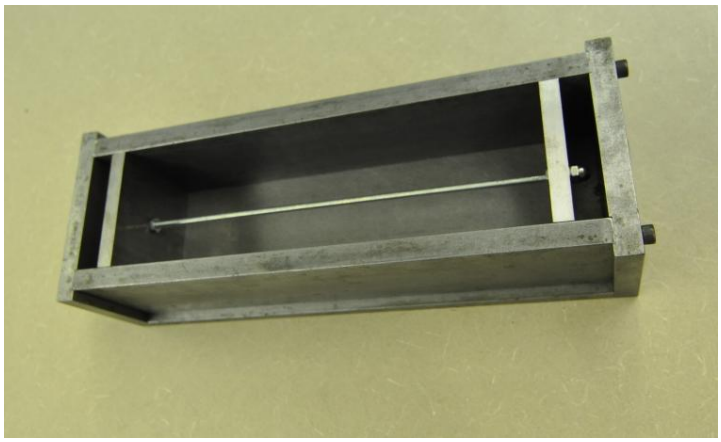


Figure 8.2 A typical mold for restrained expansion according to ASTM C878

8.4.2 Compressive Strength

Concrete samples of size 4 inch (100 mm) × 8 inch (200 mm) were prepared and cured in moist room after 24 hours of casting. Triplicate of samples were tested according to ASTM C39 for compressive strength.

8.5 RESULTS

8.5.1 Early-Age Properties

Early-age properties of CSA concrete was measured through slump test and was compared with OPC concrete. As shown in Figure 8.3, CSA concrete showed approximately 50% slump loss within 30 minutes of mixing period. The formation of ettringite crystals in CSA concrete resulted in rapid loss of slump [Quillin, 2001; Chaunsali et al., 2013 b]. Few previous studies have demonstrated the role of citric acid in retarding the hydration of CSA cement

[Mehta, 1973 c; Pelletier et al., 2010]. However, when CSA cement is used with OPC, the retarder used for OPC should be able to reduce the slump loss [Chaunsali et al., 2013 b].

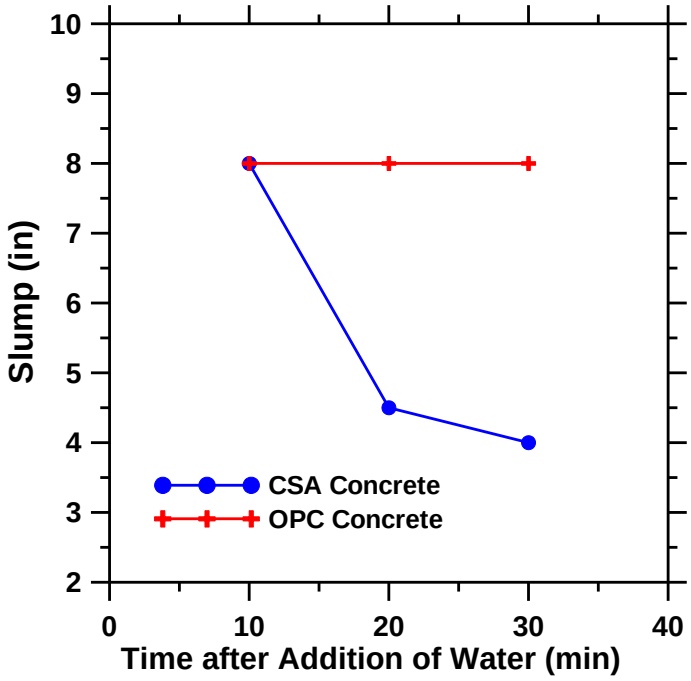
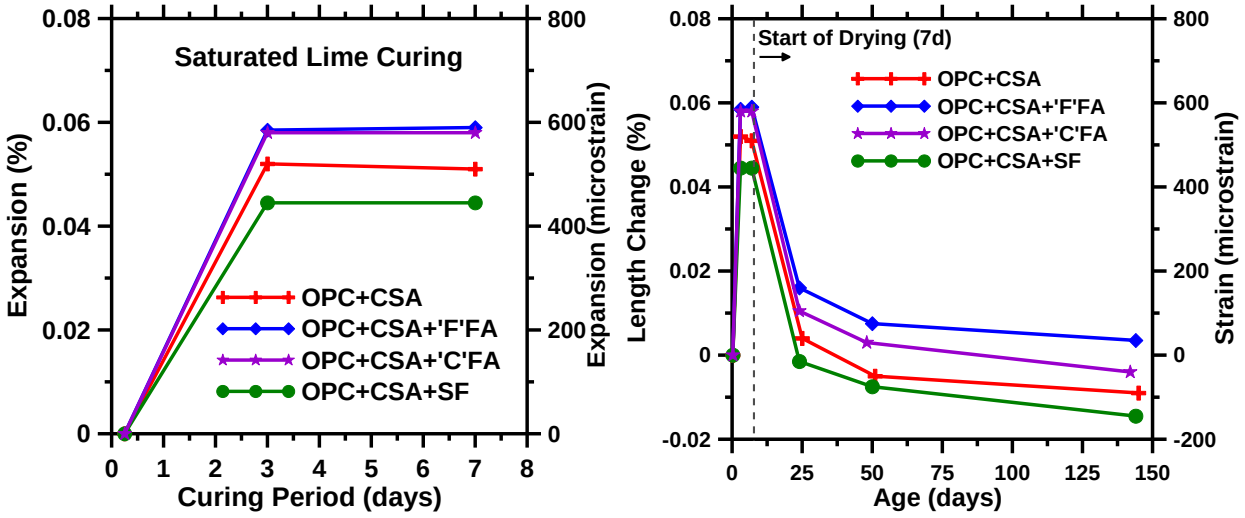


Figure 8.3 Slump loss in OPC and CSA cement concretes according to ASTM C143

8.5.2 Restrained Expansion and Shrinkage of Expansive Concretes

Figure 8.4 compares length change (expansion and shrinkage) of Portland cement concrete and CSA cement concrete. It is evident that early-age expansion reduced the shrinkage strain at later age although the amount of shrinkage is similar in plain and expansive concrete. As shown in Figure 8.4, the Class C FA and Class F FA increased the restrained expansion whereas SF reduced the expansion in CSA cement system. It is also evident that all mixtures undergo similar amount of drying shrinkage. The expansion of concrete samples was an order of magnitude lower than that of the paste samples (Figure 4.6). The reduction in expansion can be attributed to the presence of aggregate and restraint in form of reinforcing bar. The effect of

mineral admixtures on expansion behavior of OPC-CSA-MA concrete has some similarities to that of OPC-CSA-MA paste. As seen in the paste samples (Figure 4.6), Class F FA increased the expansion whereas SF reduced it. The Class C FA increased the expansion in OPC-CSA-MA concrete whereas the Class C FA reduced the expansion of OPC-CSA-MA paste.



(a) (b)

Figure 8.4 The influence of mineral admixtures on restrained expansion of CSA-based concrete: a) at early-age (7 days), and b) at later age (150 days) at w/cm – 0.44

In this study, the diameter of the reinforcing bar used in ASTM C878 was varied to examine the role of restraint on the extent of expansion. Figure 8.5 shows the effect of three levels of restraint on expansion. It is evident that the expansion of CSA concrete was twice as high in the absence of any restraint in the form of reinforcing bar. Additionally, increase in restraint by increasing the diameter of the bar decreased the expansion.

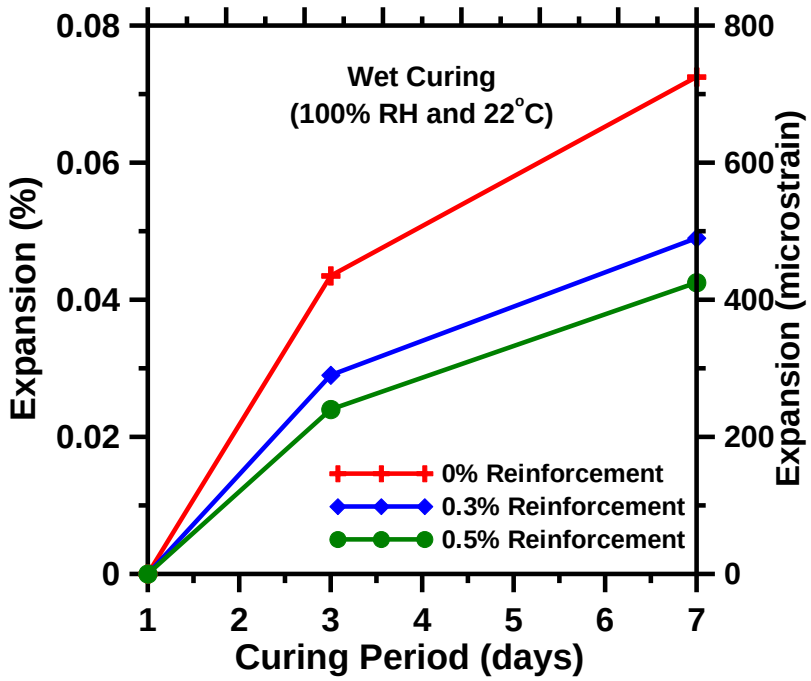


Figure 8.5 Effect of restraint on the expansion of OPC-CSA concrete (measurements started at 1 day)

8.5.3 Mechanical Properties of Expansive Concretes

Figure 8.6 compares the 28-day compressive strength of expansive concretes with ordinary Portland cement concrete. The strength of OPC-CSA concrete was similar to OPC concrete although a small increase is evident. The addition of Class F FA reduced the strength whereas SF increased the strength. The reduction in strength due to the addition of Class C FA was smaller than observed for Class F FA. It is evident that the compressive strength of CSA-based concrete was found to be similar to the Portland cement concrete at the end of 28 days [Chaunsali et al., 2013 b].

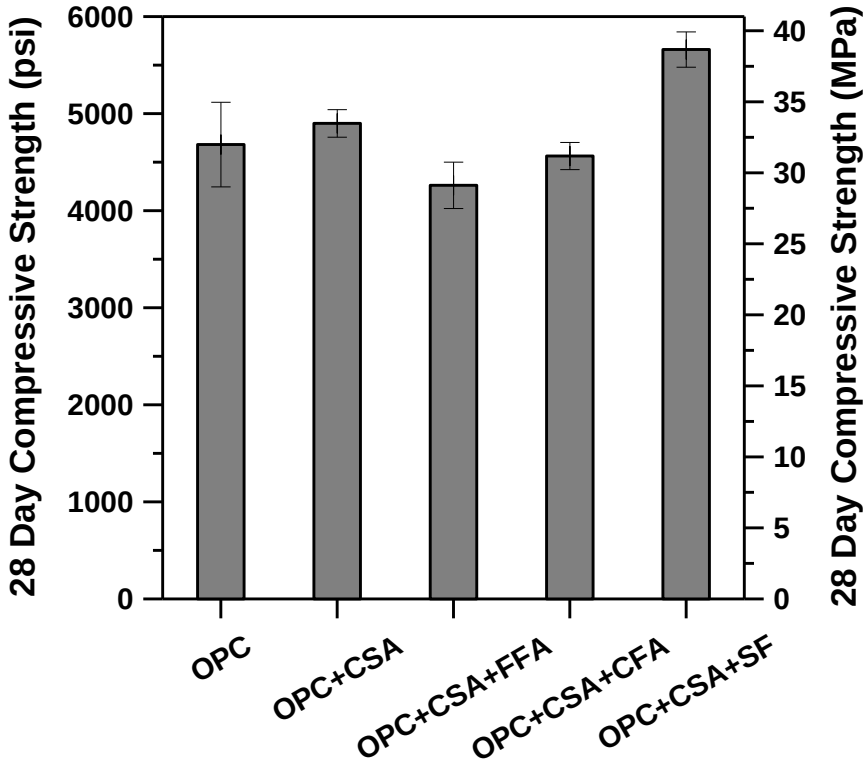


Figure 8.6 Mechanical properties of CSA-based concrete at w/cm – 0.44 (Error bars represent 1 standard deviation of three measurements)

8.6 CONCLUSIONS

The main conclusions can be summarized as below:

- CSA concrete showed a drastic loss in slump which could be attributed to the formation of ettringite crystals.
- Mineral admixtures altered the restrained expansion characteristics of CSA concrete. Class F FA and Class C FA increased the expansion whereas SF reduced its extent. There were some similarities in restrained expansion behavior of paste and concrete.
- Early-age expansion of CSA concrete was an order of magnitude lower than that of the CSA cement paste due to the presence of aggregates and reinforcing bar used for

the restrained test. Increase in percentage of reinforcement reduced the extent of expansion.

- The 28 day compressive strength of CSA concrete was found to be similar to that of the OPC concrete. The addition of Class FFA reduced the strength whereas SF increased it.

CHAPTER 9: CONCLUSIONS AND FUTURE DIRECTIONS

9.1 THESIS SUMMARY

The research summarized in this dissertation involves the investigation of early-age behavior of CSA cement-based binders with the focus on expansion mechanism, early-age expansion characteristics, and modeling the crystallization stress. The CSA cement based-binders used in this study covered a wide range of mixture proportions which included OPC-CSA and OPC-CSA-MA binders. The study validated the crystallization stress theory by showing the presence of higher supersaturation levels of ettringite, and therefore, higher crystallization stress in CSA cement-based binders. For the first time, the interaction between mineral admixtures (Class F FA, Class C FA, and SF) and OPC-CSA binder was studied. The expansion characteristics of CSA cement-based binders were found to be governed by physico-chemical factors such as material stiffness, amount of ettringite, and hydration kinetics of ye'elimite. The amount of ettringite (wt. %) which is often used to explain expansion behavior of CSA cement was found to have lower degree of correlation with expansion than the ettringite volume in given pore volume (S_c). Additionally, the study shows the importance of material stiffness in interpreting expansion as the stiffness changes rapidly at early age.

The current research showed successful application of various models in estimating macroscopic tensile stress due to crystallization, when viscoelastic effects were not considered. For the first time, the model based on poromechanics was used to calculate the macroscopic tensile stress. All models utilized in this study enabled the prediction of failure of samples incorporating high dosage of CSA cement. During the modeling effort, it was found that the viscoelastic properties of cementitious matrix need to be considered in order to improve accuracy.

9.2 PRIMARY CONCLUSIONS

The main objectives of this research were to understand early-age expansion of CSA cement-based binders, and model the crystallization stress due to the formation of ettringite crystals. The goal was achieved by monitoring physico-chemical properties of OPC-CSA and OPC-CSA-MA binders. Along the way, many significant conclusions were drawn, and are summarized below:

- Supersaturation with respect to ettringite was found to be the precursor for crystallization stress in CSA cement-based binders. The expansion at 1 day was strongly linked to saturation index with respect to ettringite at 1 day. The incremental change in expansion of all mixtures beyond 1 day has reasonable correlation with saturation index, but this correlation improved for selected mixtures (i.e., OPC-CSA binders without any MA). Higher supersaturation allows the growth of ettringite crystals in smaller pores which results in an increase in crystallization stress and possibly higher expansion.
- Dynamic modulus was found to be an important factor governing the expansion behavior beyond 1 day. The study highlights the importance of dynamic modulus in examining early-age expansion of CSA cement-based binders as the material stiffness changes considerably at early-age.
- The study reveals that the volume fraction of ettringite in total pore volume is more important factor than the ettringite weight fraction while considering the expansion potential. The results highlight a good correlation between the expansion and volume fraction of ettringite in total pore volume.
- The initial ye'elimite and total calcium sulfate contents were found to have a strong influence on the amount of ettringite and the extent of expansion at 1 day.

- Mineral admixtures were found to alter the expansion behavior of CSA cement-based binder. The expansion studies revealed that the effect of different fly ashes can be different and is influenced by their phase composition. In this study, Class C FA mixture ceased expanding beyond 2 days whereas Class F FA expanded until 5-7 days. X-ray diffraction analysis revealed that the ye'elimite was consumed earlier in Class C FA mixture due to the presence of C_3A. The expansion of Class F FA was highest among all mixtures when CSA cement content was kept constant. Class C FA and SF reduced the extent of expansion.
- The isothermal calorimetric studies highlighted the presence of an additional peak in Class C FA mixture due to early consumption of gypsum. The addition of gypsum not only resulted in disappearance of the peak, but it also increased the expansion of Class C FA mixture. The hydration rate of OPC-CSA binder was increased with the increase in temperature.
- The pore solution of CSA cement-based binders showed reduced pH in the presence of CSA cement, supporting the results of previous findings. Thermodynamic modeling enabled the estimation of saturation index with respect to ettringite which was found to decrease with time as a consequence of formation of ettringite and consumption of ye'elimite. The increase in the CSA cement and gypsum content increased the supersaturation with respect to ettringite.
- The application of various models enabled a reasonable prediction of tensile stress developed due to crystallization of ettringite. The tensile failure of OPC-CSA binder with 30% CSA cement due to excessive expansion could be predicted by all models.

- Comparison of the trend of the observed expansions (using elastic analysis) with that of the calculated expansions showed that they are in reasonably good agreement. However a mismatch between the magnitudes of the two was clear. The calculated expansion was found to be only 20-30% of the observed expansion highlighting the importance of early-age creep.
- Early-age volume change of concrete showed some resemblance to paste behavior. The effect of Class F FA and SF was similar in both paste and concrete. Due to the presence of restraint in concrete samples, the extent of expansion was reduced by an order of magnitude.

9.3 RECOMMENDATIONS FOR FUTURE WORK

The main challenge in successful application of expansive concretes is the prediction of its field performance from small-scale lab tests. Figure 9.1 describes the samples/tests used at different scale (small-to-large) in a related IDOT sponsored project. The tests on cement paste according to ASTM C1698 provide insight on unrestrained expansion characteristics but they do not consider the influence of restraint. Small-scale concrete prism test (ASTM C878) simulates the restraint present only in the form of reinforcement. Figure 9.2 also shows a large scale slab which is supposed to simulate the actual behavior of concrete in field conditions. Figure 9.2 compares the deformation characteristics of Portland cement and expansive concrete at small- and large-scale. The difference in restrained expansion levels was smaller at large-scale by an order of magnitude. This disparity in results highlights the importance of restraint (internal and external) and early-age creep in order to understand the behavior at large-scale. In light of these preliminary results, it becomes important to characterize early-age creep of CSA cement. The creep data on CSA cement is scarce in literature, and therefore, requires a better understanding

before the behavior of CSA materials can be predicted in field. In addition, most of the current research has focused on the behavior of paste samples in controlled lab environment. The main challenge lies in assessing the performance of CSA cement concrete in field conditions. The performance with respect to scaling, sulfate attack, and carbonation need to be evaluated in order for its successful implementation.

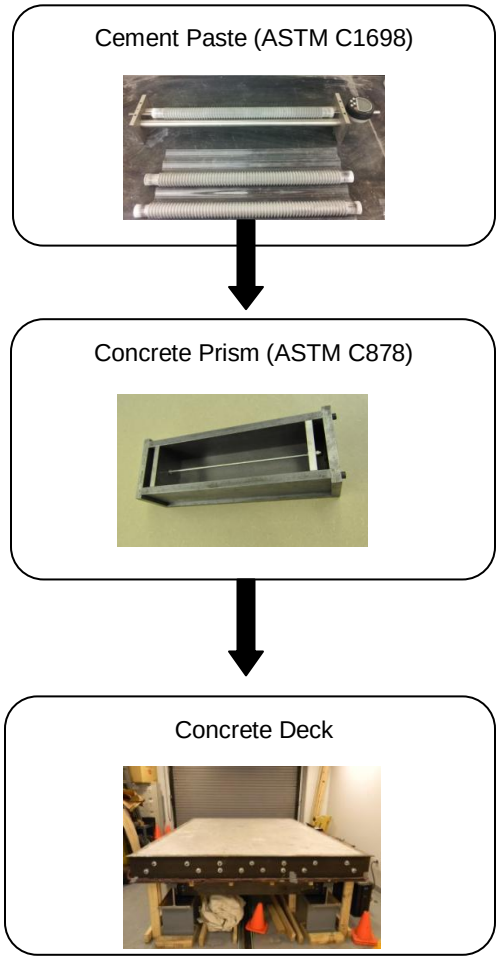
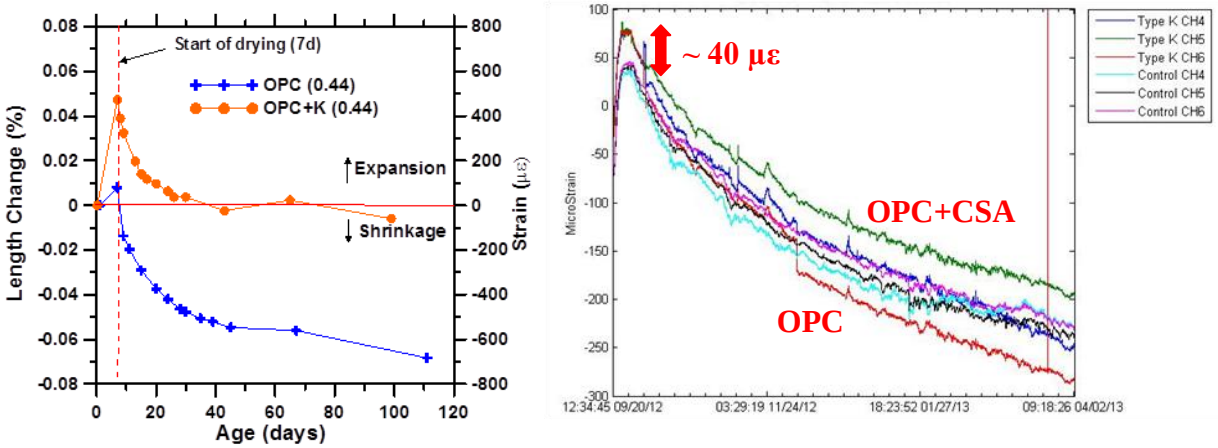


Figure 9.1 Schematic showing the small-scale and large-scale test



(a) (b)

Figure 9.2 Deformation characteristics of Portland cement and CSA-based concrete in: (a) small-scale test (ASTM C878) performed at University of Illinois, and (b) large-scale test (concrete deck) performed at St. Louis University

REFERENCES

1. ACI 223-R. Guide for the Use of Shrinkage-Compensating Concrete, American Concrete Institute. Farmington Hills. MI (2010).
2. S. A. Altoubat, Early Age Stresses and Creep-Shrinkage Interaction of Restrained Concrete, PhD Thesis. University of Illinois. 2000.
3. S. A. Altoubat, D.A. Lange, Creep, shrinkage, and cracking of restrained concrete at early age, ACI Mater. J. 98 (2001 a) 323-331.
4. S. A. Altoubat, D. A. Lange, Tensile Basic Creep: Measurements and Behavior at Early Age, ACI Mater. J. 98 (2001 b) 386-393.
5. H. Ai, J.F. Young, Mechanisms of shrinkage reduction using a chemical admixture, Proceedings of the 10th International Congress on the Chemistry of Cement, Justnes ed. Gothenburg, Sweden, 3 (1997) 18-22.
6. M. M. Ali, S. Gopal, S.K. Handoo, Studies on the formation kinetics of calcium sulphoaluminate, Cem. Concr. Res. 24 (1994) 715-720.
7. M. Andac, F. Glasser, Pore solution composition of calcium sulfoaluminate cement, Advances in cement research. 11 (1999) 23-26.
8. M. Balonis, F. P. Glasser, The density of cement phases, Cem. Concr. Res. 39 (2009) 733-739.
9. R. Barneyback Jr., S. Diamond, Expression and analysis of pore fluids from hardened cement pastes and mortars, Cem. Concr. Res. 11 (1981) 279-285.
10. A. Bentur, S. Igarashi, K. Kovler, Prevention of autogenous shrinkage in high-strength concrete by internal curing using wet lightweight aggregates, Cem. Concr. Res. 31 (2001) 1587-1591.

11. A. Bentur, M. Ish-Shalom, Properties of type K expansive cement of pure components IV. hydration of mixtures of C_3S with pure expansive component, Cem. Concr. Res. 5 (1975) 597-606.
12. D.P. Bentz, M.R. Geiker, K.K. Hansen, Shrinkage-reducing admixtures and early-age desiccation in cement pastes and mortars, Cem. Concr. Res. 31 (2001) 1075-1085.
13. D.P. Bentz, O.M. Jensen, Mitigation strategies for autogenous shrinkage cracking, Cem. Concr. Comp. 26 (2004) 677-685.
14. N. Berke, M. Dallaire, M. Hicks, A. Kerkar, New developments in shrinkage-reducing admixtures, ACI Special Publication. 173 (1997).
15. J. Beretka, B. de Vito, L. Santoro, N. Sherman, G.L. Valenti, Hydraulic behaviour of calcium sulfoaluminate-based cements derived from industrial process wastes, Cem. Concr. Res. 23 (1993) 1205-1214.
16. J. Beretka, M. Marroccoli, N. Sherman, G.L. Valenti, Influence of C_4A_3S content and W/S ratio on the performance of calcium sulfoaluminate-based cements, Cem. Concr. Res. 26 (1996) 1673-1681.
17. M. Bianchi, F. Canonico, L. Capelli, M. Pace, A. Telesca, G. Valenti, Hydration Properties of Calcium Sulfoaluminate-Portland Cement Blends, ACI Special Publication. 261 (2009).
18. J. Bizzozero, C. Gosselin, K.L. Scrivener, Expansion mechanisms in calcium aluminate and sulfoaluminate systems with calcium sulfate, Cem. Concr. Res. 56 (2014) 190-202.
19. J. Bizzozero, Hydration and dimensional stability of calcium aluminate cement based systems, PhD Thesis. École Polytechnique Fédérale de Lausanne. (2014) Switzerland.

20. J.W. Bullard, H.M. Jennings, R.A. Livingston, A. Nonat, G.W. Scherer, J.S. Schweitzer, K.L. Scrivener, J.J. Thomas, Mechanisms of cement hydration, Cem. Concr. Res. 41 (2011) 1208-1223.

21. S. Brunauer, D. Kantro, L.E. Copeland, The stoichiometry of the hydration of β-dicalcium silicate and tricalcium silicate at room temperature, J. Am. Chem. Soc. 80 (1958) 761-767.

22. J.W. Cahn, Surface stress and the chemical equilibrium of small crystals—I. The case of the isotropic surface, Acta Metallurgica. 28 (1980) 1333-1338.

23. T. Chappex, K. Scrivener, Alkali fixation of C–S–H in blended cement pastes and its relation to alkali silica reaction, Cem. Concr. Res. 42 (2012) 1049-1054.

24. P. Chaunsali, S. Lim, P. Mondal, D. H. Tobias, D. H. Tobias, Factors Influencing the Early-Age Volume Change of Expansive Cements Relevant for Bridge Deck Concrete, Trans. Res. Board 92nd Annual Meeting [13-3748] (2013 a).

25. P. Chaunsali, S. Lim, P. Mondal, D. Foutch, D. Richardson, Y. Tung, R. Hindi, Bridge Decks: Mitigation of Cracking and Increased Durability, Illinois Center for Transportation Report FHWA-ICT-13-023 (2013 b).

26. P. Chaunsali, P. Mondal, Early-Age Volume Change and Hydration of Expansive Cements, 10th fib International PhD Symposium, Quebec City (2014) 117-122.

27. P. Chaunsali, P. Mondal, Influence of Mineral Admixtures on Early-Age Behavior of Calcium Sulfoaluminate Cement, ACI Mat. J. 112 (2015) 59-68.

28. I.A. Chen, C.W. Hargis, M.C. Juenger, Understanding expansion in calcium sulfoaluminate–belite cements, Cem. Concr. Res. 42 (2012) 51-60.

29. I.A. Chen, M.C.G. Juenger, Synthesis and hydration of calcium sulfoaluminate-belite cements with varied phase compositions, J. Mater. Sci. 46 (2011) 2568-2577.

30. M.D. Cohen, Theories of Expansion in Sulfoaluminate Type Expansive Cements: Schools of thought, Cem. Concr. Res. 13 (1983) 809-818.

31. M. Collepardi, R. Turriziani, A. Marcialis, Paste hydration of $4CaO.3Al_2O_3.SO_3$ in presence of calcium sulphate, tricalcium silicate and dicalcium silicate, Cem. Concr. Res. 2 (1972) 213-223.

32. C.W. Correns, Growth and dissolution of crystals under linear pressure, Discuss. Faraday Soc. 5 (1949) 267-271.

33. O. Coussy, Poromechanics of freezing materials, J. Mech. Phys. Solids. 53 (2005) 1689-1718.

34. O. Coussy, Poromechanics, John Wiley & Sons, 2004.

35. M. D'Ambrosia, S. Altoubat, C. Park, D. Lange, Early age tensile creep and shrinkage of concrete with shrinkage reducing admixtures, Creep, Shrinkage, and Durability Mechanics of Concrete and Other Quasi-Brittle Materials, ed., Ulm, FJ, Bazant, ZP, and Wittman, FH, Elsevier, August. (2001) 685-690.

36. D. Damidot, B. Lothenbach, D. Herfort, F. Glasser, Thermodynamics and cement science, Cem. Concr. Res. 41 (2011) 679-695.

37. J.S. Damtoft, J. Lukasik, D. Herfort, D. Sorrentino, E.M. Gartner, Sustainable development and climate change initiatives, Cem. Concr. Res. 38 (2008) 115-127.

38. R.L. Day, B.K. Marsh, Measurement of porosity in blended cement pastes, Cem. Concr. Res. 18 (1988) 63-73.

39. S. Diamond, Effects of two Danish fly ashes on alkali contents of pore solutions of cement-fly ash pastes, Cem. Concr. Res. 11 (1981) 383-394.

40. A. De La Torre, S. Bruque, M. Aranda, Rietveld quantitative amorphous content analysis, J. Appl. Crystallogr. 34 (2001) 196-202.
41. T. Desbois, R. Le Roy, A. Pavoine, G. Platret, A. Feraille, A. Alaoui, Effect of gypsum content on sulfoaluminate mortars stability, European Journal of Environmental and Civil Engineering. 14 (2010) 579-597.
42. F. Deschner, F. Winnefeld, B. Lothenbach, S. Seufert, P. Schwesig, S. Dittrich, F. Goetz-Neunhoeffer, J. Neubauer, Hydration of Portland cement with high replacement by siliceous fly ash, Cem. Concr. Res. 42 (2012) 1389-1400.
43. R.M. Espinosa-Marzal, A. Hamilton, M. McNall, K. Whitaker, G.W. Scherer, The chemomechanics of crystallization during rewetting of limestone impregnated with sodium sulfate, J. Mater. Res. 26 (2011) 1472-1481.
44. W. Fajun, M.W. Grutzeck, D.M. Roy, The retarding effects of fly ash upon the hydration of cement pastes: The first 24 hours, Cem. Concr. Res. 15 (1985) 174-184.
45. C. Famy, K. Scrivener, A. Atkinson, A. Brough, Influence of the storage conditions on the dimensional changes of heat-cured mortars, Cem. Concr. Res. 31 (2001) 795-803.
46. R.J. Flatt, F. Caruso, A.M.A. Sanchez, G.W. Scherer, Chemo-mechanics of salt damage in stone, Nature communications. 5 (2014).
47. R.J. Flatt, G.W. Scherer, Thermodynamics of crystallization stresses in DEF, Cem. Concr. Res. 38 (2008) 325-336.
48. K.J. Folliard, M. Ohta, E. Rathje, P. Collins, Influence of mineral admixtures on expansive cement mortars, Cem. Concr. Res. 24 (1994) 424-432.
49. H. Freundlich, Colloid and chemistry, Methuen London. (1926).

50. M. García-Maté, A.G. De la Torre, L. León-Reina, M.A.G. Aranda, I. Santacruz, Hydration studies of calcium sulfoaluminate cements blended with fly ash, Cem. Concr. Res. 54 (2013) 12-20.

51. E. Gartner, Industrially interesting approached to "low-CO_2" cements, Cem. Concr. Res. 34 (2004) 1489-1498.

52. D. Gastaldi, F. Canonico, L. Capelli, L. Bianchi, M. Pace, A. Telesca, G. Valenti, Hydraulic behaviour of calcium sulfoaluminate cement alone and in mixture with Portland cement, Proc. 13th Int. Congr. Chem. Cem. Madrid. Spain. (2011).

53. S. Ghabezloo, J. Sulem, S. Guédon, F. Martineau, J. Saint-Marc, Poromechanical behaviour of hardened cement paste under isotropic loading, Cem. Concr. Res. 38 (2008) 1424-1437.

54. F.P. Glasser, L. Zhang, High-performance cement matrices based on calcium sulfoaluminate–belite compositions, Cem. Concr. Res. 31 (2001) 1881-1886.

55. Z.C. Grasley, G.W. Scherer, D.A. Lange, J.J. Valenza, Dynamic pressurization method for measuring permeability and modulus: II. cementitious materials, Mater. Struct. 40 (2007) 711-721.

56. G.C. Hoff, The use of expansive cements in large sections of grout and mortar, ACI Special Publication. 38 (1973) 299-340.

57. M.C.G. Juenger, F. Winnefeld, J. L. Provis, J.H. Ideker, Advances in alternative cementitious binders, Cem. Concr. Res. 41 (2011) 1232-1243.

58. V. Kasselouri, P. Tsakiridis, C. Malami, B. Georgali, C. Alexandridou, Study on the hydration products of a non-expansive sulfoaluminate cement, Cem. Concr. Res. 25 (1995) 1726-1736.

59. J.R. Keeton, Thin Shells Expansive Cement Concretes, ACI Special Publication. 38 (1973).

60. A. Klein, C. Troxell, Studies of calcium sulfoaluminate admixtures for expansive cements, 58 (1958) 986-1008.

61. A. Klein, T. Karby, M. Polivka, Properties of an expansive cement for chemical prestressing, ACI J. Proc. 58 (1961) 59-62.

62. D.A. Kulik, T. Wagner, S.V. Dmytrieva, G. Kosakowski, F.F. Hingerl, K.V. Chudnenko, U.R. Berner, GEM-Selektor geochemical modeling package: revised algorithm and GEMS3K numerical kernel for coupled simulation codes, Computational Geosciences. 17 (2013) 1-24.

63. W. Kunther, B. Lothenbach, K.L. Scrivener, On the relevance of volume increase for the length changes of mortar bars in sulfate solutions, Cem. Concr. Res. 46 (2013) 23-29.

64. W. Kurdowski, A. Thiel, On the role of free calcium oxide in expansive cements, Cem. Concr. Res. 11 (1981) 29-40.

65. G. Le Saoût, B. Lothenbach, A. Hori, T. Higuchi, F. Winnefeld, Hydration of Portland cement with additions of calcium sulfoaluminates, Cem. Concr. Res. 43 (2013) 81-94.

66. C. Lobo, A study of type K expansive cement paste and concrete and the influence of silica fume, PhD Thesis. Purdue University. (1991) USA.

67. C. Lobo, M.D. Cohen, Hydration of type K expansive cement paste and the effect of silica fume: II. Pore solution analysis and proposed hydration mechanism, Cem. Concr. Res. 23 (1993) 104-114.

68. B. Lothenbach, Thermodynamic equilibrium calculations in cementitious systems, Mater. Struct. 43 (2010) 1413-1433.

69. B. Lothenbach, T. Matschei, G. Möschner, F.P. Glasser, Thermodynamic modelling of the effect of temperature on the hydration and porosity of Portland cement, Cem. Concr. Res. 38 (2008) 1-18.

70. S. T. Li, V. Ramakrishnan, Expansion-Shrinkage, Creep, and Elastic-Modulus of Shrinkage-Compensating Gap-Graded Concrete, J. Am. Conc. Inst. 77 (4) (1980) 292-292.

71. P. Lura, D.P. Bentz, D.A. Lange, K. Kovler, A. Bentur, K. van Breugel, Measurement of water transport from saturated pumice aggregates to hardening cement paste, Mater. Struct. 39 (2006) 861-868.

72. B. Mather, A discussion of the paper "theories of expansion in sulfoaluminate-type expansive cements: Schools of thought," by M.D. Cohen, Cem. Concr. Res. 14 (1984) 603-609.

73. T. Matschei, B. Lothenbach, F.P. Glasser, Thermodynamic properties of Portland cement hydrates in the system $CaO–Al_2O_3–SiO_2–CaSO_4–CaCO_3–H_2O$, Cem. Concr. Res. 37 (2007) 1379-1410.

74. P. K. Mehta, A. Klein, Investigations on the Hydration Products in System $4CaO.3Al_2O_3.SO_3$-$CaSO_4$-CaO-H_2O, Special Report-National Research Council. Highway Research Board. (1966) 328-352.

75. P. K. Mehta, Expansion Characteristics of Calcium Sulfoaluminate Hydrates, J. Am. Ceram. Soc. 50 (1967) 204-208.

76. P. K. Mehta, Mechanism of Expansion Associated with Ettringite Formation, Cem. Concr. Res. 3 (1973 a) 1-6.

77. P. K. Mehta, Effect of Lime on Hydration of Pastes Containing Gypsum and Calcium Aluminates or Calcium Sulfoaluminate, J. Am. Ceram. Soc. 56 (1973 b) 315-319.

78. P. K. Mehta, Studies of Slump Loss in Expansive Cement Concretes, ACI Sp. Pub. 38 (1973 c) 57-68.

79. P. K. Mehta, Scanning Electron Micrographic Studies of Ettringite Formation, Cem. Concr. Res. 6 (1976) 169-182.

80. P. K. Mehta, F. Hu, Further evidence for expansion of ettringite by water adsorption, J. Am. Ceram. Soc. 61 (1978) 179-181.

81. P. K. Mehta, Investigations on energy-saving cements, World cement technology. 11 (1980) 166-177.

82. D. Min, T. Mingshu, Formation and expansion of ettringite crystals, Cem. Concr. Res. 24 (1994) 119-126.

83. S. Nagataki, K. Yoneyama, Studies on Continuously Reinforced Concrete and Prestressed Concrete Pavements Made with Expansive Cement Concrete, ACI Sp. Pub. 38 (1973).

84. A. Negro, A. Bachiorrini, Expansion associated with ettringite formation at different temperatures, Cem. Concr. Res. 12 (1982) 677-684.

85. L. Østergaard, D. A. Lange, S. A. Altoubat, H. Stang, Tensile basic creep of early-age concrete under constant load. Cem. Concr. Res. 31 (2001) 1895-1899.

86. W. Nocun-Wczelik, A. Bochenek, M. Migda, Calorimetry and other methods in the studies of expansive cement hydrating mixtures, J. Therm. Anal. Calorim. 109 (2012) 529-535.

87. I. Odler, Special inorganic cements. CRC Press, 2003.

88. I. Odler, J. Colan-Subauste, Investigations on cement expansion associated with ettringite formation, Cem. Concr. Res. 29 (1999) 731-735.

89. L. Pelletier, F. Winnefeld, B. Lothenbach, The ternary system Portland cement–calcium sulphoaluminate clinker–anhydrite: hydration mechanism and mortar properties, Cem. Concr. Comp. 32 (2010) 497-507.

90. M. Polivka, Factors influencing expansion of expansive cement concretes, ACI Sp. Pub. 38 (1973) 239-250.

91. M. Polivka, C. Willson, Properties of Shrinkage-Compensating Concretes, ACI Sp. Pub. 38 (1973) 227-237.

92. K. Quillin, Performance of belite-sulfoaluminate cements, Cem. Concr. Res. 31 (2001) 1341-1349.

93. H. Rietveld, A profile refinement method for nuclear and magnetic structures, J. App. Crystallogr. 2 (1969) 65-71.

94. D. Rothstein, J.J. Thomas, B.J. Christensen, H.M. Jennings, Solubility behavior of Ca-, S-, Al-, and Si-bearing solid phases in Portland cement pore solutions as a function of hydration time, Cem. Concr. Res. 32 (2002) 1663-1671.

95. H. Russell, Design of Shrinkage-Compensating Concretes Slabs, ACI Sp. Pub. 38 (1973) 193-226.

96. H. Russell, Performance of Shrinkage-Compensating Concretes in Slabs, ACI Sp. Pub. 64 (1980) 81-114.

97. S. Sahu, J. Havlica, V. Tomková, J. Majling, Hydration behaviour of sulphoaluminate belite cement in the presence of various calcium sulphates, Thermochim. Acta. 175 (1991) 45-52.

98. G. Sant, F. Rajabipour, P. Lura, J. Weiss, Examining residual stress development in cementitious materials experiencing an early-age expansion, Proc., 9th CANMET-ACI Int. Conf.—T.C. Holland Symp. (2007) 21–29.

99. G.W. Scherer, Stress from crystallization of salt, Cem. Concr. Res. 34 (2004) 1613-1624.

100. N. Sherman, J. Beretka, L. Santoro, G.L. Valenti, Long-term behaviour of hydraulic binders based on calcium sulfoaluminate and calcium sulfosilicate, Cem. Concr. Res. 25 (1995) 113-126.

101. M. Steiger, Crystal growth in porous materials—I: The crystallization pressure of large crystals, J. Cryst. Growth. 282 (2005) 455-469.

102. L. Struble, T. Y. Kim, H. Zhang, Setting of Cement and Concrete, Cem. Concr. Aggr. 23 (2001) 88-93.

103. H.F. Taylor, Cement Chemistry, Thomas Telford, 1997.

104. S. Taber, The growth of crystals under external pressure, Am. J. Sci. (1916) 532-556.

105. S. Timoshenko, J. N. Goodier, Theory of elasticity, Hill Book Co. (1970) New York.

106. G. Valenti, L. Santoro, R. Garofano, High-temperature synthesis of calcium sulphoaluminate from phosphogypsum, Thermochim. Acta. 113 (1987) 269-275.

107. T. Wagner, D.A. Kulik, F.F. Hingerl, S.V. Dmytrieva, GEM-Selektor geochemical modeling package: TSolMod library and data interface for multicomponent phase models, The Canadian Mineralogist. 50 (2012) 1173-1195.

108. F. Winnefeld, S. Barlag, Calorimetric and thermogravimetric study on the influence of calcium sulfate on the hydration of ye'elimite, J. Therm. Anal. Calorim. 101 (2010) 949-957.

109. F. Winnefeld, B. Lothenbach, Hydration of calcium sulfoaluminate cements - Experimental findings and thermodynamic modelling, Cem. Concr. Res. 40 (2010) 1239-1247.

110. W. J. Weiss, Early-Age Shrinkage Cracking in Concrete, PhD Thesis. Northwestern University. (1999) USA.

111. L. Zhang, Microstructure and Performance of Calcium Sulfoaluminate Cements, PhD Thesis. University of Aberdeen. (2000) Scotland.

112. L. Zhang, G. W. Scherer, Comparison of methods for arresting hydration of cement, Cem. Concr. Res. 41 (2011) 1024–1036.

113. http://www.panalytical.com/Xray-diffraction-software/HighScore.htm

114. http://gems.web.psi.ch/

APPENDIX A. RIETVELD REFINEMENT OF OPC-CSA BINDERS

This section provides the Rietveld refinement of OPC-CSA binders using HighScore Plus. The phase composition of samples interground with TiO_2 (15% by wt.) is plotted and shown below:

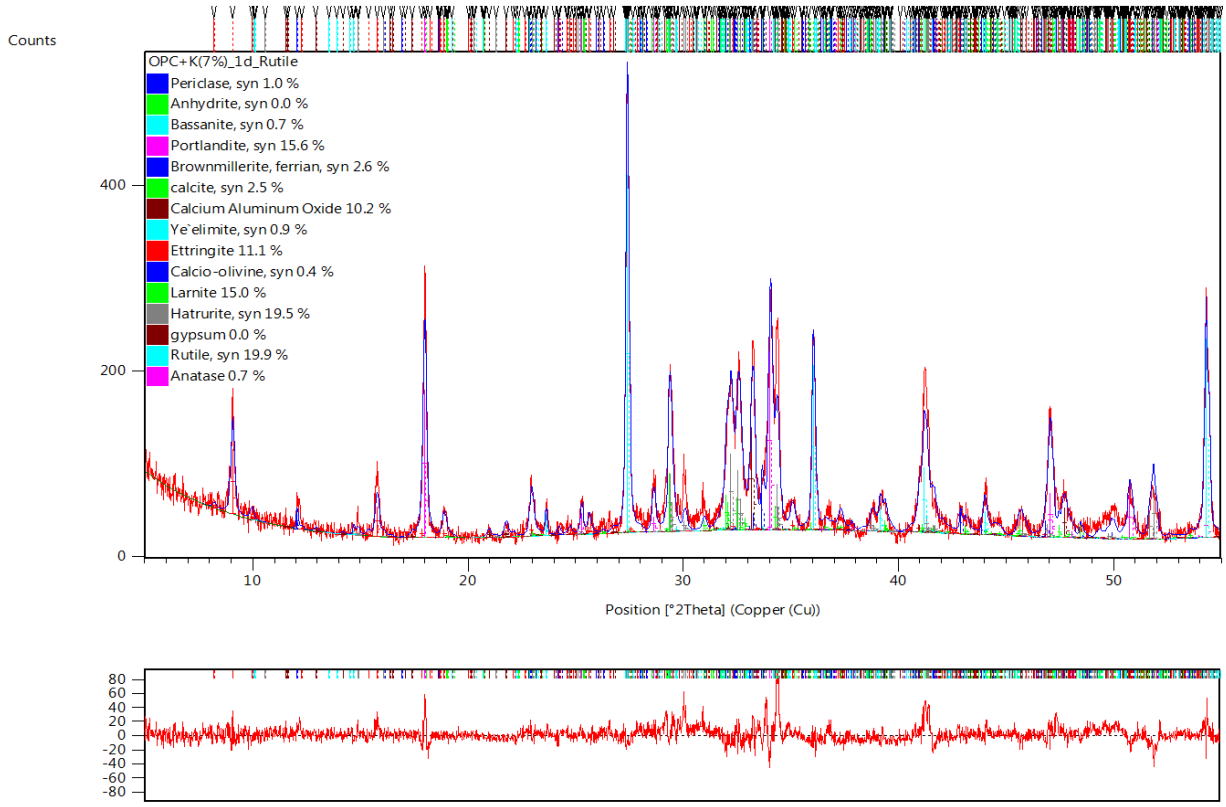


Figure A.1 Rietveld refinement of hydrated OPC-CSA binder with 7% CSA cement after 1 day

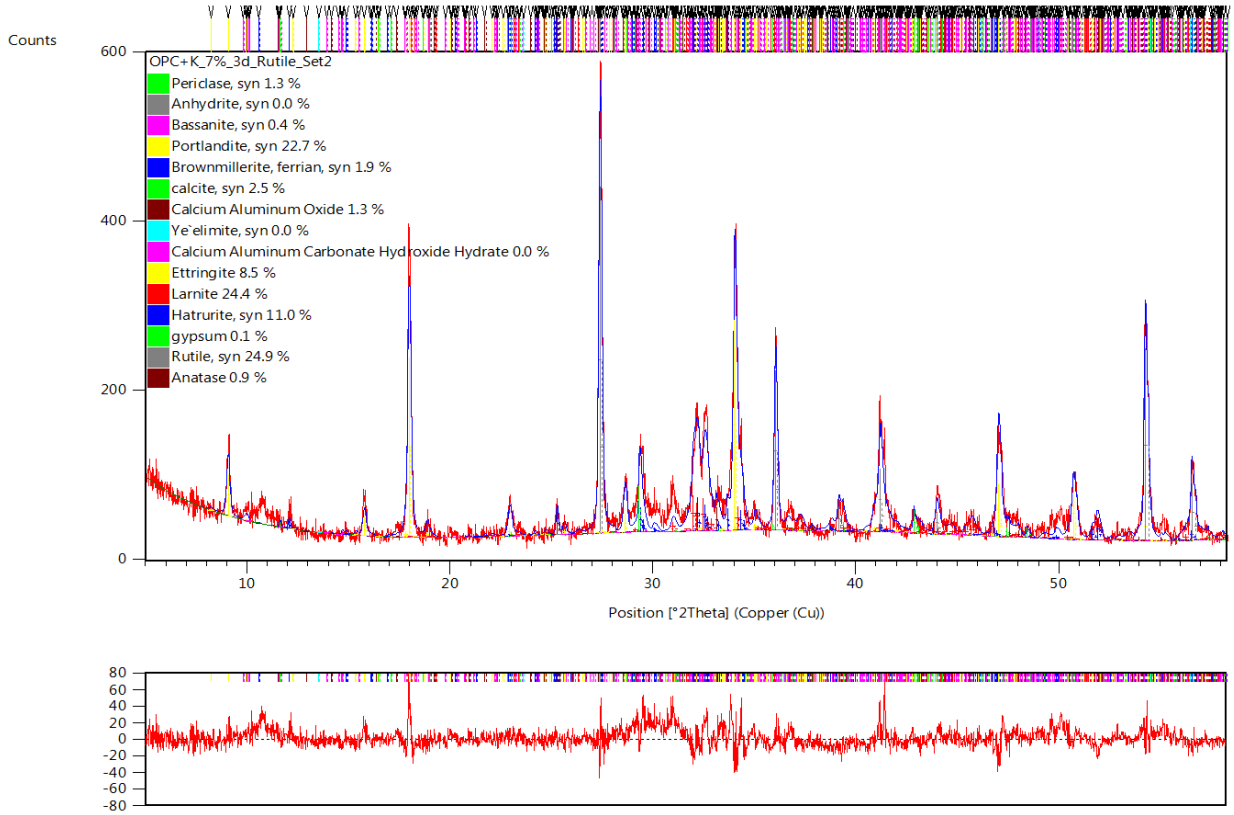


Figure A.2 Rietveld refinement of hydrated OPC-CSA binder with 7% CSA cement after 3 days

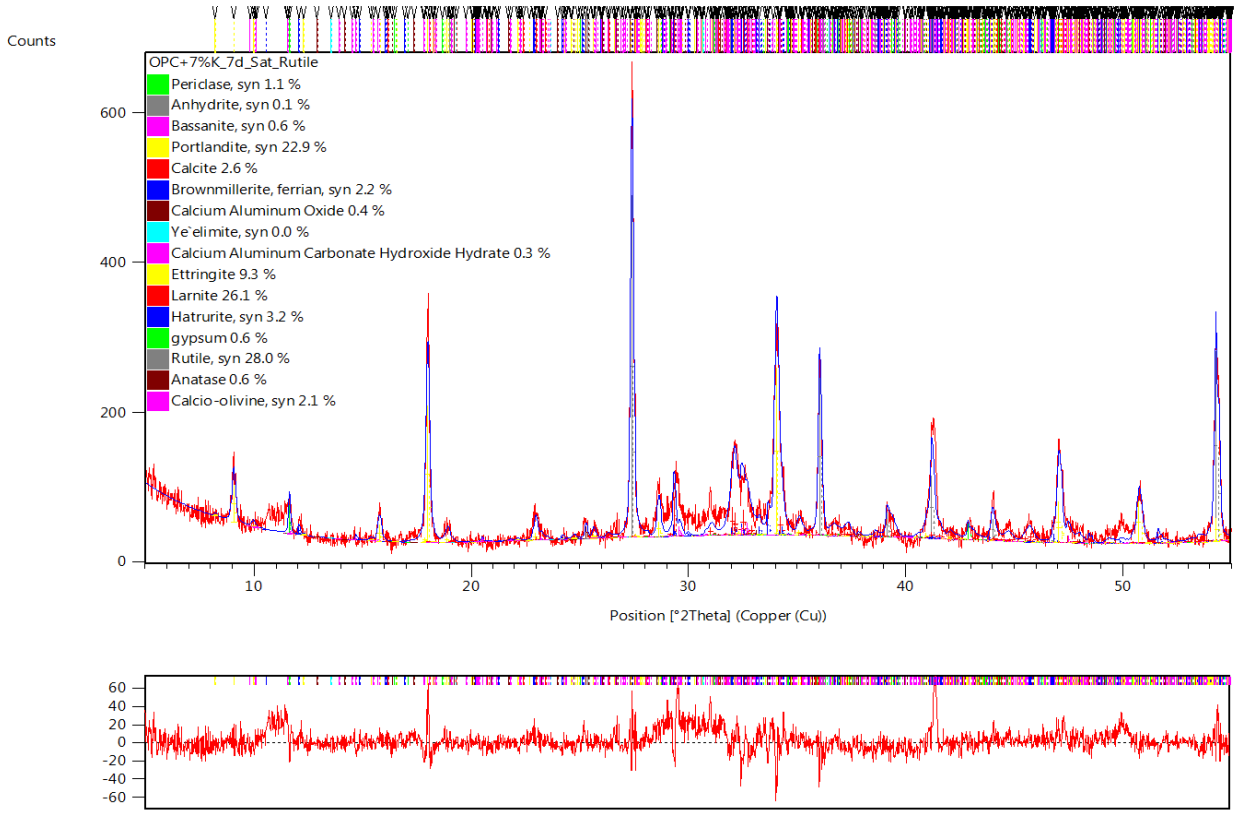


Figure A.3 Rietveld refinement of hydrated OPC-CSA binder with 7% CSA cement after 7 days

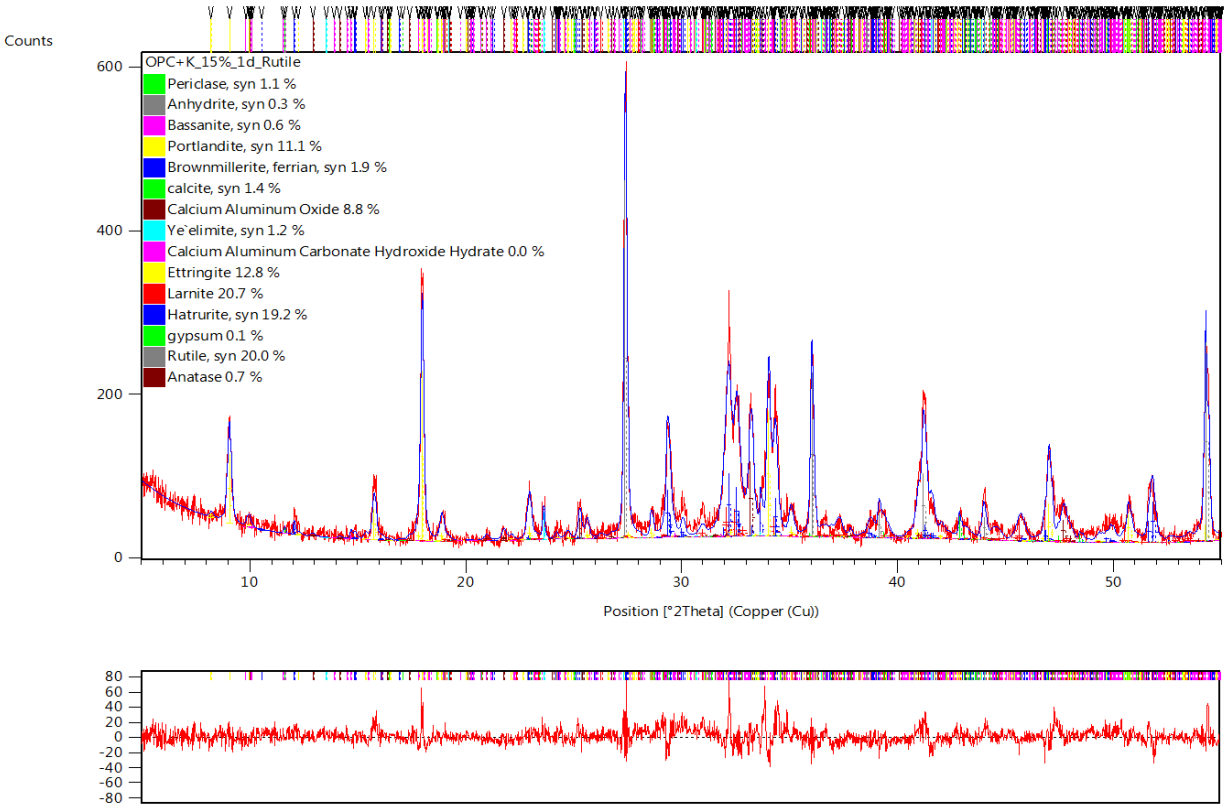


Figure A.4 Rietveld refinement of hydrated OPC-CSA binder with 15% CSA cement after 1 day

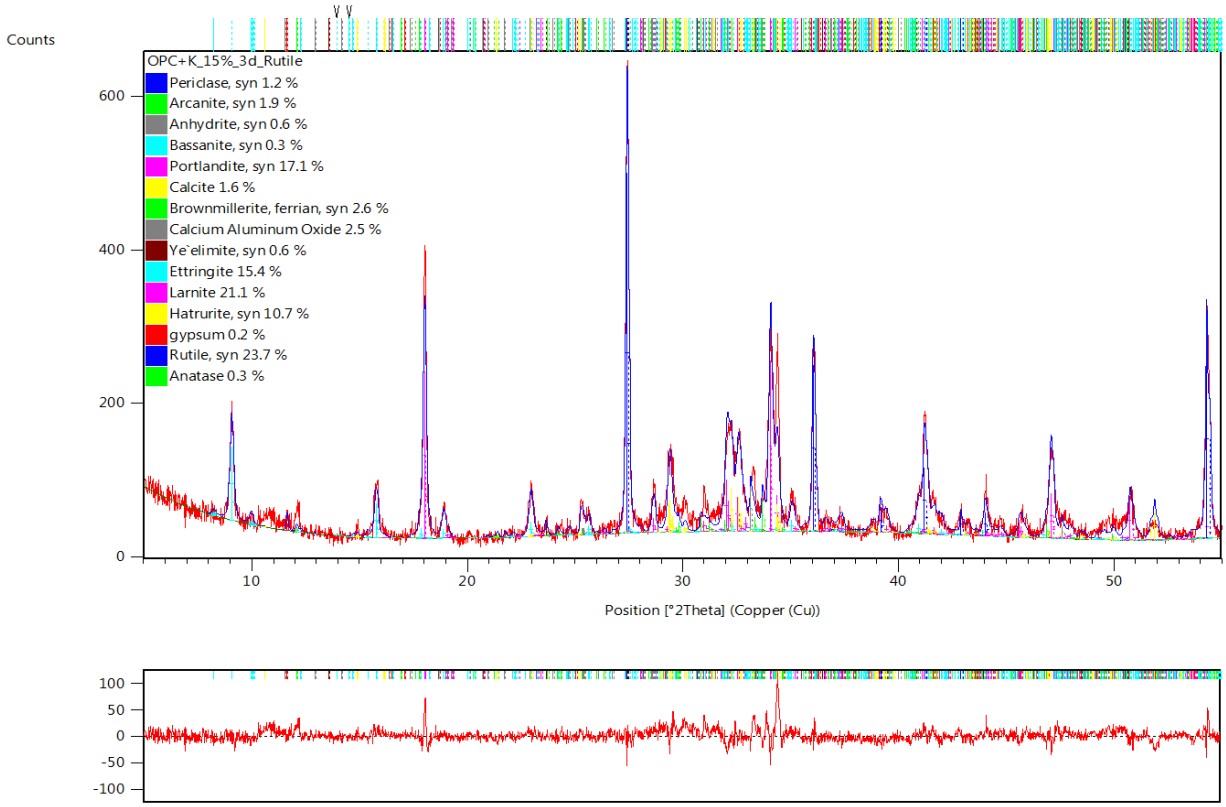


Figure A.5 Rietveld refinement of hydrated OPC-CSA binder with 15% CSA cement after 3 days

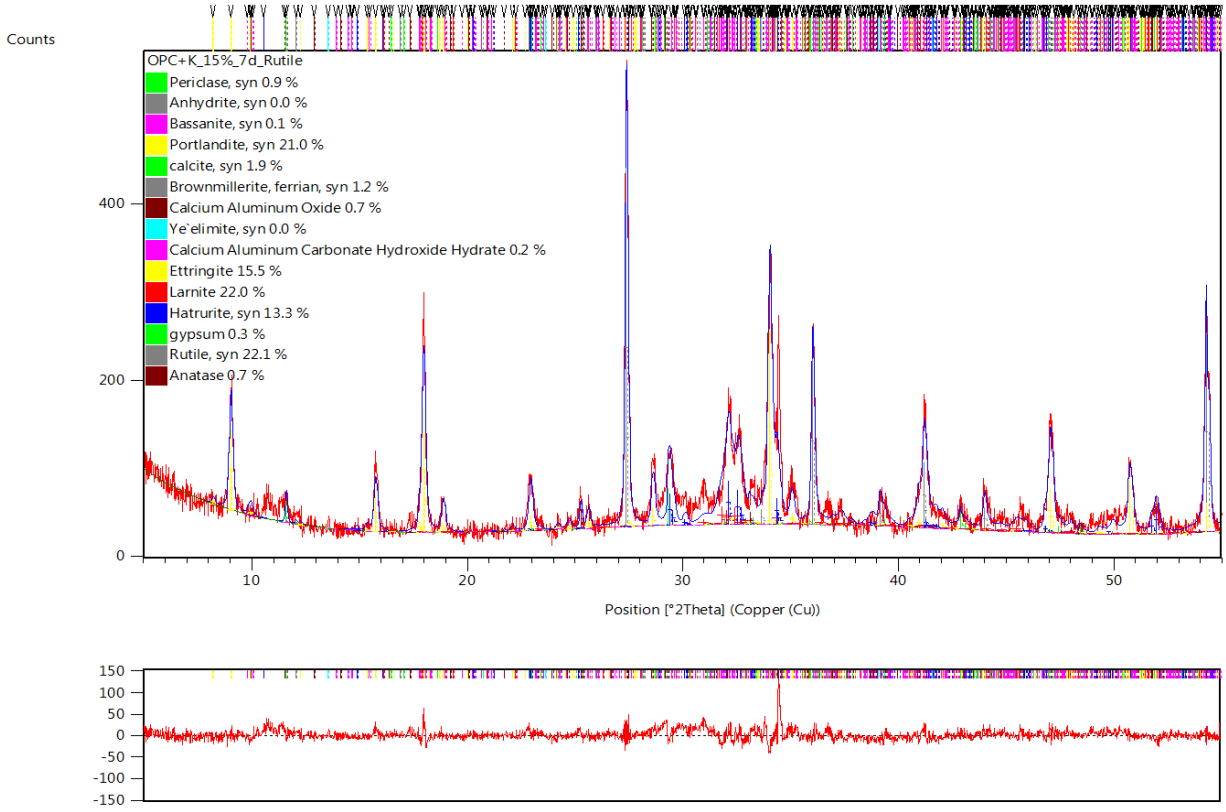


Figure A.6 Rietveld refinement of hydrated OPC-CSA binder with 15% CSA cement after 7 days

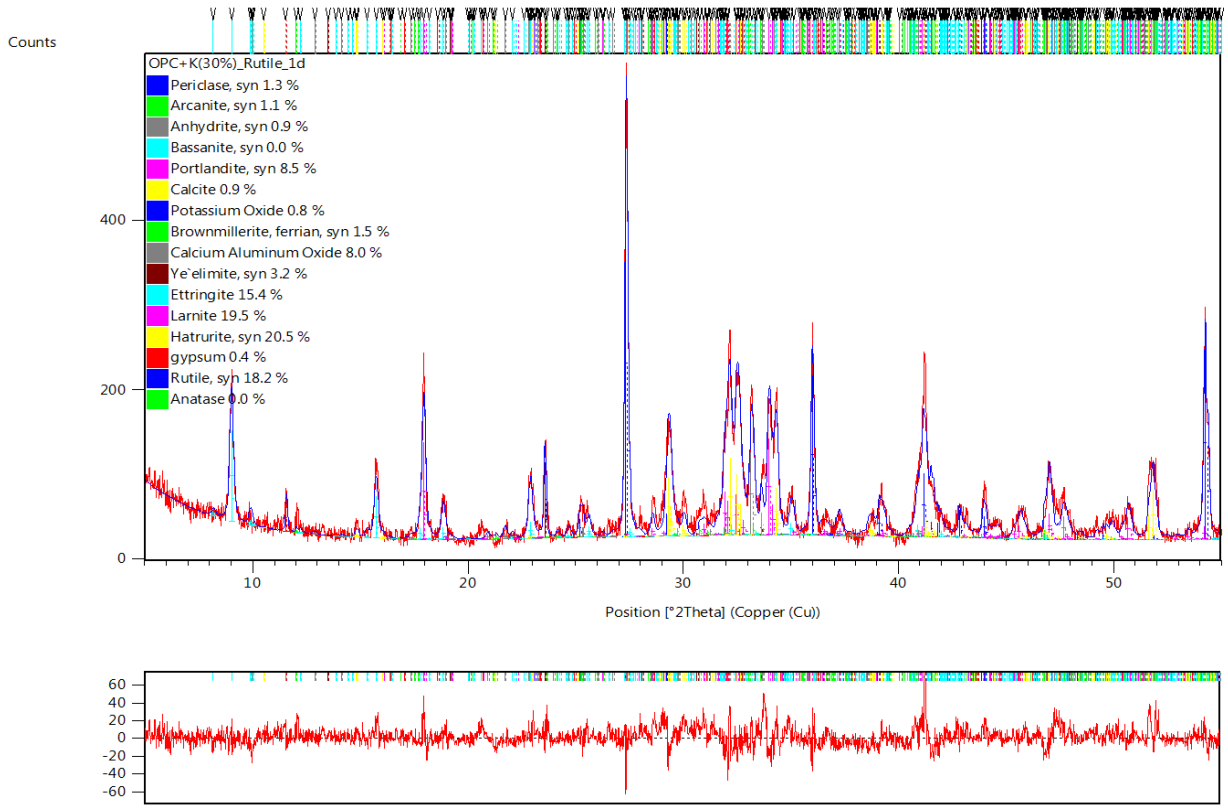


Figure A.7 Rietveld refinement of hydrated OPC-CSA binder with 30% CSA cement after 1 day

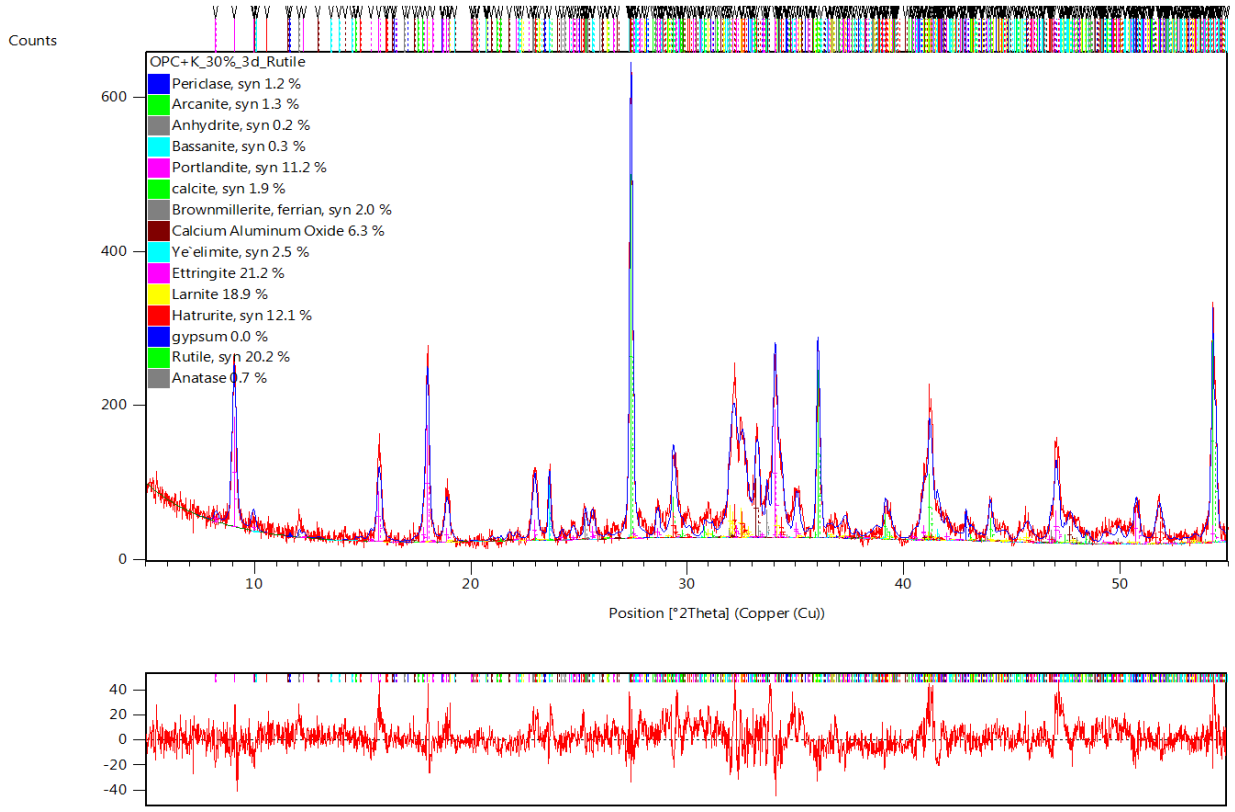


Figure A.8 Rietveld refinement of hydrated OPC-CSA binder with 30% CSA cement after 3 days

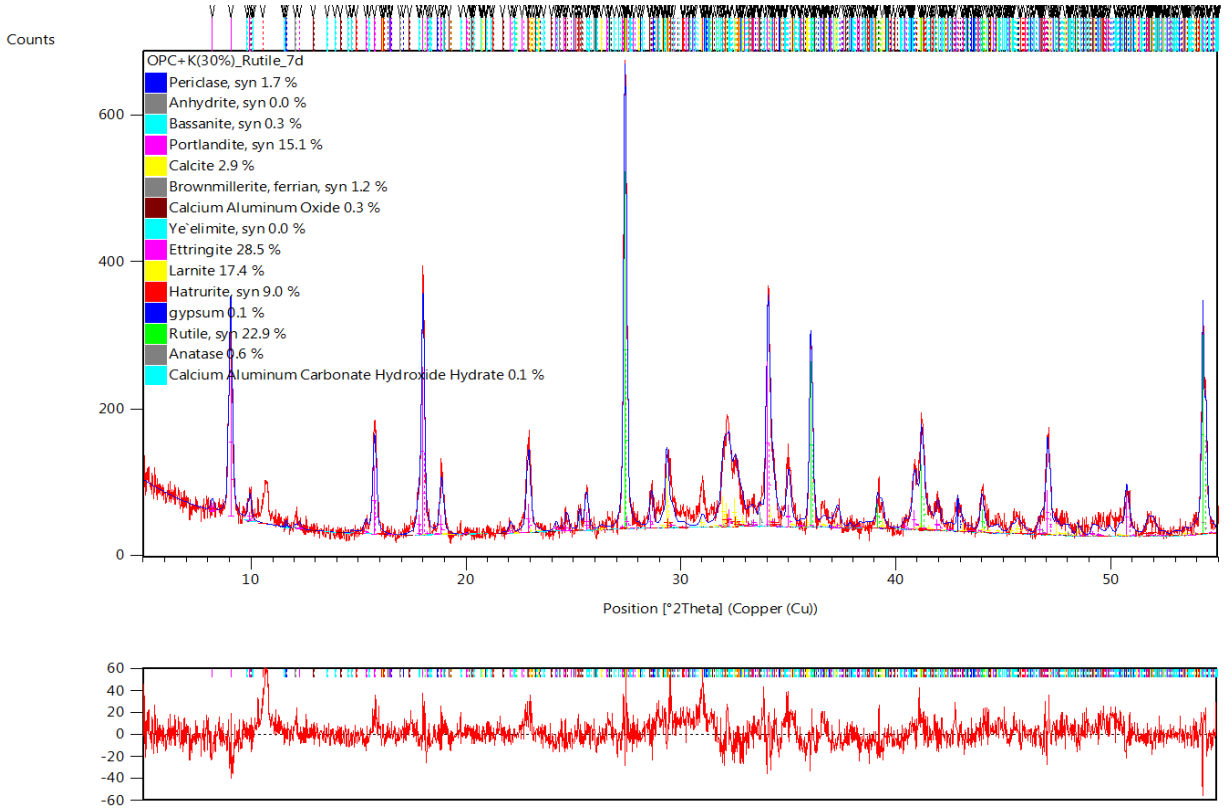


Figure A.9 Rietveld refinement of hydrated OPC-CSA binder with 30% CSA cement after 7 days

APPENDIX B. RIETVELD REFINEMENT OF OPC-CSA-MA BINDERS

This section provides the Rietveld refinement of OPC-CSA-MA binders using HighScore Plus. The phase composition of samples interground with TiO_2 (15% by wt.) is plotted and shown below:

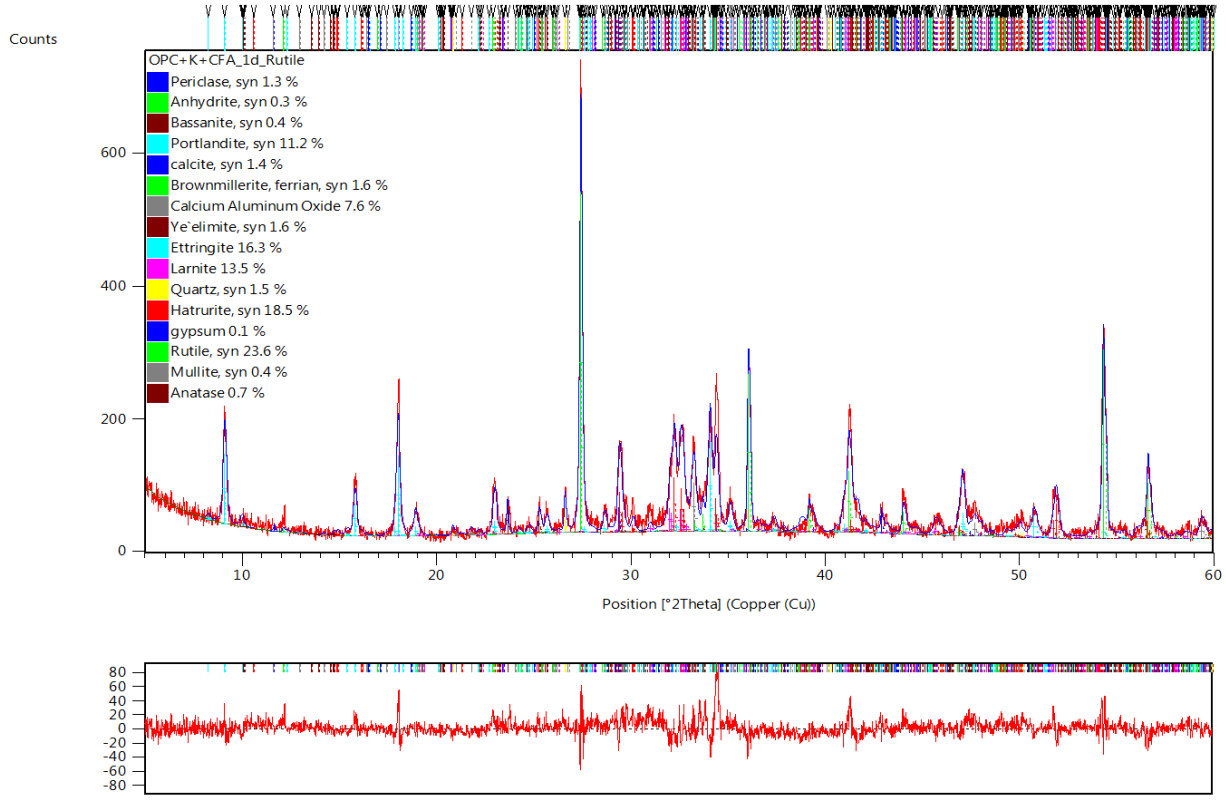


Figure B.1 Rietveld refinement of hydrated OPC-CSA-CFA binder after 1 day

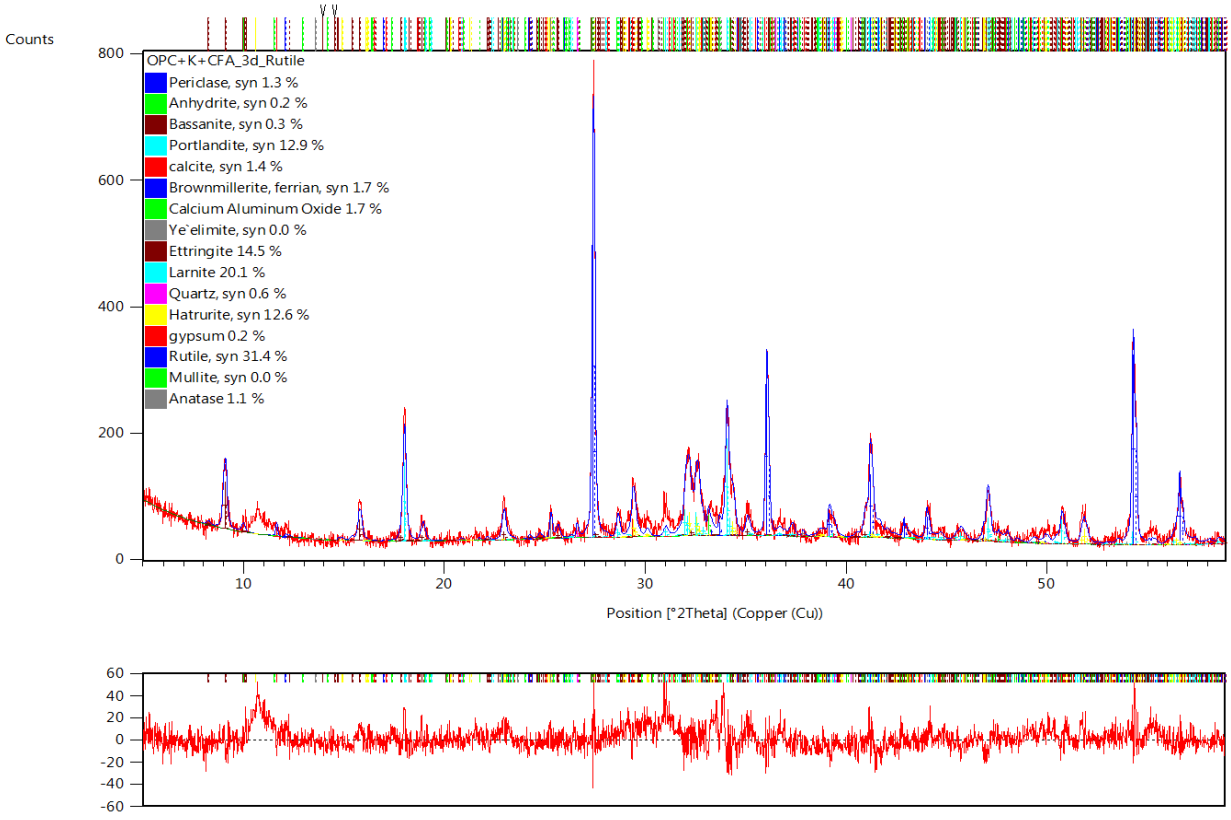


Figure B.2 Rietveld refinement of hydrated OPC-CSA-CFA binder after 3 days

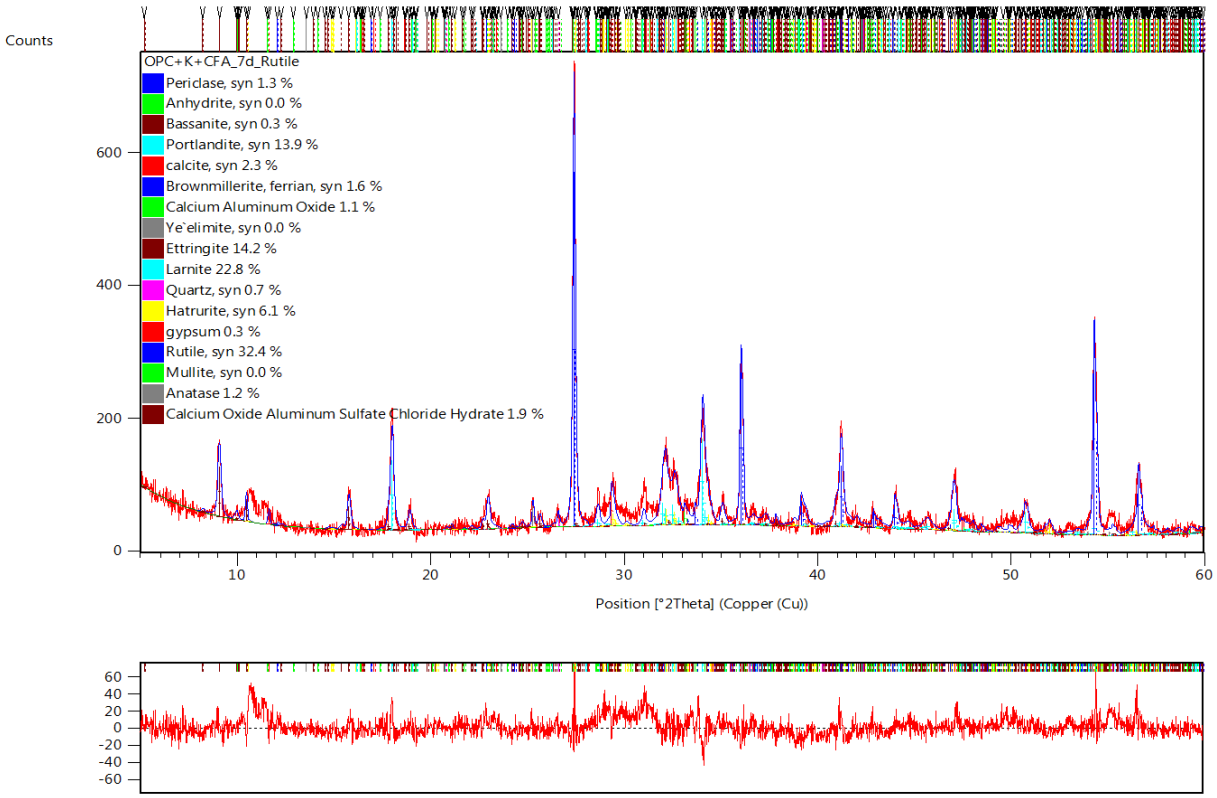


Figure B.3 Rietveld refinement of hydrated OPC-CSA-CFA binder after 7 days

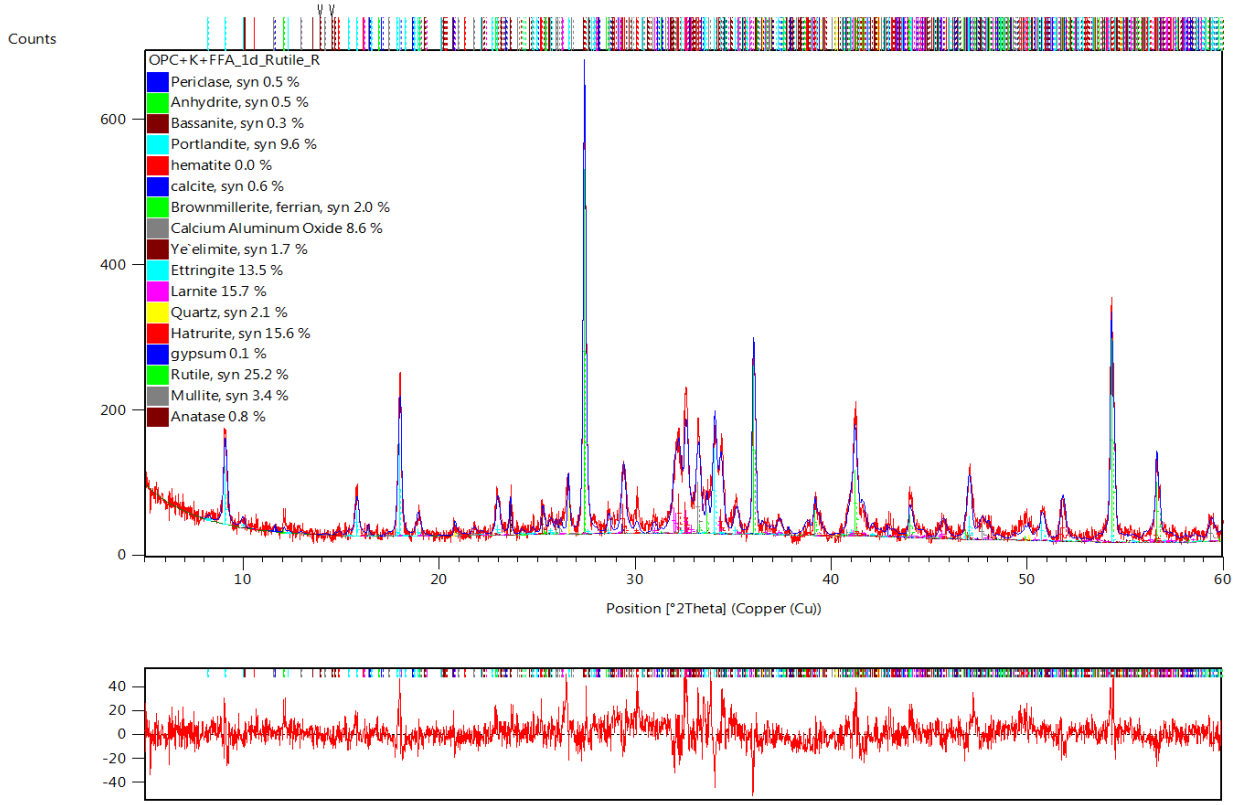


Figure B.4 Rietveld refinement of hydrated OPC-CSA-FFA binder after 1 day

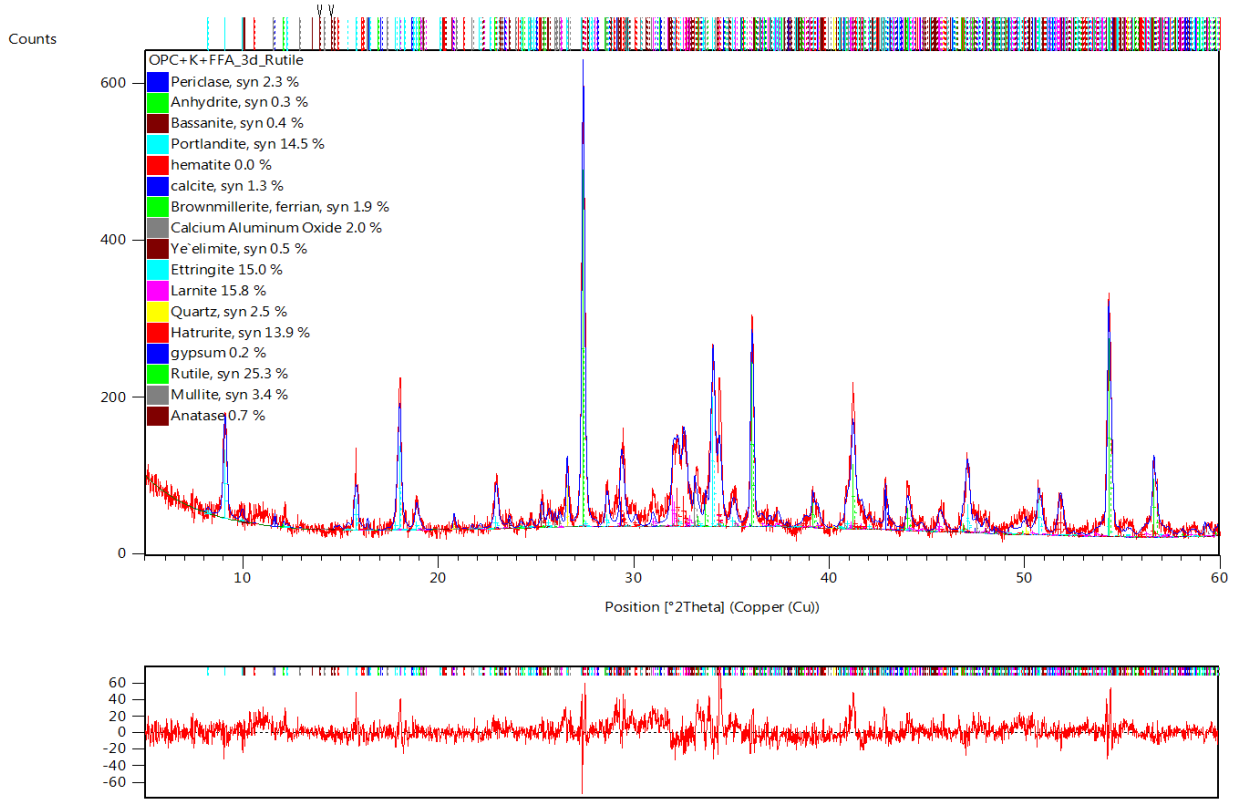


Figure B.5 Rietveld refinement of hydrated OPC-CSA-FFA binder after 3 days

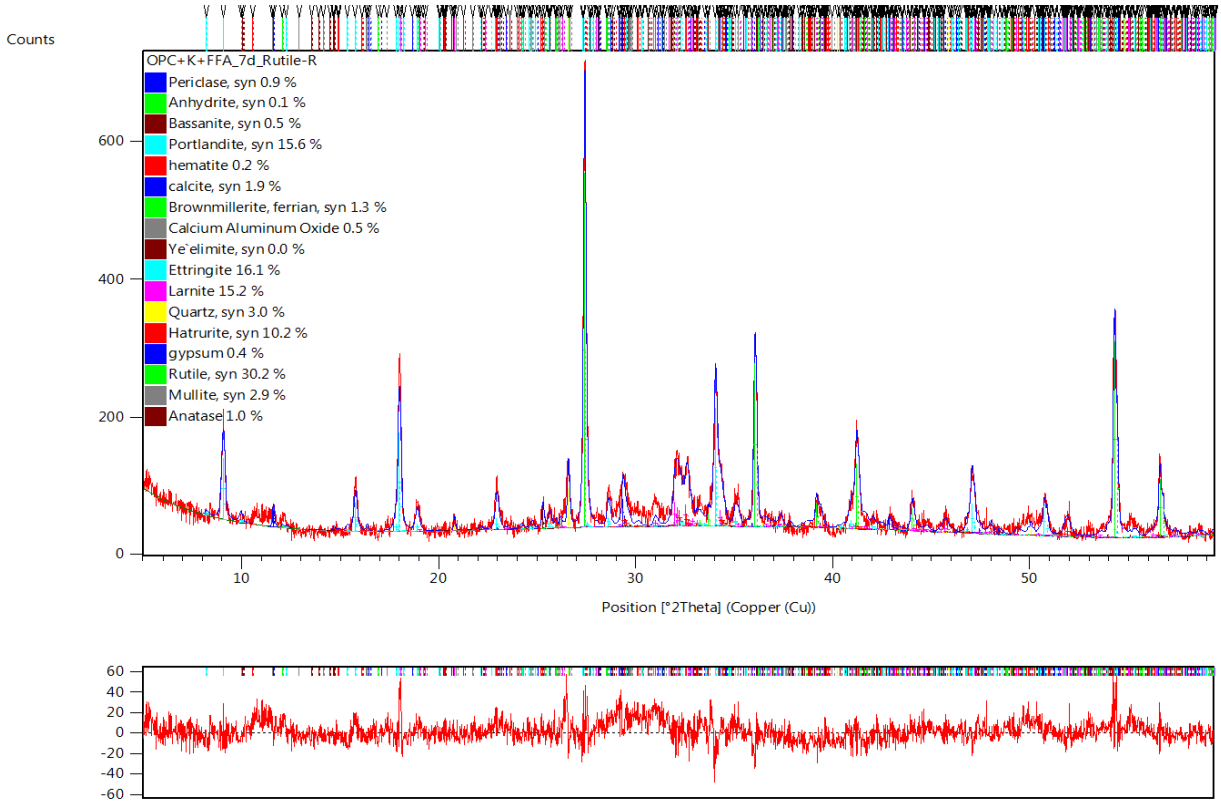


Figure B.6 Rietveld refinement of hydrated OPC-CSA-FFA binder after 7 days

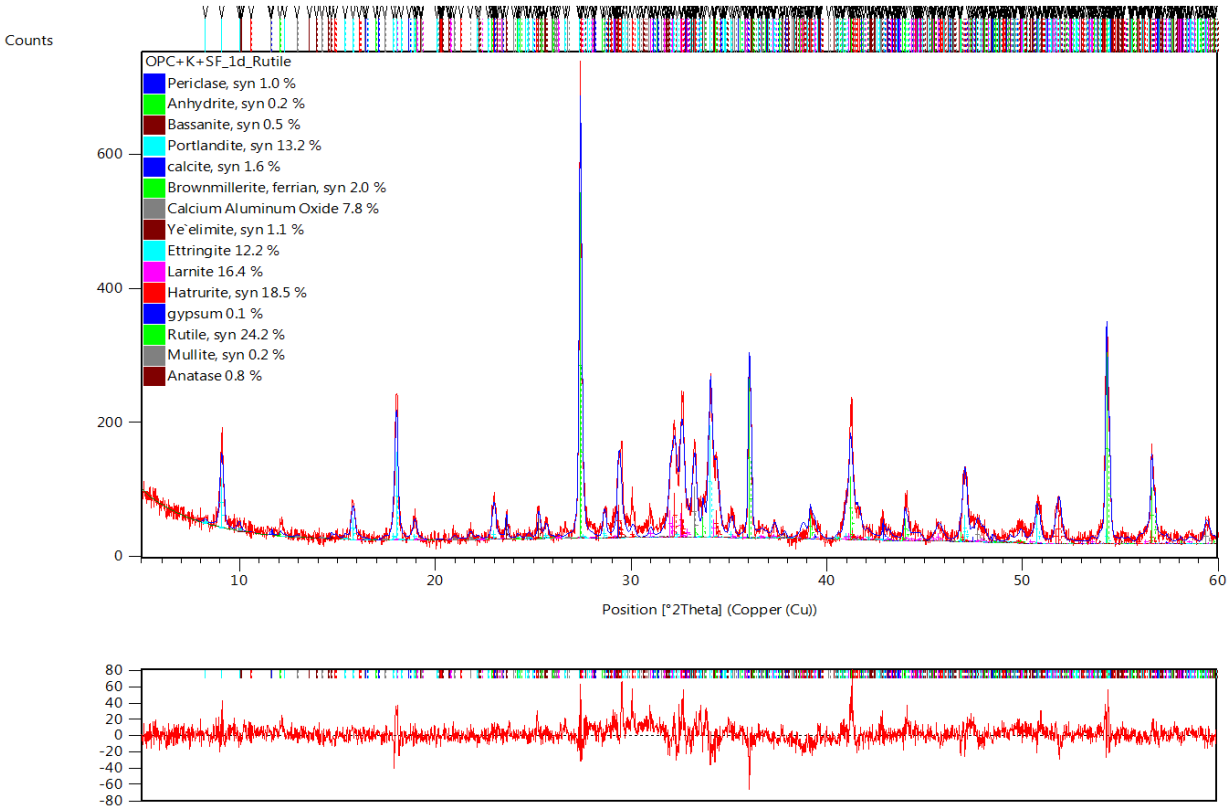


Figure B.7 Rietveld refinement of hydrated OPC-CSA-SF binder after 1 day

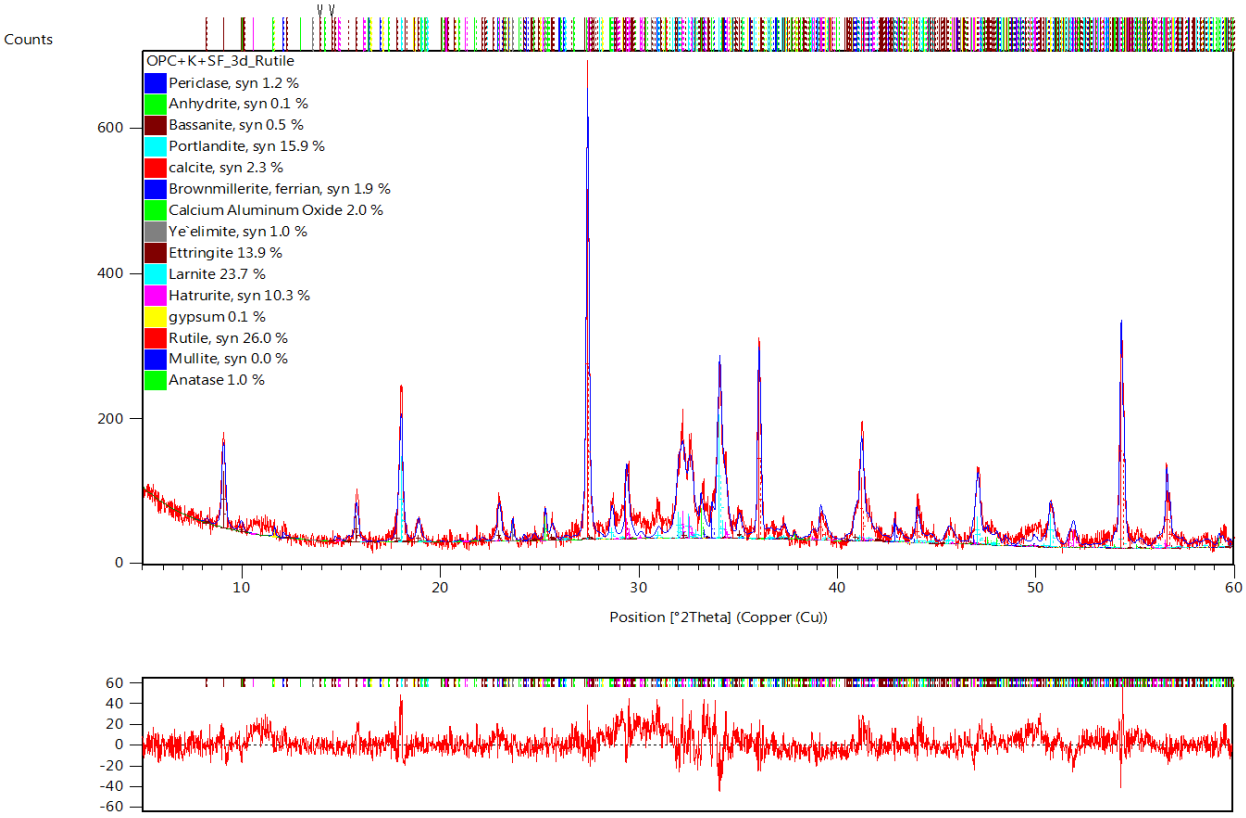


Figure B.8 Rietveld refinement of hydrated OPC-CSA-SF binder after 3 days

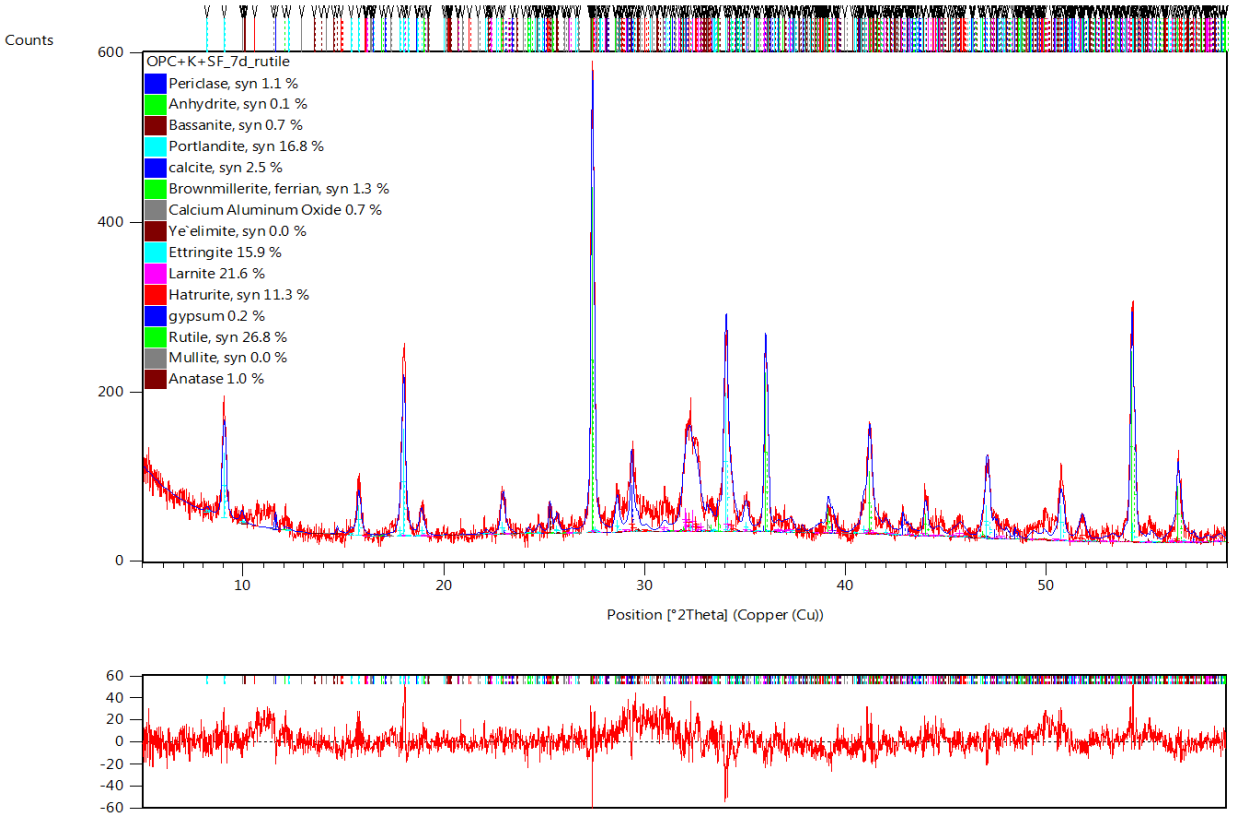


Figure B.9 Rietveld refinement of hydrated OPC-CSA-SF binder after 7 days

APPENDIX C. RIETVELD RFINEMENT OF OPC-CSA-CFA-GYP BINDER

The phase composition of OPC-CSA-CFA-Gyp binder interground with TiO_2 (15% by wt.) is plotted and shown below:

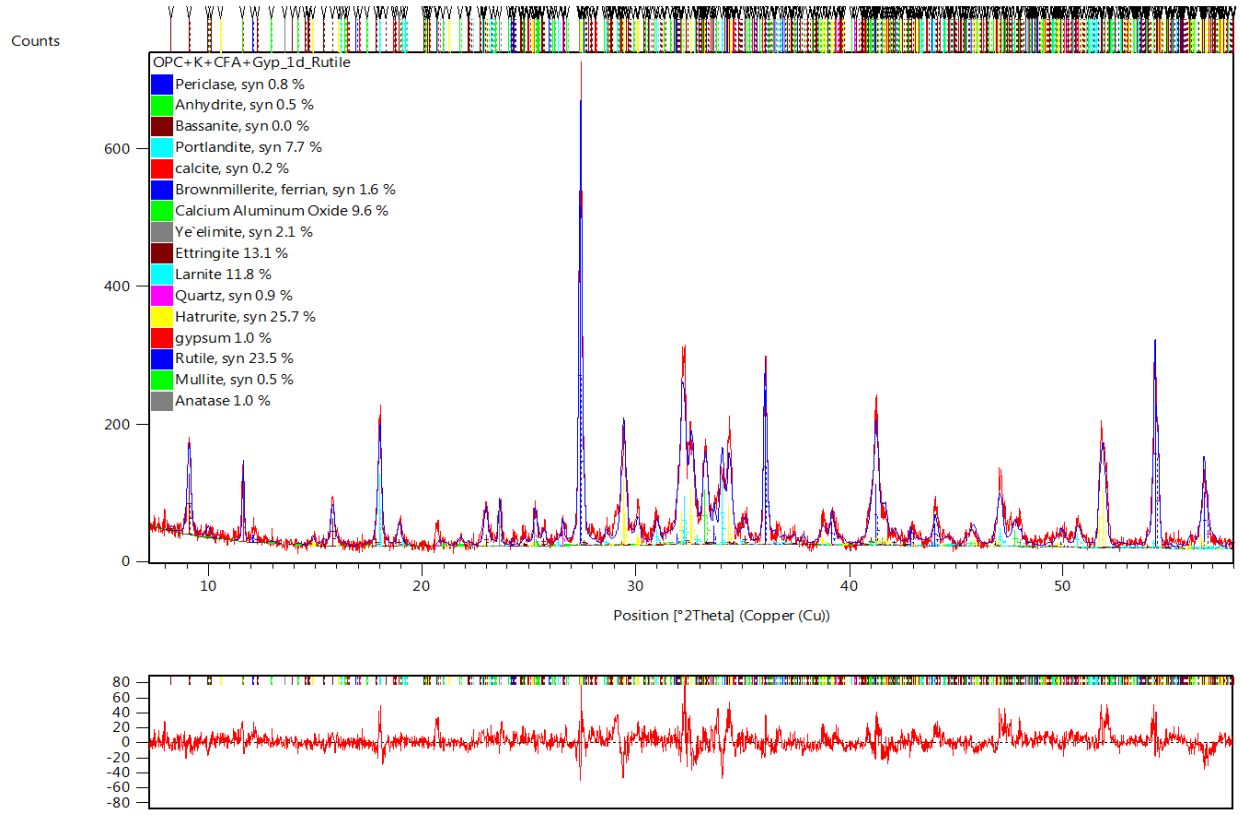


Figure C.1 Rietveld refinement of hydrated OPC-CSA-CFA-Gyp binder after 1 day

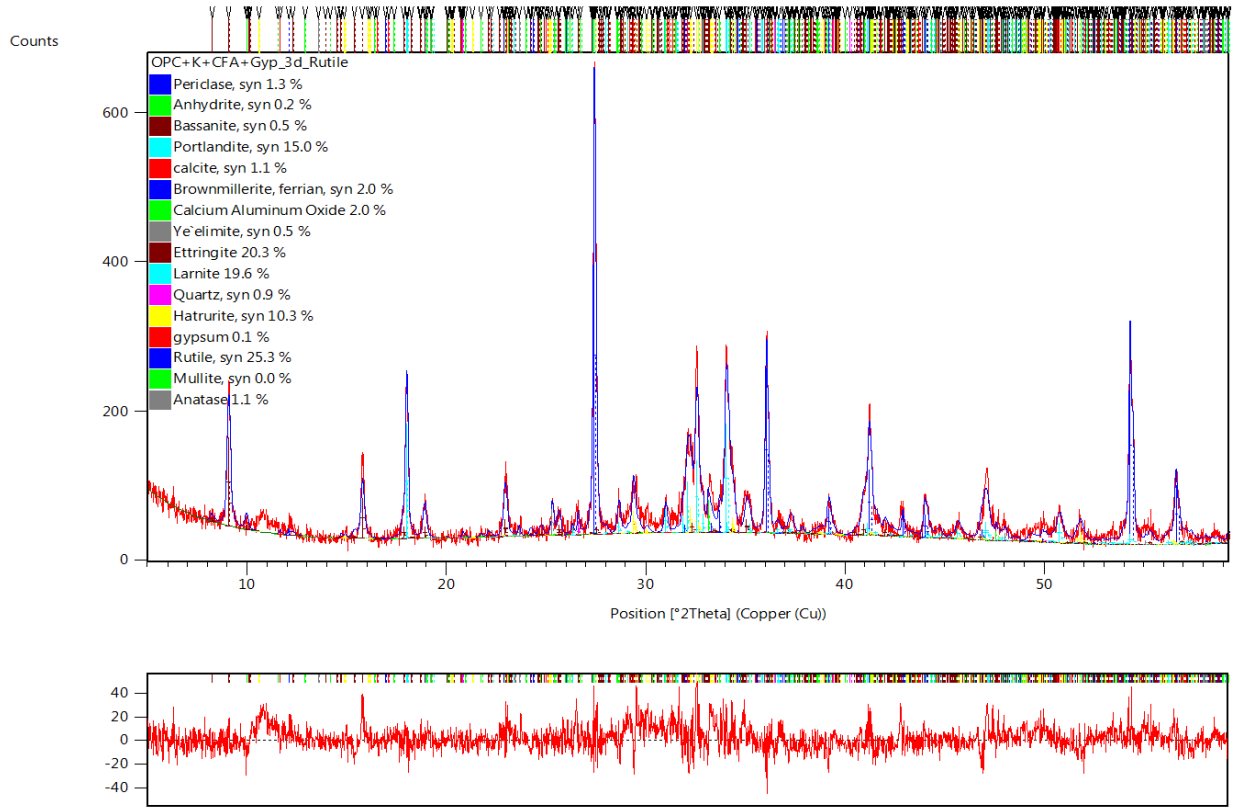


Figure C.2 Rietveld refinement of hydrated OPC-CSA-CFA-Gyp binder after 3 days

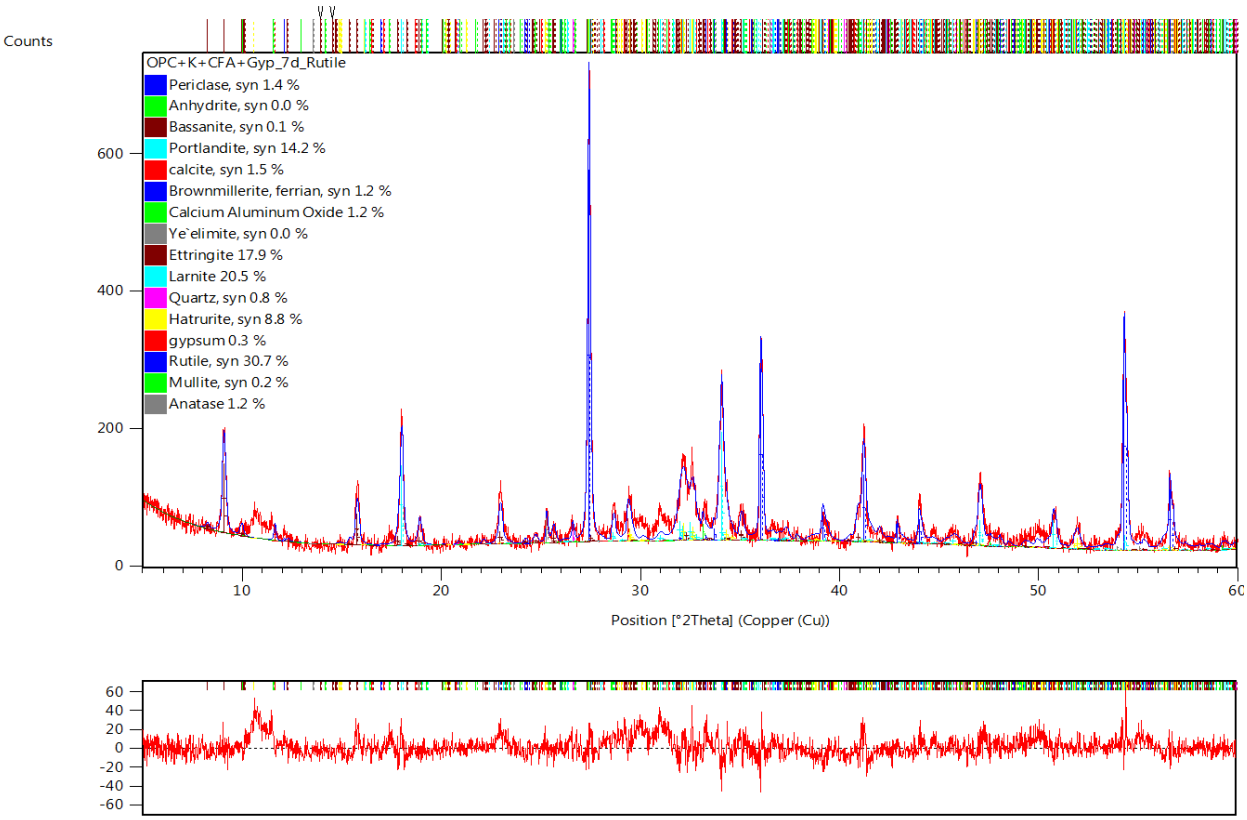


Figure C.3 Rietveld refinement of hydrated OPC-CSA-CFA-Gyp binder after 7 days

APPENDIX D. ESTIMATION OF AMORPHOUS CONTENT USING INTERNAL STANDARD

Rietveld analysis only provides the phase composition of crystalline phases. And, it is known that hydration of Portland cement results in the formation of C-S-H which is poorly crystalline or amorphous. Various attempts have been made to estimate the amorphous content using internal and external standard method. The following method describes the internal standard method which involves the intergrinding of an internal standard. The restriction on the selection of an internal standard is that it has to be purely crystalline, and also the main XRD peaks should not overlap with the peaks of a given sample. TiO_2, ZnO and Al_2O_3 are commonly used internal standards for Rietveld refinement of hydrated cement paste. The following procedure describes the method to estimate amorphous content using internal standard method.

Let's assume that the sample of interest has one crystalline phase, *Cr*, and one amorphous phase, *Am*. The amounts of crystalline and amorphous phases are W_{cr} and W_{Am}, respectively. We are interested in determine the amorphous content in the sample which can be expressed as:

$$Amorphous,\% = \frac{W_{Am}}{W_{Cr} + W_{Am}} \times 100 \qquad \text{Eq. D-1}$$

Now, let's add a known weight percentage (W_x) of an internal standard, X , in the sample which already has *Cr* and *Am* phases. The weight percentage of internal standard can be expressed as:

$$W_{IS},\% = \frac{W_x}{W_x + W_{Cr} + W_{Am}} \times 100 \qquad \text{Eq. D-2}$$

As Rietveld refinement only considers crystalline phase, the weight percentage of internal standard as determined through Rietveld, W_{RIT}, can be written as:

$$W_{RIT},\% = \frac{W_x}{W_x + W_{Cr}} \times 100 \qquad \text{Eq. D-3}$$

Now performing following manipulation, the actual weight fraction of amorphous content can be derived.

$$Amorphous,\% = \frac{1 - \frac{W_{IS}}{W_{RIT}}}{100 - W_{IS}} \times 10^4\,\% \qquad \text{Eq. D-4}$$

In order to verify the above expression, let us consider right hand side of the above expression and substitute for W_{IS} and W_{RIT} from Eqs. D-2 and D-3,

$$\frac{1 - \frac{W_{IS}}{W_{RIT}}}{100 - W_{IS}} \times 10^4 = \frac{1 - \frac{\frac{W_x}{W_x + W_{Cr} + W_{Am}}}{\frac{W_x}{W_x + W_{Cr}}}}{100 - \frac{W_x}{W_x + W_{Cr} + W_{Am}} \times 100} \times 10^4 = \frac{1 - \frac{W_x + W_{Cr}}{W_x + W_{Cr} + W_{Am}}}{\left(\frac{W_{Cr} + W_{Am}}{W_x + W_{Cr} + W_{Am}}\right)} \times 10^2 = \frac{W_{Am}}{W_{Cr} + W_{Am}} \times 10^2$$

Amorphous Content

The right most expression in the above calculation is the amorphous phase content (% wt.) as shown in Eq. D-1. Therefore, the amorphous phase can be estimated using known amount of internal standard (W_{IS}) and Rietveld determined internal standard (W_{RIT}).